Review

Nanomaterial-Based Sensors for the Detection of Glyphosate

Karem Zúñiga [1], Georgette Rebollar [2], Mayra Avelar [3], José Campos-Terán [4,*] and Eduardo Torres [5,*]

[1] Posgrado en Ciencias Naturales e Ingenieria DCNI, Universidad Autónoma Metropolitana, Unidad Cuajimalpa, Av. Vasco de Quiroga 4871, Col. Santa Fe, Delegación Cuajimalpa de Morelos, Mexico City 05348, Mexico

[2] Facultad de Ingeniería Química, Benemérita Universidad Autónoma de Puebla, Puebla 72570, Mexico

[3] Laboratorio de Síntesis Asimétrica y Bioenergética (LSAyB), Ingeniería Química (UACQ), Universidad Autónoma de Zacatecas, Campus XXI Km 6 Carr. Zac-Gdl, Zacatecas 98160, Mexico

[4] Departamento de Procesos y Tecnología, Universidad Autónoma Metropolitana, Unidad Cuajimalpa, Av. Vasco de Quiroga 4871, Col. Santa Fe, Delegación Cuajimalpa de Morelos, Mexico City 05348, Mexico

[5] Instituto de Ciencias, Benemérita Universidad Autónoma de Puebla, Puebla 72570, Mexico

* Correspondence: jcampos@correo.cua.uam.mx (J.C.-T.); eduardo.torres@correo.buap.mx (E.T.)

Abstract: Due to its chemical properties, glyphosate [N-(phosphonomethyl)glycine] is one of the most commonly used agricultural herbicides globally. Due to risks associated with human exposure to glyphosate and its potential harmfulness, the need to develop specific, accurate, online, and sensitive methods is imperative. In accordance with this, the present review is focused on recent advances in developing nanomaterial-based sensors for glyphosate detection. Reported data from the literature concerning glyphosate detection in the different matrices using analytical methods (mostly chromatographic techniques) are presented; however, they are expensive and time-consuming. In this sense, nanosensors' potential applications are explained to establish their advantages over traditional glyphosate detection methods. Zero-dimensional (0D), one-dimensional (1D), two-dimensional (2D), and three- dimensional (3D) materials are reviewed, from biomolecules to metallic compounds. Bionanomaterials have generated research interest due to their selectivity with respect to using enzymes, DNA, or antibodies. On the other hand, Quantum Dots also are becoming relevant for their vast surface area and good limit of detection values (in the range of pM). This review presents all the characteristics and potential applications of different nanomaterials for sensor development, bearing in mind the necessity of a glyphosate detection method with high sensitivity, selectivity, and portability.

Keywords: Glyphosate; nanomaterials; sensor; water-detection; herbicide

1. Introduction

Pesticides are produced in millions of tons annually for agricultural purposes [1]. However, this intensive use poses a potential toxicological risk for humans [2] and the ecosystems [3,4]. Among the different pesticides used, the herbicide Glyphosate (GLYP), N-(phosphonomethyl) glycine, has been applied extensively over the last 40 years, assuming minimal side effects. However, concerns about the direct and indirect potential health effects of large-scale GLYP usage have recently increased worldwide [5–8].

GLYP is widely used compared to other herbicides because of its non-selective, post-emergence, and systemic properties. Its action mechanism disrupts the shikimate metabolic pathway and the aromatic amino acid synthesis [9–11]. The impact of this herbicide on the ecological environment and human health is of international concern [12–14].

Chemically, GLYP (Figure 1a) is a white crystalline and odorless solid with one basic amino group and three acidic sites. GLYP is commonly used as a salt despite its acid characteristic, particularly the isopropylamine salt. GLYP is a highly polar and, consequently, water-soluble substance. It can form complexes quickly with some metals; it has low

volatility, high density, and low octanol-water partition coefficient [15]. It presents an average half-life of 45–60 days and may persist up to 170 days in soil [16]. Its primary breakdown product is aminomethylphosphonic acid (AMPA, Figure 1b), which degrades slowly in the ground.

Further degradation breaks down this compound into phosphate, ammonia, and carbon dioxide. As polar molecules, GLYP and AMPA could be readily found in water bodies such as rivers and streams or can enter the atmosphere bound to soil dust, which can be dissolved in rivers and streams through the rainwater [11,17,18]. Consequently, and due to its intensive and unregulated use, GLYP represents a potential pollutant of water [19–22].
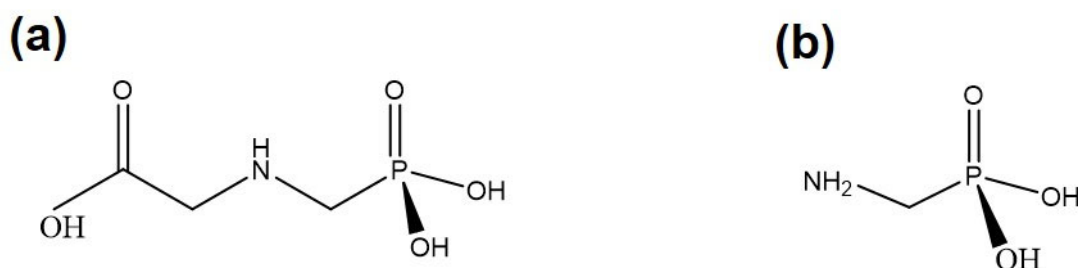
(a)

(b)

Figure 1. Chemical structure of (**a**) glyphosate (GLYP); (**b**) aminomethylphosphonic acid (AMPA).

The high human exposure to GLYP has carried out an intense debate about its potential harmfulness [8,20,23,24]. Besides acute and chronic toxicity in aquatic species, its use has been associated with cancer and endocrine disruption in humans [17,25–31]. Thus, determining its presence in environmental, food, or biological samples is imperative and, consequently, the requirement to develop sensitive, specific, accurate, and online GLYP detection methods [11,22,32]. It is important to note that the maximum concentrations allowed for GLYP in water vary according to each country's or even region's regulations. For instance, the European Union established a maximum level of 0.1 µg/L for this herbicide in drinking water [33,34].The United States Environmental Protection Agency (USEPA) set a maximum level of 700 µg/L [35], and Canada has a maximum concentration of 280 µg/L [36]. There is a remarkable difference in the allowed maximum limits between countries such as Mexico, where local regulations permit a maximum of 10 µg/L per the local regulations [37]. These differences are due to the legislation in each country, as some may focus on hazard identification and regulatory assessments.

In contrast, others refer to estimating the substance's toxicity in question [38–40]. For example, the USEPA official method to detect GLYP in drinking water [41] uses tandem liquid chromatography and fluorescence, which conforms to the USA's regulations. However, its lowest limit of detection (LOD) falls above the minimum concentration allowed in the European Union.

Environmental monitoring of glyphosate, and in general of environmental pollutants, requires certain parameters for the correct diagnosis of environmental problems; among them is the reliability of the measurement of the concentration of the pollutant; for this, the methods, instruments and devices must show their capacity to measure ultra-low concentrations, be selective, accurate and precise; in addition, they are expected to be sufficiently robust to be stable under working and storage conditions. The development of methods, devices or sensors is a very active field of research, with a number of very numerous reports in the scientific literature. To date, sensors are focused on meeting these performance aspects, with the challenge of their application in environmental conditions, and their validation with officially recognized techniques. This review aims to present the recent advances in the development of nanosensors and nanomaterials-based sensors for the detection of GLYP. For this purpose, a comprehensive study was carried out in the SCOPUS database over the past three years concerning (nano) sensors for GLYP detection,

especially emphasizing the application of the nanosensor in water samples. First, the analysis is focused on the sensibility of the different preparations; then, an analysis of selectivity is provided for the application in field conditions.

2. Glyphosate Detection Techniques

Chromatographic methods are currently used as the analytical methods of reference for GLYP detection [42,43] as these methods can be automated, are accurate and highly specific, and can be performed simultaneously [43–45]. However, their requirement for expensive equipment, strict experimental conditions, drawn-out assay times, expensive reagents, time-consuming analyses, sample pre-treatment, their slow response time, and their requirement for skilled personnel limit their applications, mainly in developing countries [19,46–50]. Furthermore, the physicochemical properties of GLYP have led to the development of a wide variety of alternative analytical methods to improve the LOD and the linear range associated with the techniques and overcome the high requirements of conventional HPLC-MS or GC-MS methods (Table 1) [51].

The research and development of an analytical methodology using sensors for environmental applications can help resolve these problems. According to the International Union of Pure and Applied Chemistry (IUPAC), a sensor "is a device that transforms chemical information, ranging from the concentration of a specific sample component to total composition analysis, into an analytically useful signal." Usually, a sensor uses a recognition element in direct contact with a transducing element to provide specific, quantitative, or semi-quantitative analytical information [52–54]. With this definition, a sensor in general has the following components (Figure 2): (a) a recognition element, able to selectively recognize analytes from a matrix source; (b) a physical transducer to transform the interplay between the recognition element and the analyte into a measurable signal; and (c) an electronic system for signal amplification and signal processing [55–57].

Table 1. LOD values of some methods for the detection of GLYP in water.

Matrix	Analytical Technique	LOD	Linear Range	Reference
Groundwater	Solid-phase extraction followed by liquid chromatography coupled to tandem mass spectrometry (SPE-LC-MS/MS)	18.9 pM	0.3–3 nM	[58]
Tap water and irrigation water	Electrochemiluminescence	0.2 mM	0.2–16.6 mM	[59]
Tap water	High-performance liquid chromatography (HPLC) and ultraviolet spectroscopy	0.4 μM	29.6 μM–0.6 mM	[60]
Groundwater	Fluorescence spectroscopy	0.25 μM	0.59–2.96 μM	[61]
Potable, treated wastewater, urban, and groundwater	Spectrophotometric: 5-Phenyldipyrrinate of Nickel (II)	0.20 μM	0.59 μM–11 μM	[62]
Canal water	Liquid chromatography fluorescence (LC-FLD) + tandem mass spectrometry (MS-MS)	0.6 nM	0.6 nM–0.3 μM	[63]
Surface water	Chromatography-tandem mass spectrometry (LC-MS/MS)	0.89 nM	2.96–2957 nM	[64]
Pearl River water	Fluorescence	47.3 nM	59.1 nM–47.3 μM	[65]

|				
Deionized water	Optical: prism coupling optical waveguide	1.4 nM	1.4–5.0 nM	[66]
	Laser induced fluorescence (LIF)	0.3 nM	0.1 nM–5.0 μM	[67]
	Enzyme-linked immunosorbent assay (ELISA)	0.6 nM	3.2–4.5 nM	[68]
	Solid-phase extraction (SPE) Derivatized/Gas chromatography-flame photometric detection (GC-FPD)	0.6 nM	59.15–5915 nM	[69]
	Sequential-injection reversed-phase chromatography	30 nM	0.10–12.8 μM.	[70]
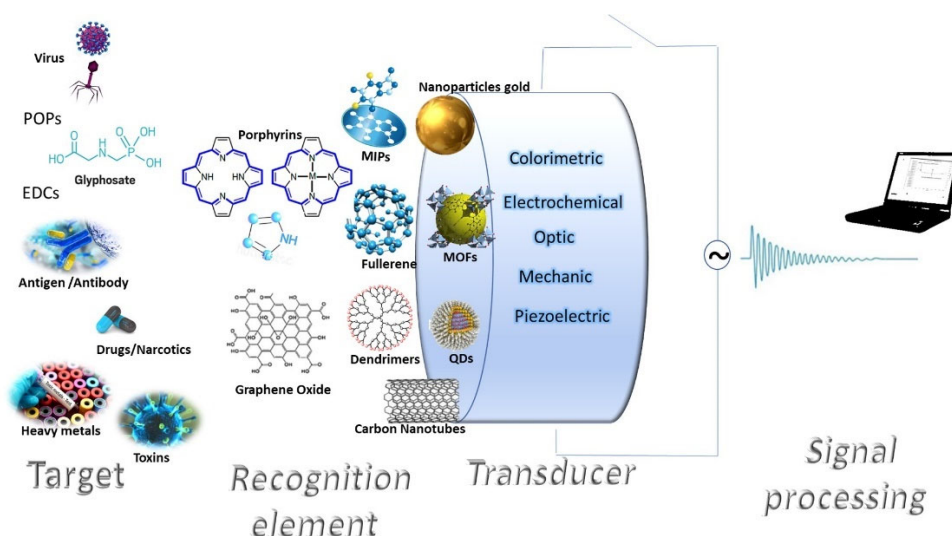
Figure 2. The schematic representation of sensor parts includes recognition elements, transducers, and detectors.

In addition, nanosensors are nanoscale element devices engineered to identify a particular chemical, biological compound, or environmental event [55,71]. These sensors are highly specific, cost-effective, and much more sensible than their macroscale versions.

The performance of these kinds of devices is usually evaluated in terms of their response time, dynamic range, LOD, and selectivity. This performance could be enhanced using nanomaterials.

In recent years, many nanomaterials have been introduced in sensor fabrication to detect and quantify analytes at trace levels in the environment [72,73]. The use of nanomaterials in sensors may have at least three leading roles: first, as part of the recognition element, they present a large surface area that allows for an analyte's more efficient capture [74–77]; second, they can be used as an immobilization platform for biological recognition elements such as enzymes, aptamers, DNA, RNA, etc.; and the third role, the nanomaterial can be by itself the transducer or amplifier of the signal coming from the recognition element [78,79]. These (nano)sensors are portable, potentially cost-effective, fast, and easy-to-operate with competitive performance characteristics compared to conventional methods, with the potential advantage of being used for massive numbers of samples in situ.

3. Nanomaterial-Based Sensors for Monitoring Pollutants

In terms of dimension and shape, nanomaterials can be classified into four classes: (i) the zero-dimensional nanomaterials (0D), which have all their dimensions in nanoscale, i.e., their sizes are less than 100 nm, and 0D include spherical, cubic, nanorod, polygon,

hollow sphere, metal, and core–shell nanomaterials, as well as quantum dots (QDs); (ii) one-dimensional nanomaterials, (1D) which are materials with only one non-nano scale dimension, for example, 1D nanomaterials include metallic, polymeric, ceramic, nanotube, nanorod filament or fiber, nanowire, and nanofiber materials; (iii) two-dimensional NMs (named 2D), which contain just one nanoscaled length and include single-layered and multi-layered types, crystalline or amorphous types, thin films, nanoplates, and nanocoating; and finally, (iv) three-dimensional (3D) materials, which possess dimensions larger than 100 nm measurements [80]. and combine multiple nanocrystals in different directions, with examples including foams, fibers, carbon nanobuds, nanotubes, fullerenes, pillars, polycrystals, honeycombs, and layer skeletons [81,82] (Figure 3).

In addition, combining different nanomaterials has introduced new components called nanocomposites. Nanocomposites combine various properties among distinct materials and may produce enhanced or new physical and chemical properties. Therefore, nanocomposites represent a relevant element in nanosensor development [83,84]. Furthermore, an optimal sensor should fulfill characteristics such as having a fast response time, a prolonged lifetime (several months), a small size, and low-cost production [85]. To date, the integration of 0D, 1D, 2D, and 3D nanomaterials and their nanocomposites [53,86–88] represents an outstanding research field for (nano)sensor development [89–92].
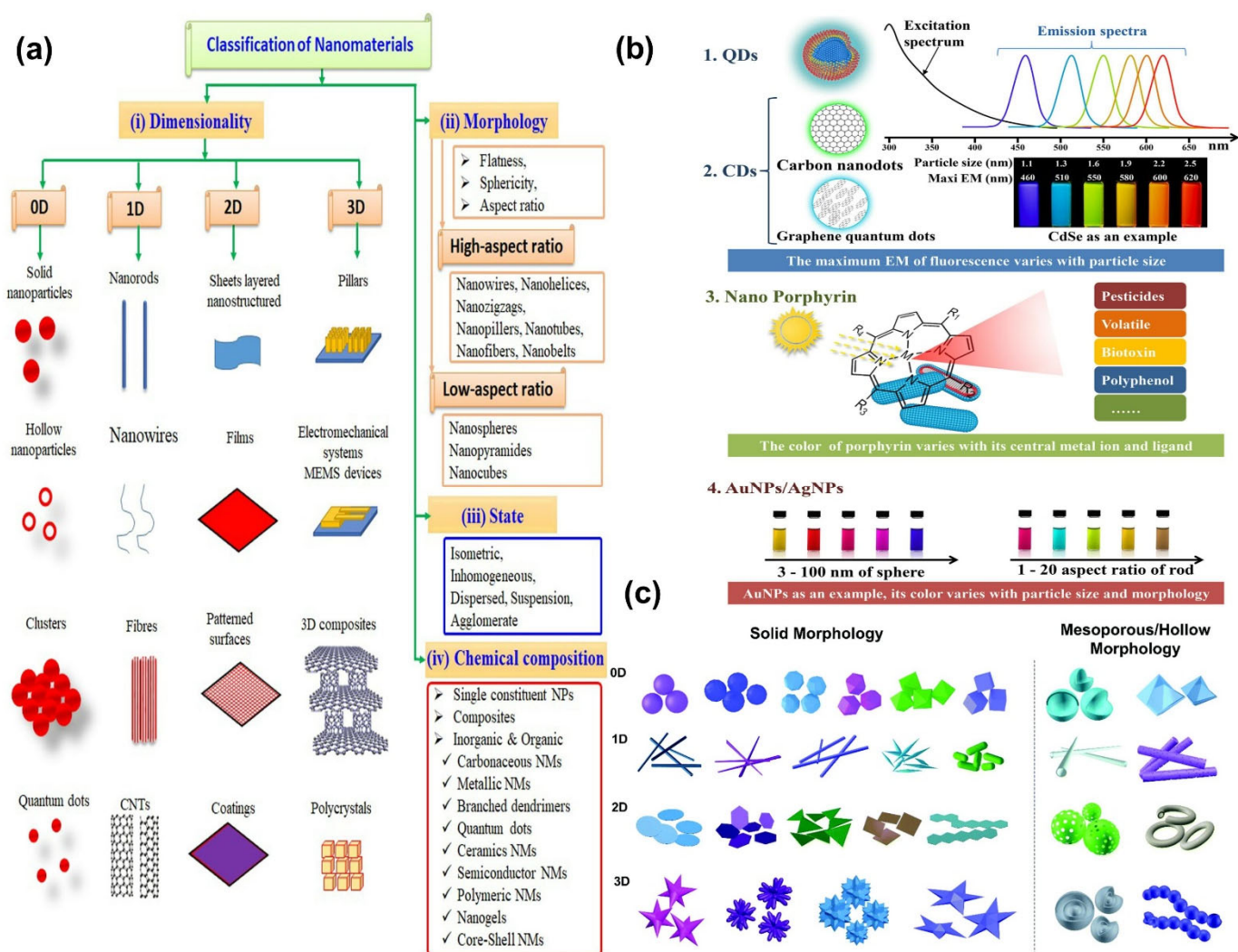

Figure 3. (**a**) Schematic illustration of nanomaterials classification. Adapted with permission from [81] Copyright 2020 Elsevier (**b**) and their optical properties. Adapted with permission from [93] Copyright 2021 Elsevier. (**c**) Typical morphologies of solid and mesoporous/hollow inorganic

nanoparticles with 0D, 1D, and 2D shapes and other 3D complex structures. Adapted with permission from [94]. Copyright 2016 Royal Society of Chemistry.

3.1. 0D Nanomaterials

Research in 0D materials includes spherical NMs, cubes, nanorods, polygons, hollow spheres, metals, and core and shell NMs, as well as inorganic quantum dots (QDs), including carbon quantum dots (CQDs), quantum dots (GQD), fullerenes, polymeric dots (Pdots), magnetic nanoparticles (MNPs); in the case of glyphosate detection, noble metal nanoparticles and upconversion nanoparticles (UCNP) have been used [82].

3.1.1. Gold Nanoparticles (AuNPs)

AuNPs possess properties that make them an ideal optical material for detecting various analytes [95], thus facilitating their use as sensors (Table 2) [96]. AuNPs commonly have a size particle distribution between 1 nm and 100 nm and are likewise known as colloidal gold. They are highly inert, stable against oxidation, have a large surface-to-volume ratio, and possess unique optical and electrochemical properties that significantly depend on their size, shape, and aggregation [96]. The color of the colloidal solution of this kind of material depends on changes or alterations in their particle size, shape, geometry[95,97], and the agglomeration states [98]. Hence, the measurement of color change could detect the AuNPs–analyte interaction through colorimetric assays. For example, when an analyte binds to the AuNPs' surface, the particle aggregation induces a color change, and the Surface Plasmon Resonance (SPR) peak is broadened and shifted. In this way, the detection of GLYP at trace concentrations through its interaction with AuNPs has been reported. For instance, the aggregation of AuNPs–Cysteamine in the presence of GLYP causes a color change from red to blue (or purple), which can be observed with the naked eye. Cysteamine-stabilized gold nanospheres were used as a colorimetric probe to detect GLYP, resulting in a linear concentration of 0.500–7.00 mM and achieving an LOD of 5.88×10^{-8} M [99].

In another example, an electrochemical molecularly imprinted sensor developed by the electropolymerization of p-amino thiophenol-functionalized with AuNPs in the presence of GLYP as a template molecule was reported (Figure 4). The electrochemical determination was based on the change in the electron transfer rate for Fe (II)/Fe (III), which flows through the MIP sensor film after incubation with GLYP. As a result, the MIP sensor facilitated the attainment of a limit of detection as low as 5 fM with a broad linear range between 5.9×10^{-9} and 5.9×10^{-3} µM [100].
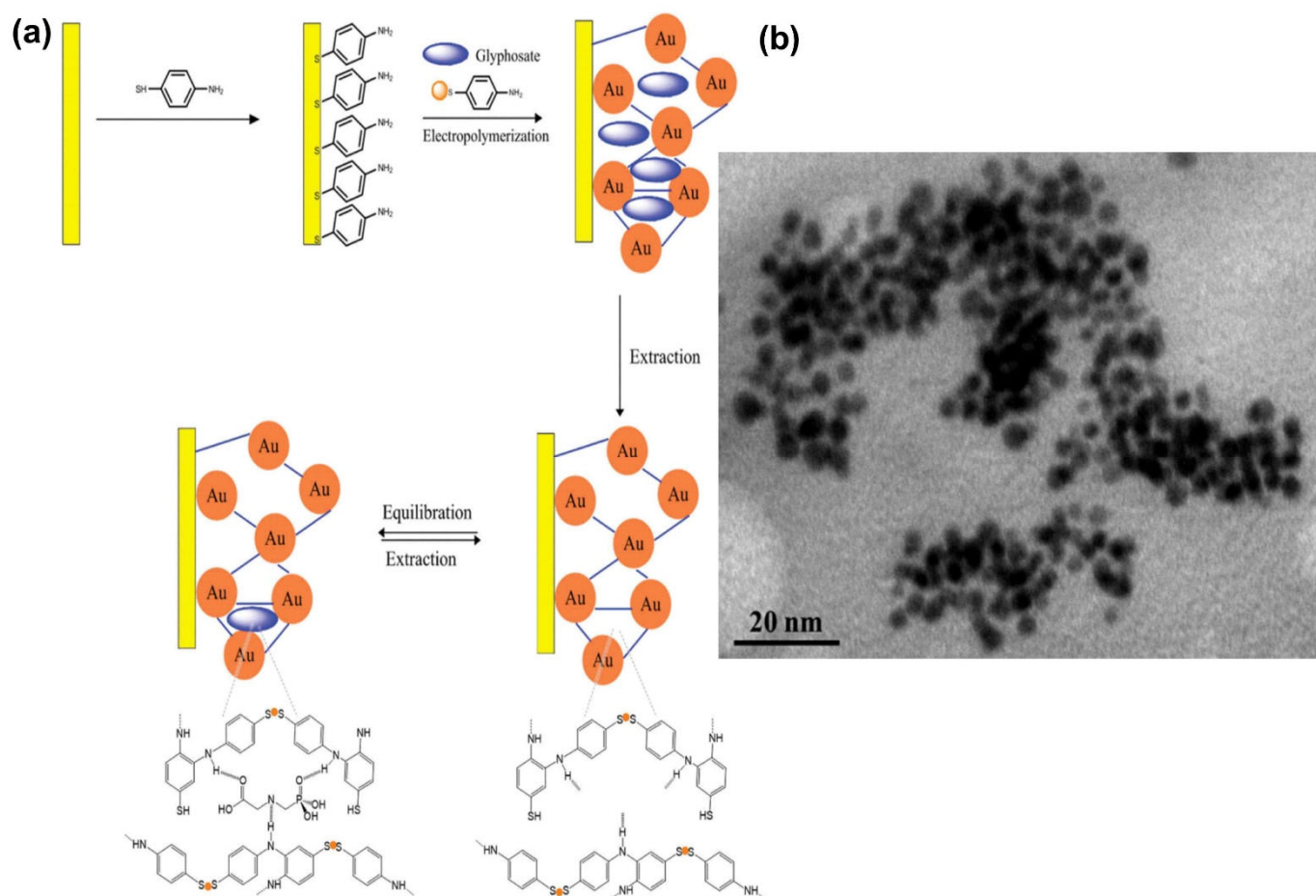
Figure 4. Fabrication steps of an imprinted sensor for GLYP detection: (**a**) electropolymerization in the template presence, template extraction, and equilibration with the unknown GLYP solution for its detection. Au bullets present AuNPs, before and after electropolymerization of polythioaniline, entrapping GLYP molecules as templates. At the bottom of the figure, the hydrogen bonds between aniline moieties and the O and N atoms of GLYP molecules in the MIP-MOF film are presented, and empty cavities after the extraction of GLYP molecules. (**b**) TEM observation of p-amino thiophenol-functionalized gold nanoparticles. Reprinted with permission from [100]. Copyright 2015 Taylor & Francis.

Another study using AuNPs, wherein the sensitivity and selectivity for GLYP were enhanced, reported using anisotropic gold nanobipyramids (GNBPs) with a localized surface plasmon resonance (LSPR) technology. In this case, the gold nanoparticles have a bipyramidal structure. The large curvature at the edge of the GNBPs increased the LSPR effect due to electron-rich sites, which enhanced the sensor's function. This system showed high sensitivity and could detect GLYP at limits as low as 5.92 μM with good stability and repeatability at 600 s and five cycling tests. Furthermore, estimating the high LOD of the plasmonic sensor compared with other reported works showed that the probe could be adapted for GLYP detection considering its fast and direct sensing mechanism with a simple preparation of GNBPs as a sensing material [101].

Another example of an organic/inorganic nanohybrid is luminol-gold-L-cysteine-Cu (II) nanoparticle composites (Lu-Au-Lcys-Cu (II)); these hybrids were previously reported as luminescent reagents using electrochemiluminescence (ECL). In this context, the luminescence intensity of the composites (Lu-Au-Lcys-Cu (II)) decreases with the GLYP concentration in the linear concentration range of 0.001–1.0 μM; the LOD could be as low as 0.5 nM [102]. The sensing principle behind this is the disruption of the copper interactions

with the nanoparticle (ON state) due to copper sequestration by GLYP, leaving the nanoparticle without copper ions (OFF state).

In addition, the AuNPs' surfaces have also been modified with carbon nanomaterials [103,104] to improve sensor potential. For instance, Tan et al. [105] functionalized an AuNP's surface with organometallic osmium carbonyl clusters [10Os]CO-Au NPs (Figure 5). By incubating these AuNPs conjugated with the enzyme acetylcholinesterase (AChE) and its substrate, the reaction product was adsorbed on the [10Os]CO-Au NPs, which induced their aggregation (Figure 5a). The thiocholine-induced aggregation of [10Os]CO-Au NPs caused a distinctive color change in the solution from red to purple and thus a variation in the intensity of the SERS signal. As GLYP inhibits AChE activity, its presence could be indirectly assessed by changes in the intensity of the SERS signal. As a result, the highly sensitive detection of GLYP of 5.92×10^{-7} µM was achieved [105].
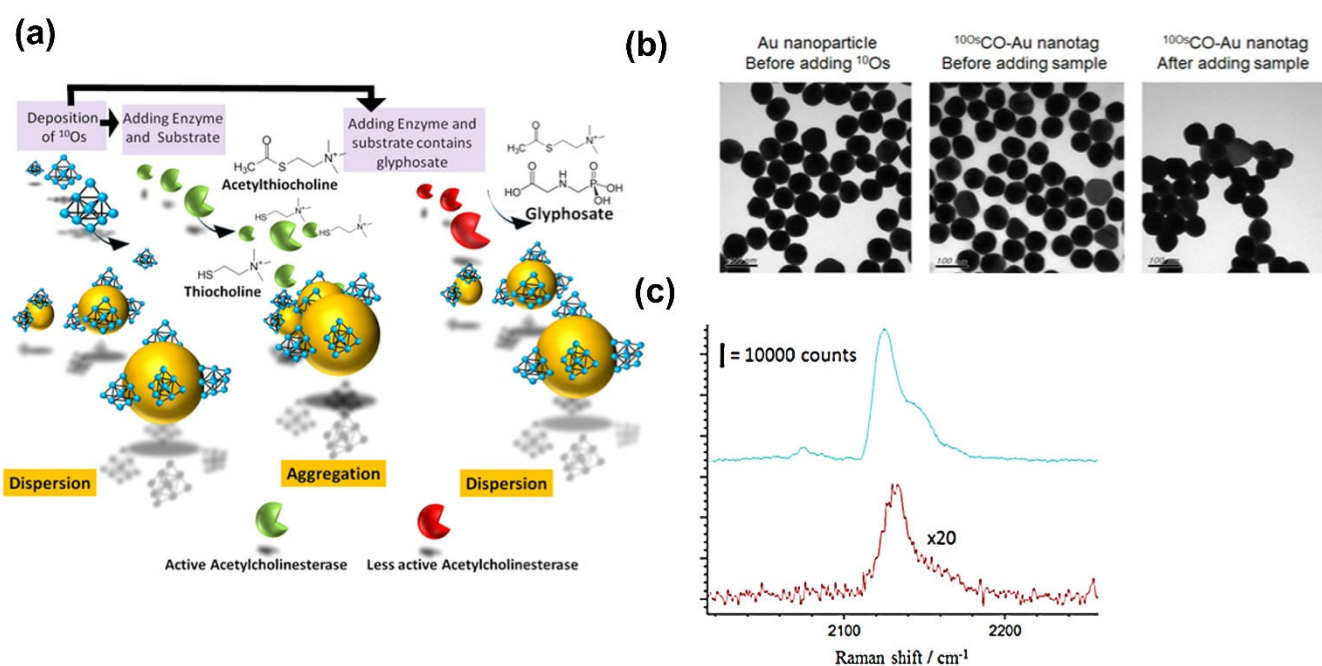

Figure 5. (**a**) Schematic representation of a GLYP sensor design strategy using [10Os]CO-Au NPs as SERS probe. (**b**) TEM images of Au nanoparticles, [10Os]CO-Au NPs and aggregated [10Os]CO-Au NPs and (**c**) SERS spectra of [10Os]CO-Au NPs scanned at 633 nm (top) and 532 nm (bottom). Reprinted/adapted with permission from [105]. Copyright 2017 Elsevier.

3.1.2. Other Metallic Nanoparticles

In addition to gold, NPs of other materials such as silver [106,107], copper [108], copper oxide[104], and silicon have been developed as sensors for GLYP. GLYP's ability to complex with copper has been exploited to create electrochemical [109–111], fluorescent [112,113], or dual-sensing systems (colorimetric and fluorometric) [114]. Conventional fluorescent materials are organic dyes, fluorescence proteins, C-dots, and quantum dots, which have photobleaching, autofluorescence, and high-energy excitation issues.

For example, Jiang et al. [115] modified an electrode with carbon paper; then, AuNPs were deposited on its surface. Finally, the electrode was modified with a copper porphyrin metal–organic framework (Figure 6). The final electrode presented excellent electrocatalytic activity towards copper oxidation due to the high conductivity provided by the AuNPs. In addition, the presence of the copper supplied a binding site for GLYP. In the presence of the herbicide, the peak current decreased proportionally to the GLYP concentration. The linear range was observed from 0.2 to 120 µM with a detection limit of 0.03 µM [115].
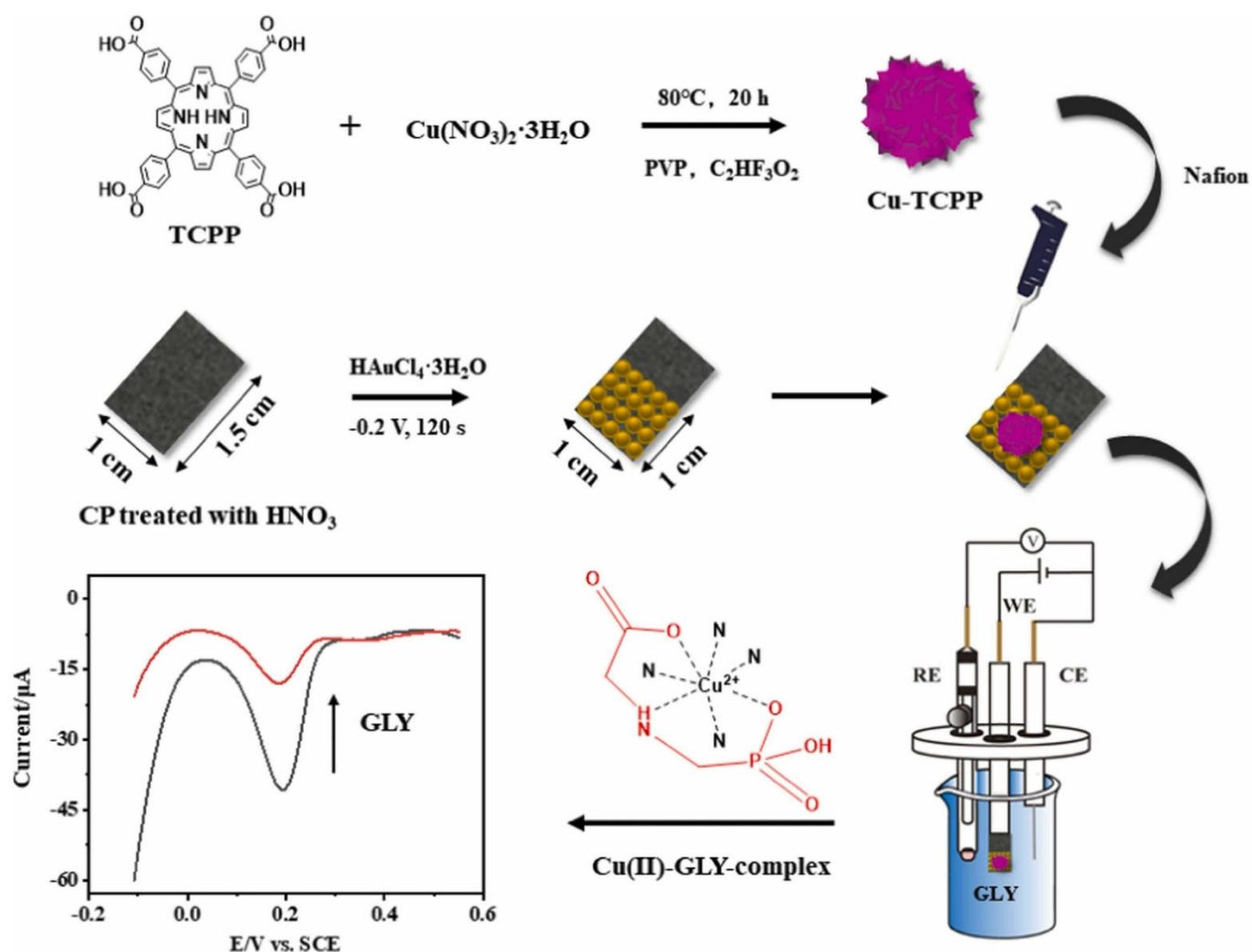
Figure 6. Scheme illustration of the fabrication of the Cu-TCPP/AuNPs/CP electrode and the electrochemical sensor for GLYP. Reprinted/adapted with permission from [115]. Copyright 2022 Elsevier.

On the other hand, silicon nanoparticles (SiNPs) possess a fluorescence intensity that can be quenched by 2,3 diaminophenazine (oxOPD). This chemical is produced by *o*-phenylenediamine's (OPD) oxidation by Cu^{2+}. In the presence of GLYP, the interaction between Cu^{2+} and GLYP decreases oxOPD production, resulting in fluorescence recovery at 446 nm. Furthermore, the addition of GLYP changed the yellow solution into a colorless state. The LOD reached with this strategy was 0.02 μM (Figure 7) [116].
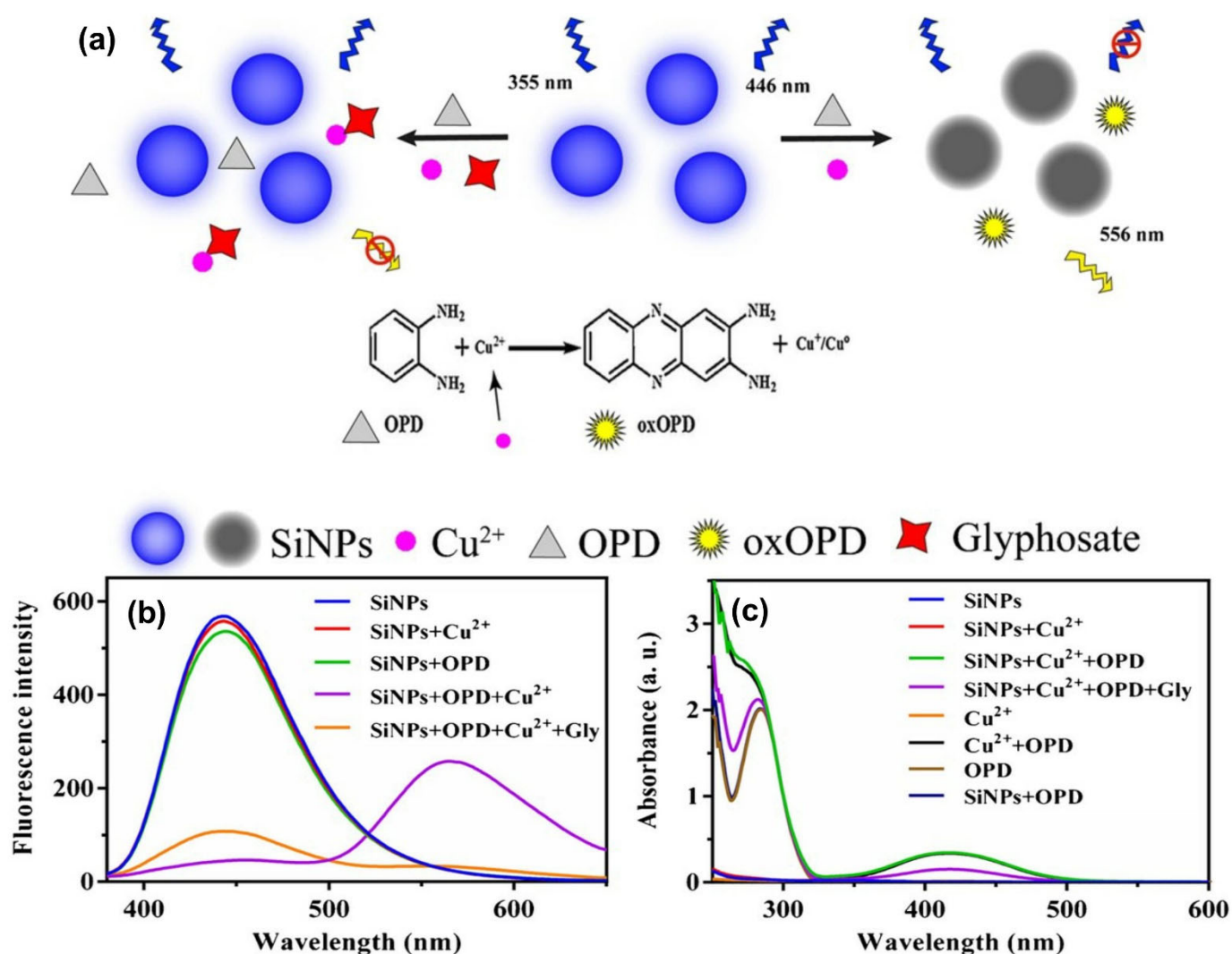
Figure 7. (**a**) Scheme of dual-signal sensing strategy based on ratiometric fluorescence and colorimetry for Cu^{2+} and glyphosate determination. (**b**) Fluorescence spectra of SiNPs, SiNPs + Cu^{2+}, SiNPs + OPD, SiNPs + OPD + Cu^{2+}, and SiNPs + OPD + Cu^{2+} +glyphosate. (**c**) UV–vis absorption spectra of SiNPs, SiNPs + Cu^{2+}, SiNPs + Cu^{2+} + OPD, SiNPs + Cu^{2+} + OPD + glyphosate, Cu^{2+}, Cu^{2+} + OPD, OPD, and SiNPs + OPD. Reprinted/adapted with permission from [116]. Copyright 2022 Springer.

Table 2. The 0D-nanomaterial metal-based nanoparticles as GLYP detection sensors.

System	Detection Method (Transducer)	Linear Range	Detection Limit	Reference
Lu-AuNPs-Lcys-Cu (II) composites	Electrochemical luminescence	0.001~1.0 μM	0.5 nM.	[102]
Organometallic osmium carbonyl clusters (10OsCO-AuNPs)	SERS	NR	5.9×10^{-7} μM	[105]
AgNPs based on inner filter effect	Fluorometric	0.15–15 μM	0.07 μM	[106]
AgNPs	UV-Vis extinction spectra SERS	0~30 μM	6 μM 7.5 μM	[107]
GC/rGO-CuNPs	(DPV) Electrochemical	0.1–1.1 μM	0.19 μM	[108]

Polyethylenimine-capped NaGdF4:Yb,Er upconversion nanoparticles (UCNPs), copper (II), hydrogen peroxide, and 3, 3′, 5, 5′-tetramethylbenzidine	Fluorometric Colorimetric	0.3–739 μM 30–739 μM	0.06 μM 5.91μM	[114]
Agarose-guar gum entrapped bio-nanoconjugate of urease with AuNPs	Potentiometric	2.96–296 μM	2.96 μM	[117]

Note: NR: Not reported.

3.1.3. Upconversion Nanoparticles (UCNPs)

UCNPs possess distinctive luminescent properties such as significant stokes shifts, high quantum yields, and a low photodegradation. A fluorescence turn-off–turn-on detection strategy was developed to detect GLYP using polyethyleneimine-capped NaGdF4:Yb,Er UCNPs (Figure 8). In the presence of Cu(II) ions, hydrogen peroxide, and 3,3′,5,5′ tetramethylbenzidine (TMB), the fluorescence of the UCNPs was quenched by the oxidation product of TMB as a result of the catalytic activity of Cu(II). The addition of GLYP to the reaction system led to the formation of a stable complex with Cu(II), N-(phosphonomethyl)glycine copper (II), which avoids the catalytic activity of the Cu (II) ions; then, the fluorescence of the UCNPs was less quenched in a concentration-dependent manner. The observed linear range was from 0.3–739 μM and the LOD was 0.058μM [114].
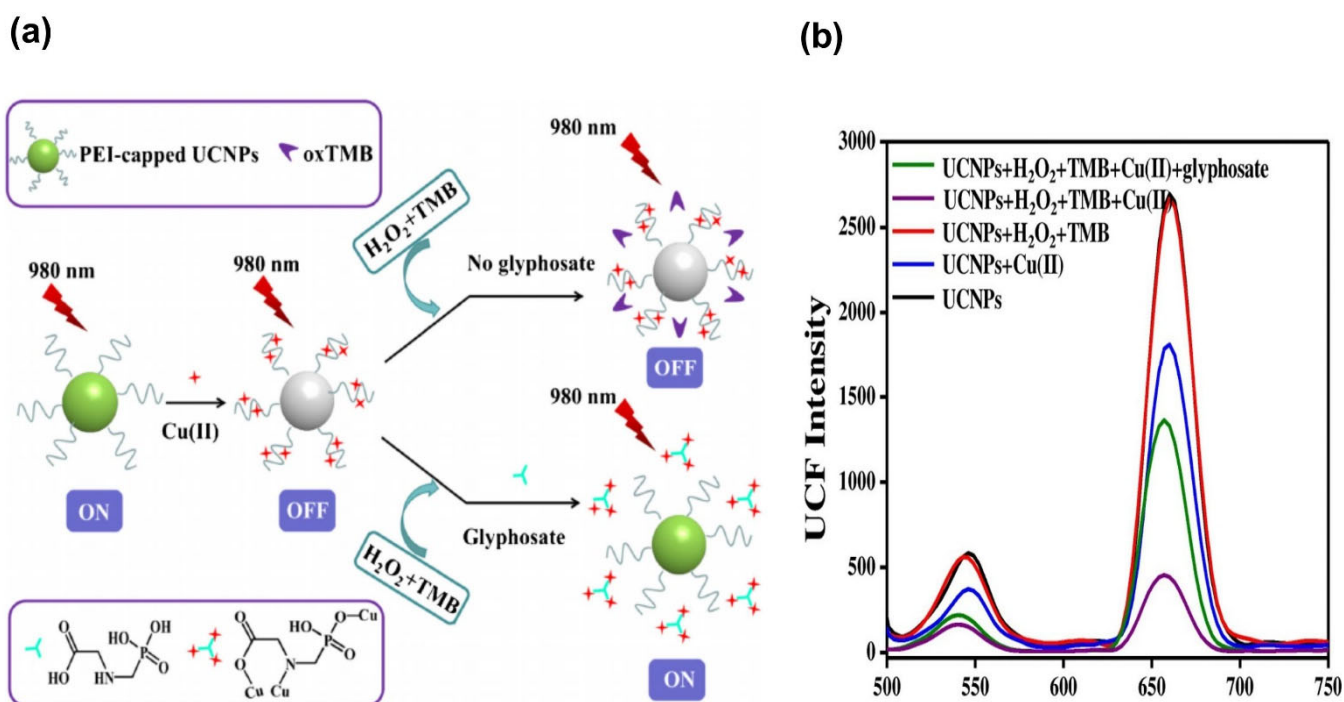

(a) **(b)**

Figure 8. (**a**) Schematic representation of UCNP-H_2O_2 -TMB-Cu (II) hybrid system for GLYP detection. (**b**) Fluorescence spectra of UCNPs (black line), UCNP-Cu(II) (blue line), UCNP-H_2O_2-TMB (red line), UCNP-H_2O_2-TMB-Cu(II) (purple line), UCNP-H_2O_2-TMB-Cu(II)-GLYP (green line). Reprinted with permission from [114]. Copyright 2019 Springer.

3.1.4. 0D Biosensors

In this section, some example (nano)sensor with biological molecules as recognition elements are described, including immunosensors [118,119], aptasensors [120–122], nanobodies [123], and nanozyme sensors [124–126], among others, as shown in (Figure 9).
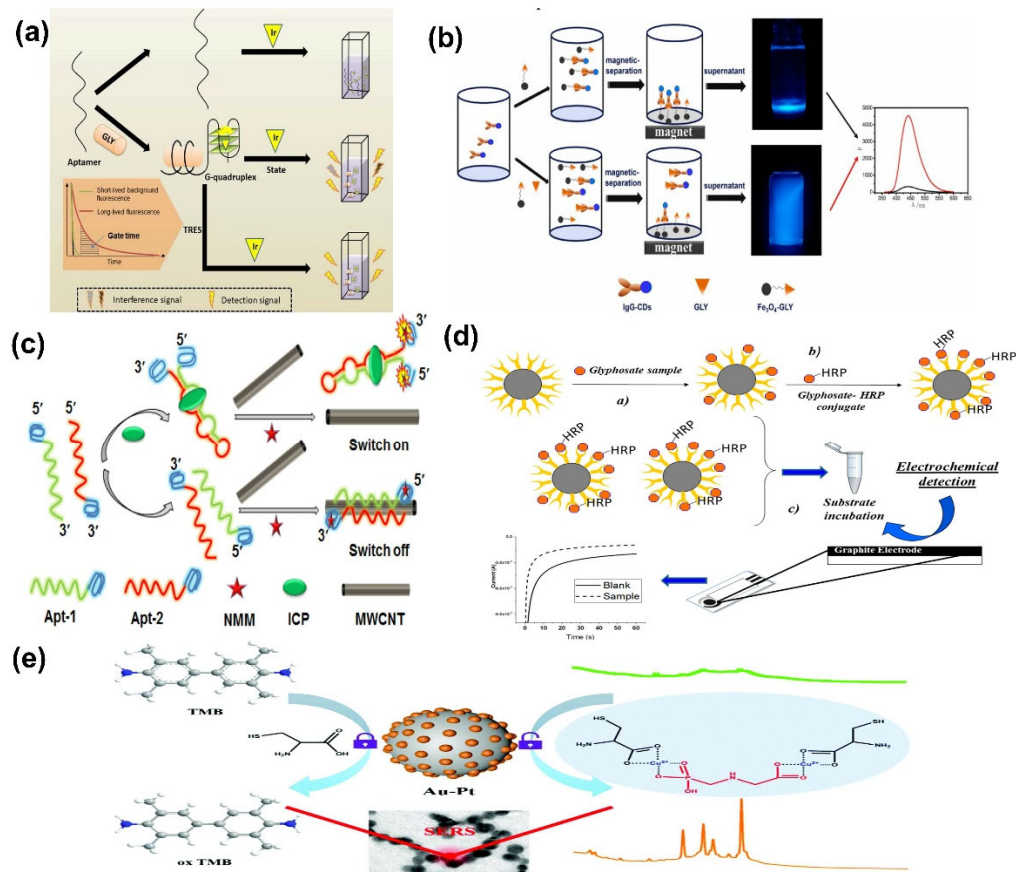

Figure 9. Schematic representation of the detection strategy by aptasensors, immunosensors, and nanozyme-based sensors and their assembled procedures used to develop pesticide sensors. (**a**) The scheme shows the aptamer-based sensing system's operation for GLYP employing G-quadruplex-selective iridium (III) complex in TRES mode. Adapted with permission from [122]. Copyright 2020 Elsevier. (**b**) Schematic representation of detection principle using carbon dots labeled antibody and antigen magnetic beads for GLYP detection. Adapted with permission from [127]. Copyright 2016 ACS Publications. (**c**) Schematic representation of the label-free and enzyme-free fluorescent isocarbophos (ICP) aptasensor using multiwalled carbon nanotubes (MWCNTs) and G-quadruplex as the signal transducers. Adapted with permission from [128]. Copyright 2018 Elsevier. (**d**) Scheme of the electrochemical immunoassay coupled with disposable screen-printed carbon electrode. Steps to develop paramagnetic beads modified with anti-GLYP antibodies and horseradish peroxidase (HRP) (a, b, and c). Adapted with permission from [129]. Copyright 2018 MPDI. (**e**) Schematic illustration of the sensing process of GLYP-based an Au–Pt nanozyme. Adapted with permission from [126]. Copyright 2021 Royal Society Chemistry.

0D Nanomaterials with Antibodies

Wang et al. [127] reported the detection of GLYP by fluorescence in a competitive mode immunoassay using carbon dots coupled to GLYP antibodies (IgG-CDs). The as-prepared IgG-CDs could specifically identify glyphosate from Fe_3O_4-GLYP or free GLYP as an environmental analyte through a competitive immune reaction. Subsequently, the magnetic antigen beads were separated from the solution by a magnetic field, and thus the freed GLYP attached to IgG-CDs could be determined. As a result, the linear range between the fluorescence intensity of lgG-CDs and glyphosate GLYP concentration was 0.06–473.18 μM, with a detection LOD of 0.05μM (Figure 10) [127].
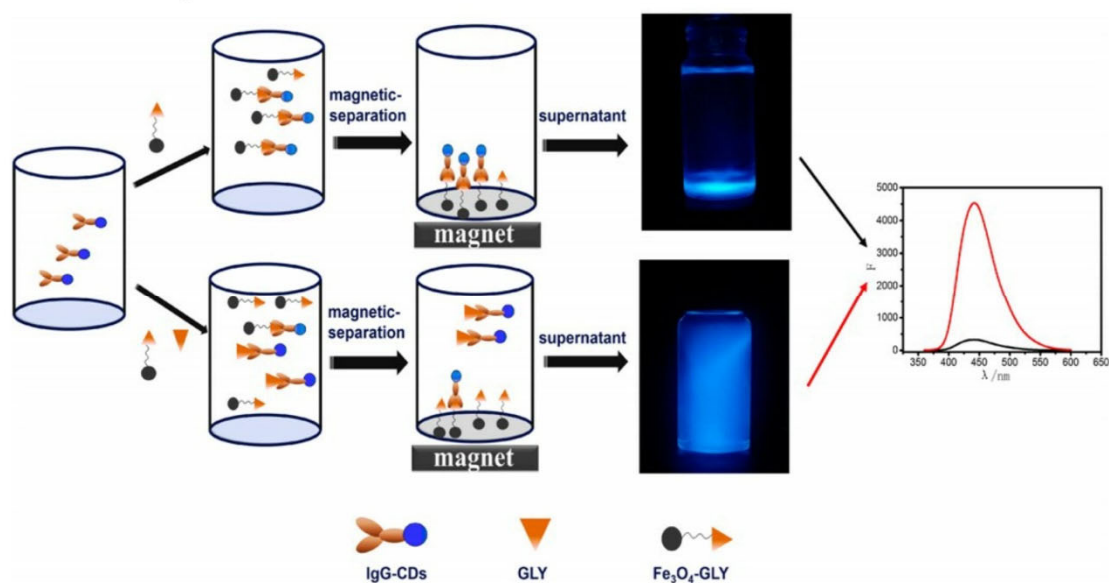
Figure 10. Strategy detection for GLYP using carbon dots coupled to glyphosate antibodies (IgG-CDs and Fe₃O₄-GLYP. Reprinted with permission from [127]. Copyright 2016 ACS Publications.

Another novel strategy reported applies the coupling of an immuno-magnetic assay with electrochemical sensors, which was developed using commercially available magnetic beads modified with an anti-glyphosate antibody and an HRP conjugated with GLYP. The competition was then performed by incubating the corresponding HRP-conjugated GLYP and free GLYP towards the magnetic nanoparticles. The oxidation of 3,3′,5,5′-tetramethylbenzidine (TMB) substrate by the enzyme generates an electroactive product (TMBox), which can be reduced at the electrode as the sensor response. In this way, the response was inversely proportional to GLYP concentration, reaching an LOD of 2.96×10^{-5} μM and an LOQ of 1.77×10^{-4} μM (Figure 11) [129].
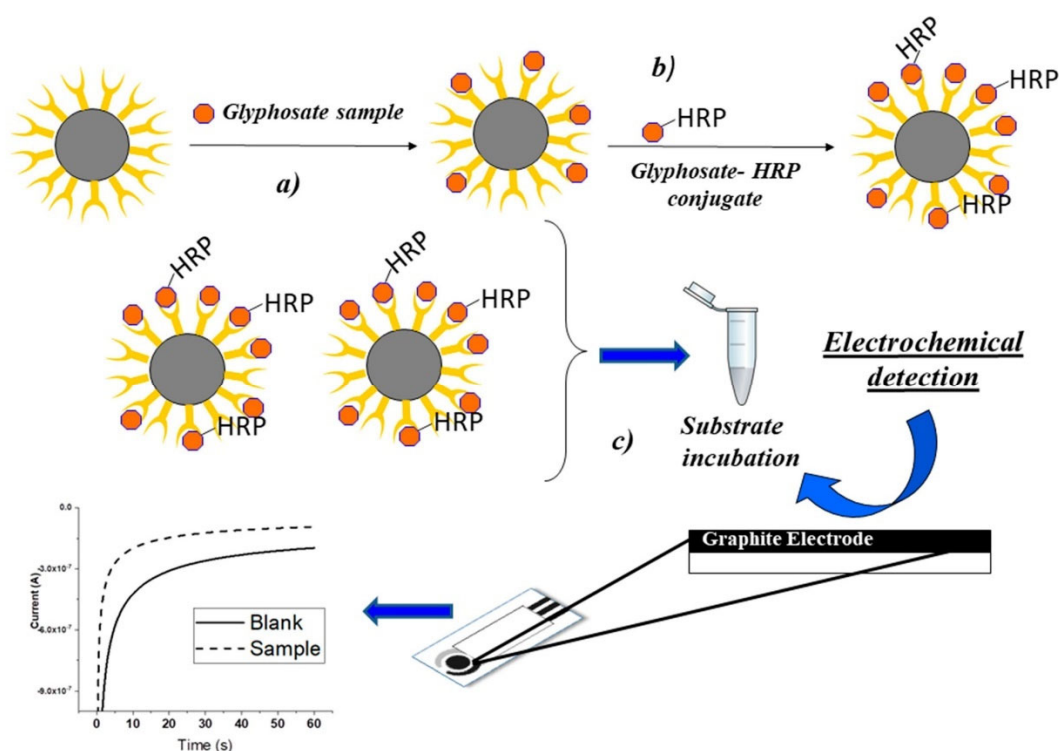
Figure 11. Electrochemical immunoassay coupled with disposable screen-printed carbon electrode: (**a**) Paramagnetic beads modified with anti-glyphosate antibodies were incubated with samples; (**b**) a solution containing horseradish peroxidase (HRP) conjugate was added; (**c**) after several washing steps, the particles were magnetically blocked, and the substrate was added. The enzymatic product was measured by chronoamperometry[129]. Free use. Copyright 2018 MDPI.

Guan et al. [130] modified gold nanoparticles with short oligonucleotide sequences and anti-GLYP antibodies; the analytical response was based on PCR amplification. The detection principle consisted of a competition assay between the immobilized GLYP derivative in the PCR tubes and the soluble GLYP from the mixture. Depending on its interaction with the GLYP species, the probe was immobilized on the tube or was soluble in bulk. The supernatant was discarded, and signal DNA (complementary to the immobilized oligo) was released and subjected to real-time PCR. This way, the amount of GLYP present was directly proportional to the Ct value (Ct, the cycle at which the response signal is higher than the noise signal) because less signal DNA was present. Then, more cycles were necessary (Figure 12) [130]. A great deal of signal DNA per antibody present in the probe, together with PCR amplification, provided a high sensitivity to the method, and an LOD of 0.052 nM was achieved.
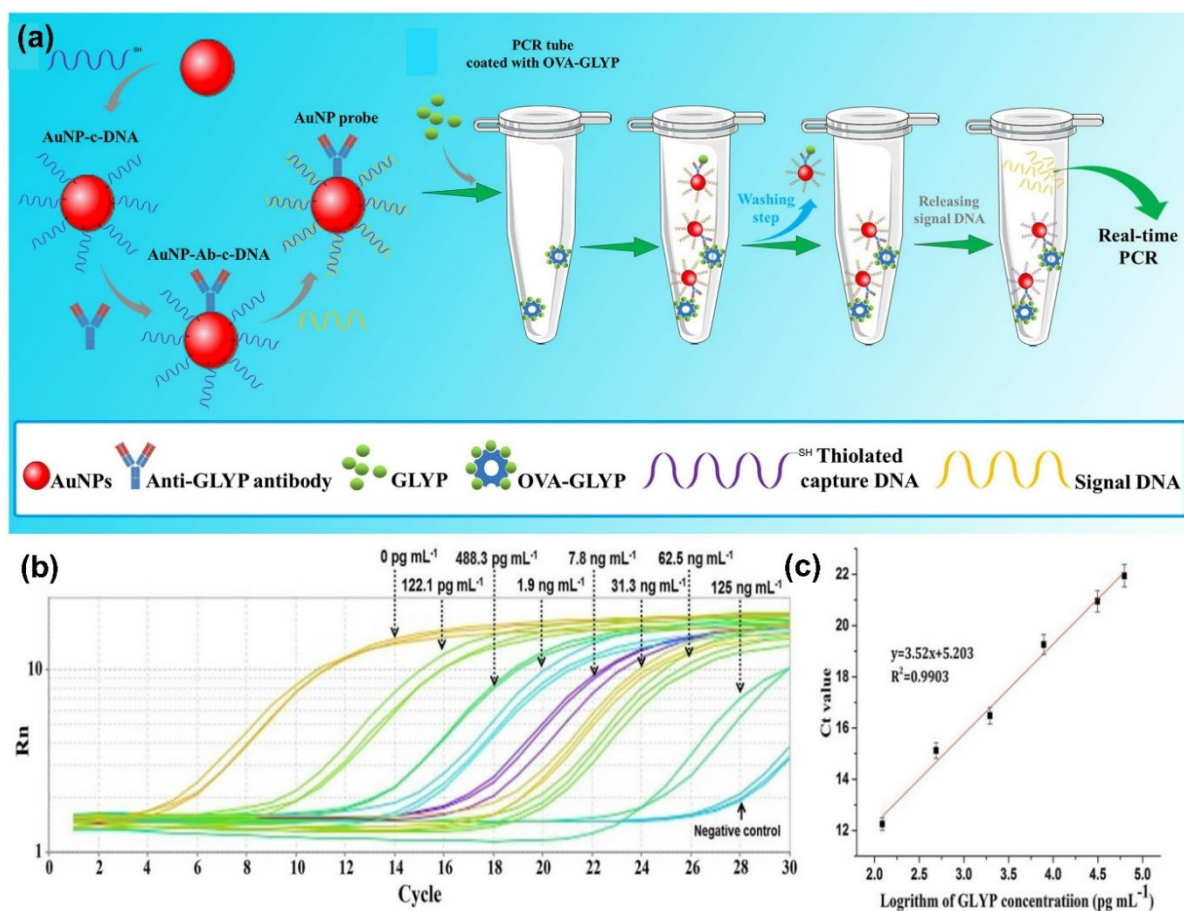
Figure 12. Schematic illustration of the AuNP-BB-iPCR. (**a**) Synthesis procedure of the AuNP probe. (**b**) Amplification curves of real-time PCR for the standard curve of Ct value against concentrations of signal DNA (from 1 fM to 0.01 μM). Water was used instead of signal DNA for negative control. (**c**) The standard curve of Ct values against logarithm concentrations of signal DNA. Reprinted with permission from [130]. Copyright 2021 Elsevier.

0D Nanomaterials with Aptamers

On the other hand, aptamers are also promising biological recognition elements that can identify various pesticides [131–139]. DNA-aptamers are synthetic single-stranded oligonucleotides selected to bind to target contaminants with favorable selectivity and sensitivity. The reported studies on aptamers and aptasensors have shown these devices to be quite promising regarding their ability to sense targets in a wide range of matrices with minimal sample pretreatment.

Jian et al. [140] developed a nanosensor using a 6-carboxy-fluorescein-labeled aptamer as the recognition probe and DNA-functionalized magnetic nanoparticles as the separation carrier. The aptamer was conjugated on the surface of the magnetic nanoparticles to form a magnetic aptamer–complementary DNA complex. Upon the introduction of GLYP, the aptamer was separated from the complementary DNA and was extracted by applying a magnetic field; then, the supernatant's fluorescence signal was measured. The sensors reached an LOD of 0.52 nM. This method produces results similar to those obtained using gas chromatography, and the relative standard deviations were also acceptable. If the aptamer can recognize other pesticides, the technique could provide a means for detecting multiple organophosphorus pesticides [140].

0D Nanomaterials with Enzymes

The conjugation of AuNPs with the enzyme urease enhanced the GLYP determination due to the synergistic effect of these two components. The catalytic reaction of urease was inhibited in a concentration-dependent manner by the presence of GLYP; the conjugation of the enzyme with the AuNPs improved the sensor's potentiometric response. This system showed a linear response in the concentration range 2.96 μM–296 μM, with an LOD of 2.96 μM, which covers the maximum residual limit set by the WHO for drinking water. In addition, other pesticides were not interferent [117]. However, the enzyme denaturation process results in the instability and short lifetime of the biosensor, which mostly limits the operational applications [141].

Moreover, the enzymes can be affected by different contaminants in environmental samples, such as heavy metals, resulting in a lack of selectivity in the direct determination of pesticides and leading to false-positive results. Therefore, nanozyme electrodes for electrochemical sensing have recently been recommended [142,143]. Nanozymes are a type of nanomaterial with enzyme-like characteristics that can be used as an alternative to natural enzymes, mimicking biological enzyme activity and overcoming the drawbacks of natural enzymes. Due to their excellent operational stability, high catalytic activity, and simple preparation, nanozymes have been widely used to establish rapid detection methods [125,144–146].

For instance, Luo et al. [147] developed a colorimetric sensor of porous Co_3O_4 nanoplates immobilized on a polyester fiber membrane. As GLYP could specifically inhibit the peroxidase-mimicking catalytic activity of Co_3O_4 nanostructures, its presence can be determined by the color change intensity in the catalytic reaction. The prepared nanozyme sheet showed an LOD of 0.175 mg/kg for GLYP, which enabled its detection by the naked eye. The assays time was 10 min, and the color spots were maintained for more than 20 min (Figure 13) [147].
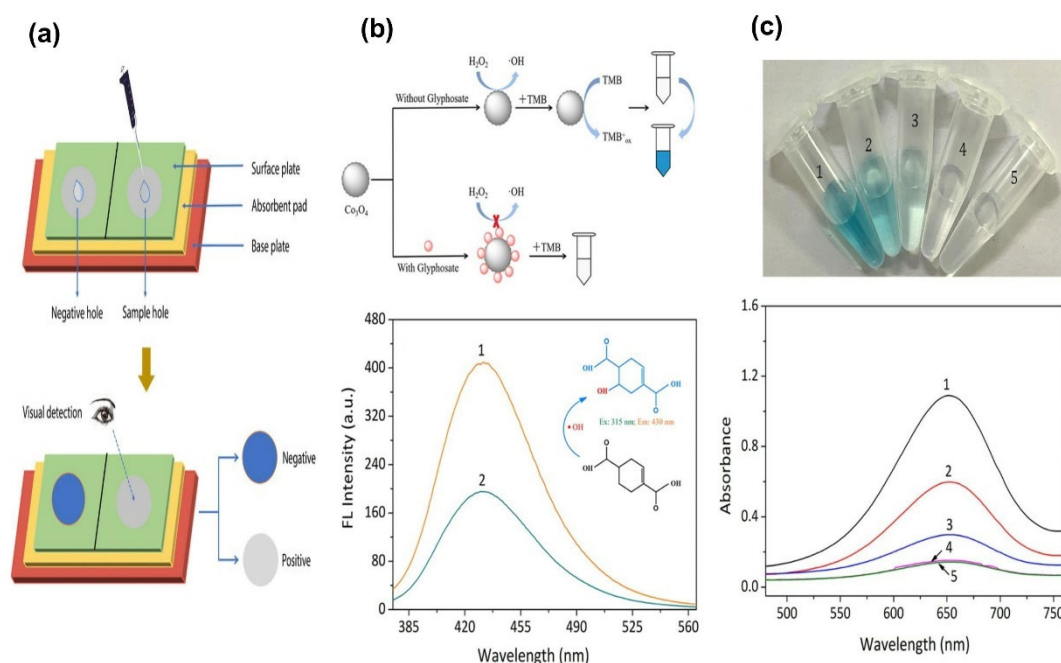
Figure 13. Detection of GLYP by Co_3O_4 nanoplates on a polyester membrane. (**a**) Representation of the inhibitory effect of GLYP on the peroxidase activity of nanoplates; (**b**) Fluorescence spectra in solution of the TMB reaction product in the presence and absence of GLYP; (**c**) Colorimetric signal changes of colorimetric nanozyme sheets without (sample 1) and with GLYP (sample 2); sample 3 and 4 are control assays without nanozyme. Reprinted with permission from [147]. Copyright 2021 ACS Publications.

In another example, an indirect SERS sensing assay was applied to determine the amount of GLYP in tap water. The detection mechanism was based on quantifying the TMB oxidation by an Au–Pt nanozyme. This oxidation was inhibited by L-cysteine (L-Cys). However, the inhibitory effect of L-Cys was avoided when GLYP and Cu ions were added, which allowed for the reaction to occur. Therefore, TMB oxidation (TMBox) depends on the amount of GLYP present. In addition, the detection was possible because chain-shaped gold and silver nanoparticles were used as a SERS substrate, which enhanced the Raman signal of the oxidized TMB and induced the SERS response of the reduced TMB. As a result, the SERS signal intensity of the TMBox (at 1605 cm^{-1}) was proportional to the concentration of GLYP over the concentration ranges of 0.059 μM to 5.9 μM. The LOD and LOQ of GLYP were 0.03 μM and 0.059 μM, respectively (Figure 14) [126].
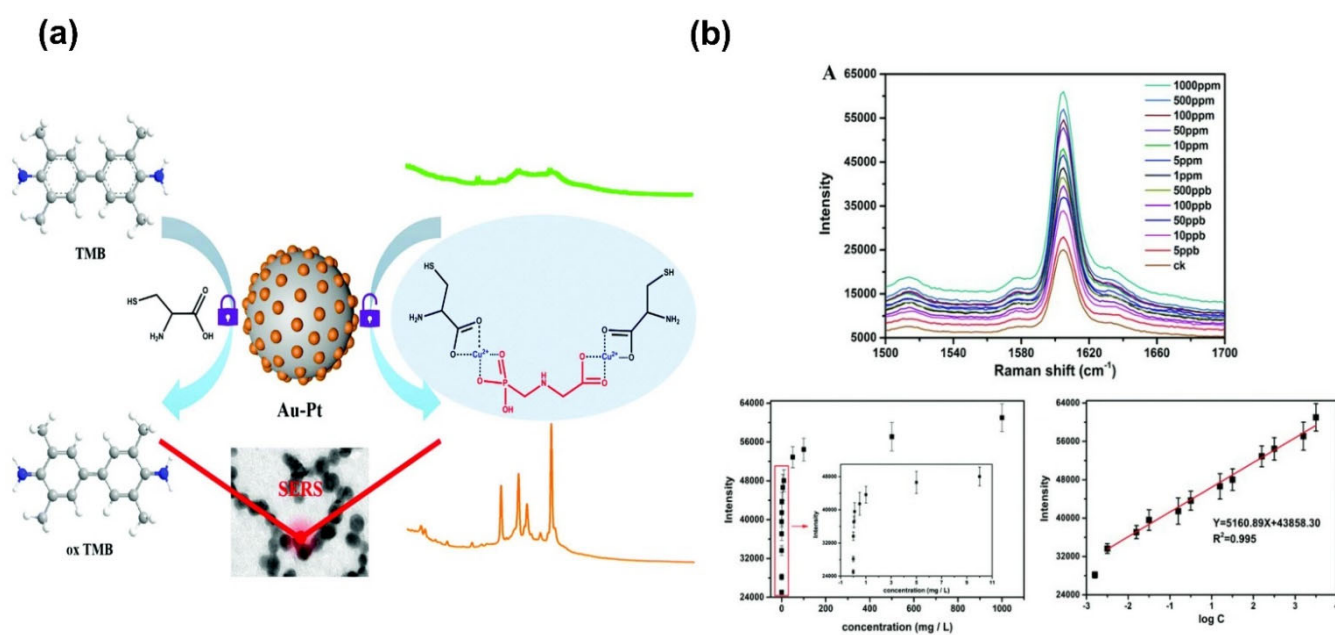
Figure 14. (**a**) Schematic illustration of the sensing process of glyphosate, (**b**) SERS spectra and reference plot of SERS intensities of a Raman shift at 1605 cm^{-1} vs. GLYP concentrations, and linear plot of SERS intensities of a Raman shift at 1605 cm^{-1} vs. logarithm of GLYP concentrations. Reprinted with permission from [126]. Copyright 2021 Royal Society Chemistry.

0D Nanomaterials with Other Biological Elements

DNA-templated AgNCs (DNA-AgNCs), produced using an oligonucleotide as a stabilizing agent, showed interesting spectral and photophysical properties. A GLYP detection application was developed based on a Cu^{2+}-modulated DNA-templated silver nanocluster (DNA-AgNCs) sensor, operating via the turn-on fluorescence strategy. The fluorescence quenching of the DNA AgNCs occurred through the presence of Cu^{2+}. Upon the presence of GLYP, the functional groups on the surface of glyphosate could chelate with Cu^{2+}, following the fluorescence recovery of DNA-AgNCs. In this system, the carboxylate, amine, and phosphonate groups of GLYP interacted with Cu^{2+} through chelation. This fluorescence sensor showed the linearity of the GLYP analysis ranging from 0.09 to 0.6 μM with a detection as low as 0.03 μM [148].

Finally, Li et al. [149] reported the use of bovine serum albumin-stabilized gold nanoclusters (BSA-AuNCs) as a conjugate for a GLYP assessment. In the BSA-AuNCs conjugate, the enzyme quenched the fluorescence signal of the AuNPs; this fluorescence attenuation was eliminated by adding a second enzyme, trypsin, which hydrolyzes BSA, thus releasing the AuNPs, and as a result, fluorescence was observed. Since GLYP

irreversibly inhibits trypsin, the herbicide can be quantified indirectly by inhibiting trypsin, monitored by the fluorescence quenching efficiency. The linear range extended from 5.9×10^{-4}–29.57 µM, and the LOD reached 2.2×10^{-4} µM [149].

3.1.5. Carbon Dots (CDs)

CDs are among the most representative 0D carbon nanomaterials. CDs as fluorescent carbon-based materials (Figure 15) possess at least one dimension less than 10 nm in size with tunable physical, chemical, electronic, thermal, mechanical, and optical properties. Sok and Fragoso [150] employed carbon nano-onions (CNOs) to improve the sensitivity of a method based on tyrosinase's (Tyr) inhibition by GLYP. CNOs are hollow spherical nanoparticles formed by concentric graphene layers with increasing diameters. In the aforementioned work, the CNOs-Tyr conjugate was immobilized on chitosan (Chi) on a screen-printed electrode. As the analytical response, the amperometric signal was monitored during the transformation of L-DOPA by the enzyme. The inhibition of tyrosinase was improved when the enzyme was conjugated with CNOs. The LOD reported was 6.5 nM. In the absence of the CNOS, the LOD was 12 nM [150].
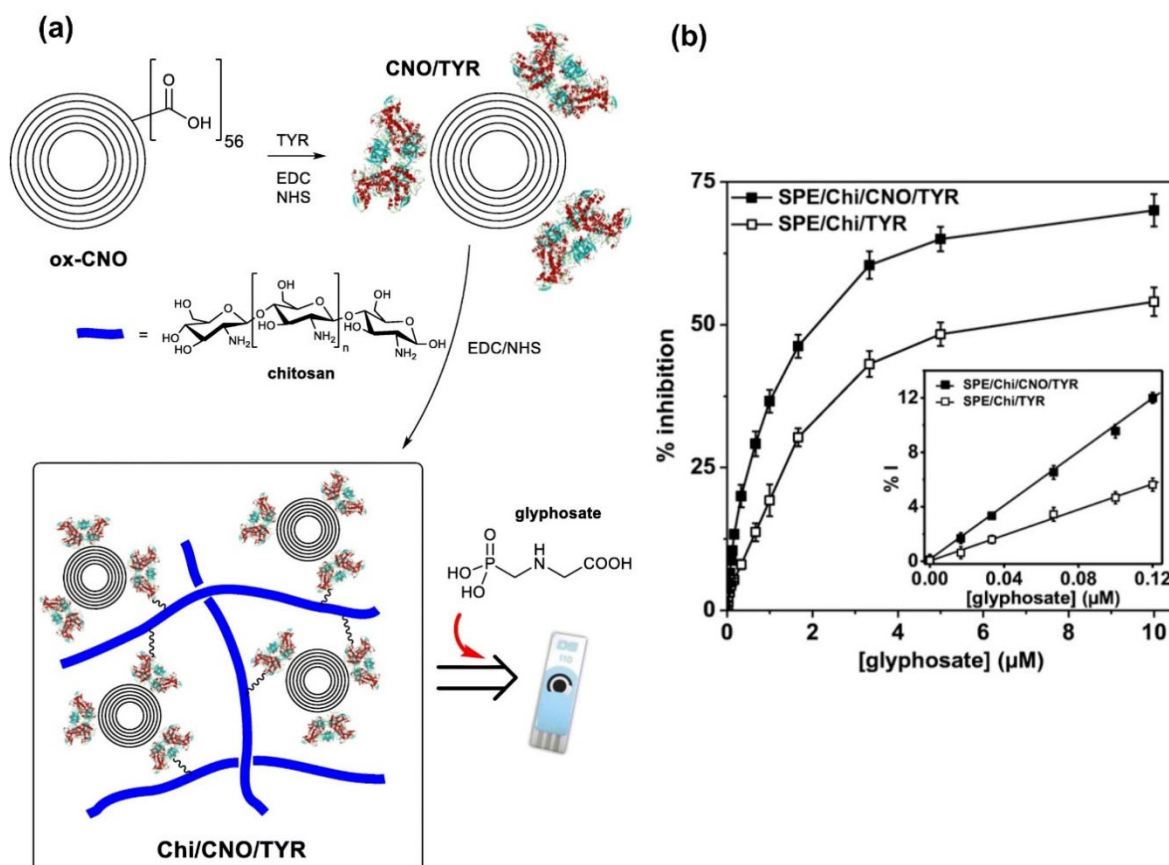
Figure 15. (**a**) Schematic representation of the preparation of SPE /Chi/ CNOs/TYR electrodes to develop a GLYP sensor. (**b**) Calibration plots for SPE/Chi/CNO/TYR and SPE/Chi/TYR at different glyphosate concentrations. Reprinted with permission from [150]. Copyright 2019 Springer.

3.1.6. Quantum Dots (QDs)

QDs are inorganic fluorescent semiconductor nanoparticles (Figure 16a) with a size range of 2–10 nm [151] and particular optical and electronic properties, representing a remarkable difference compared to larger-sized nanoparticles. Their high surface area can hold more functional groups compared to organic compounds. QDs are called 'artificial

atoms' since they behave similarly to single atoms with discrete electronic states [152]. These nanoparticles have an expanding use due to their broad absorption band (several hundreds of nm), a narrow emission band (below 40 nm), high quantum yield (up to 95%), and their chance of exhibiting an emission band tuning beyond a wide range of wavelengths (350–2000 nm). In addition, QDs present particular optical properties: (i) The fluorescence emission of QDs can be adapted by managing their chemical composition, particle size, and shape [153]; (ii) QDs have a broad absorption spectrum and symmetrical fluorescence emission spectrum (Figure 16b), with only 25−40 nm of half-width. Moreover, they can emit multicolor fluorescence when they are excited at the same wavelength [154]. Therefore, QDs can be used in multichannel analyses, ideal for the multiplex detection of several different analytes in environmental applications [155]. These characteristics make them excellent optical transducers [154,156].

Only few reports discussing the use of metal oxide quantum dots to construct sensors for pesticides have been published. However, Sahoo et al. [155] proved the effectiveness of the exciton quenching of QD in the presence of GLYP and other pesticides by steady-state, time-resolved fluorescence spectroscopy and electrochemical methods. The authors synthesized fluorescent ZnO nanoparticles and functionalized them with APTES (3-aminopropyltrimethoxy silane). The fluorescence of the nanoparticles was attenuated by the presence of different concentrations of GLYP. Although the authors did not report the LOD, the research showed that concentrations of GLYP on the order of ppm affected the fluorescence intensity (Figure 16). According to the authors, the fluorescence quenching seems to be explained by the ionic interaction between the carboxylic groups from GLYP and the amino groups from APTES [155].
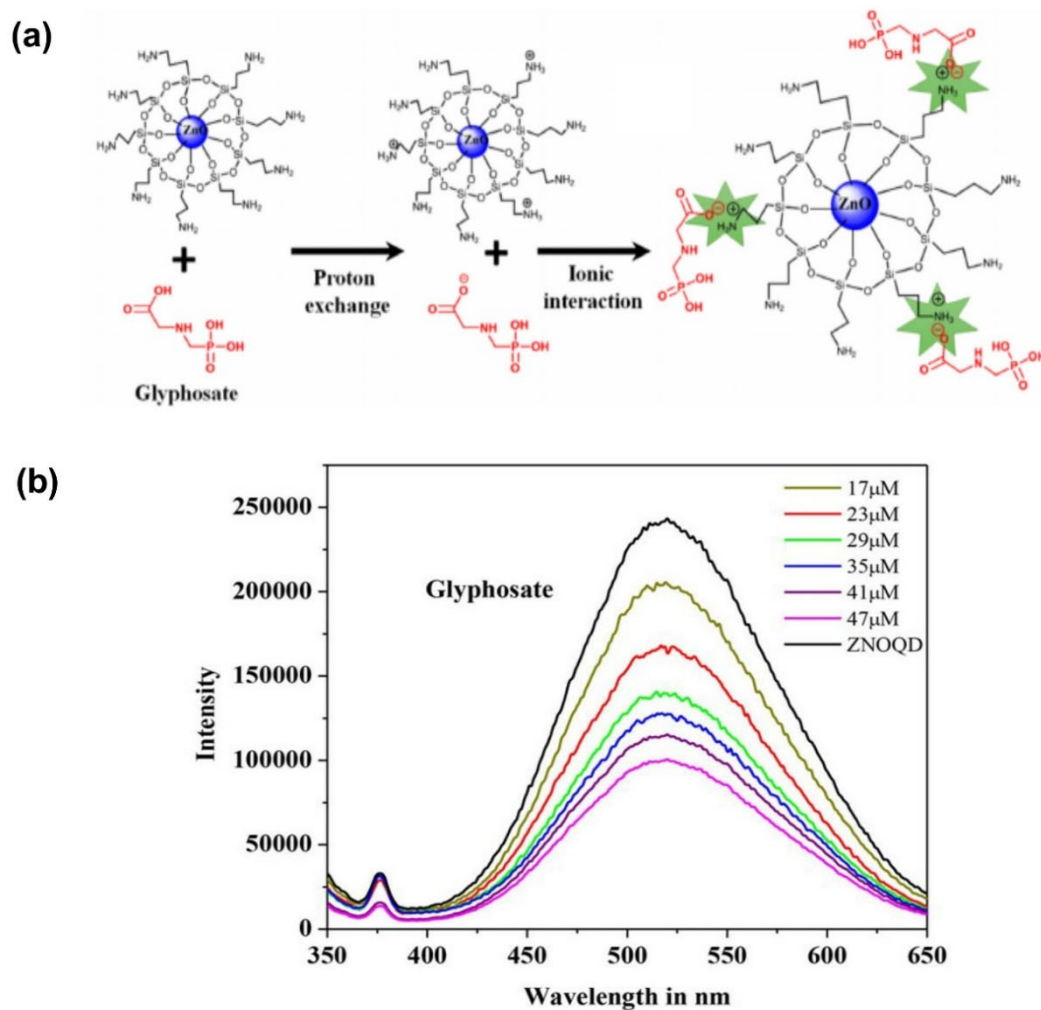
Figure 16. (**a**) Schematic Representation of Interaction of QD with Glyphosate, (**b**) Emission spectra (λex = 340 nm) of ZnO QD (5×10^{-5} M) in the presence of different GLYP concentrations. Reprinted with permission from [155]. Copyright 2018 ACS Publications.

Bera & Mohapatra [157] reported an LOD for GLYP of 2 pM (Figure 17) by applying a CdTe-carbon quantum dot (CQD)-integrated probe. Electrostatic bonding with the CQDs inhibited the photo electron transfer (PET) fluorescence of CdTe. The addition of GLYP disrupted the interaction between the quantum particles by forming a complex with the CQDs (Figure 17), significantly increasing the emission intensity at 632 nm. As a result, a remarkably sensible response was achieved, even at picomolar concentrations [157].
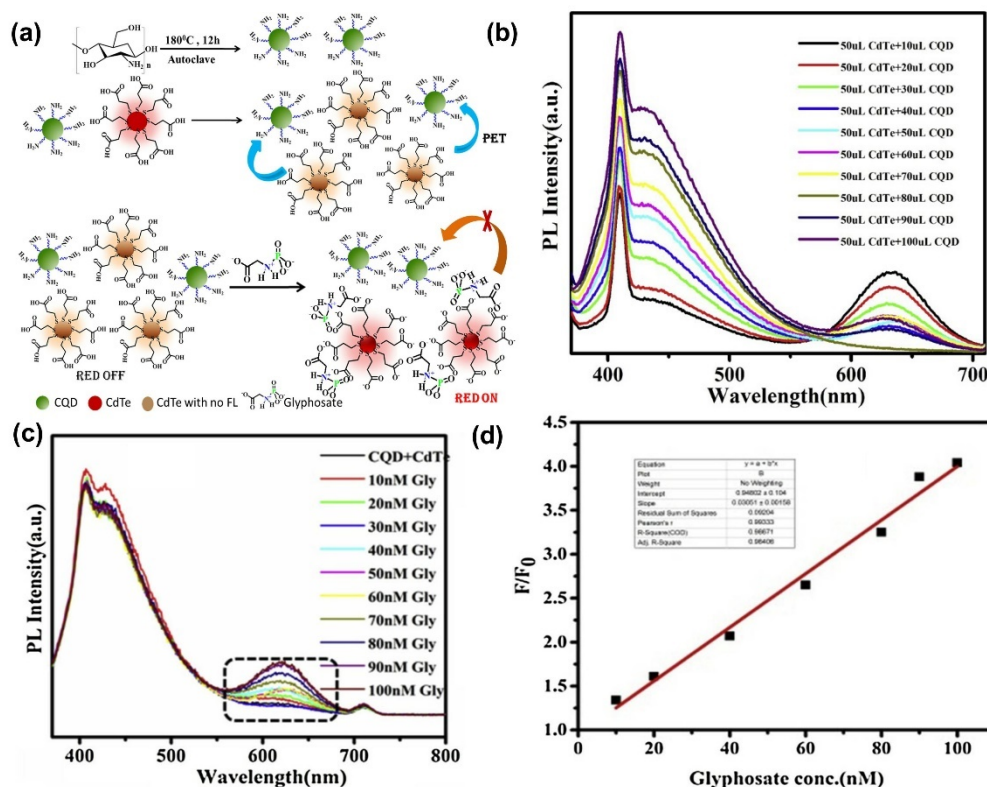
Figure 17. (**a**) The sensing mechanism of CdTe-CQD sensor towards GLYP, (**b**) Fluorescence decreasing of CdTe due to increasing concentration of CQD solution (**c**) Fluorescence response of CdTe CQD solution, (**d**) Linear range. Reprinted with permission from [157]. Copyright 2020 Elsevier.

3.2. 1D Nanomaterials

1D nanostructures are materials with one dimension not on the nanoscale while the other two dimensions are on the nanoscale. The varieties of 1D nanostructures include metallic, polymeric, ceramic, nanotube (NTs), nanorod filament or fiber, nanowires (NWs), and nanofibers, which are attractive materials because of their large surface-to-volume ratio. Their ultrasmall size makes them suitable for nanodevices.

3.2.1. Carbon Nanotubes (CNTs)

Carbon nanotubes and porous carbon are the most common carbon materials used in sensors to detect contaminant materials in water [158] (Table 3). Integrating various nanomaterials is a viable strategy to obtain a lower LOD for GLYP [159]. For example, a nanocomposite of CuO NPs and multi-walled carbon nanotubes (CuO/MWCNTs) exhibited high peroxidase-like catalytic activity. GLYP could inhibit the catalytic activity of the nanocomposite when added to the system, which diminishes the fluorescence intensity. In this way, GLYP was assessed indirectly by measuring the degree of inhibition of the nanosystem. A detection limit of 3.96×10^{-3} µM was reached with a linear range from 0.012 to 0.059 µM (Figure 18) [112].
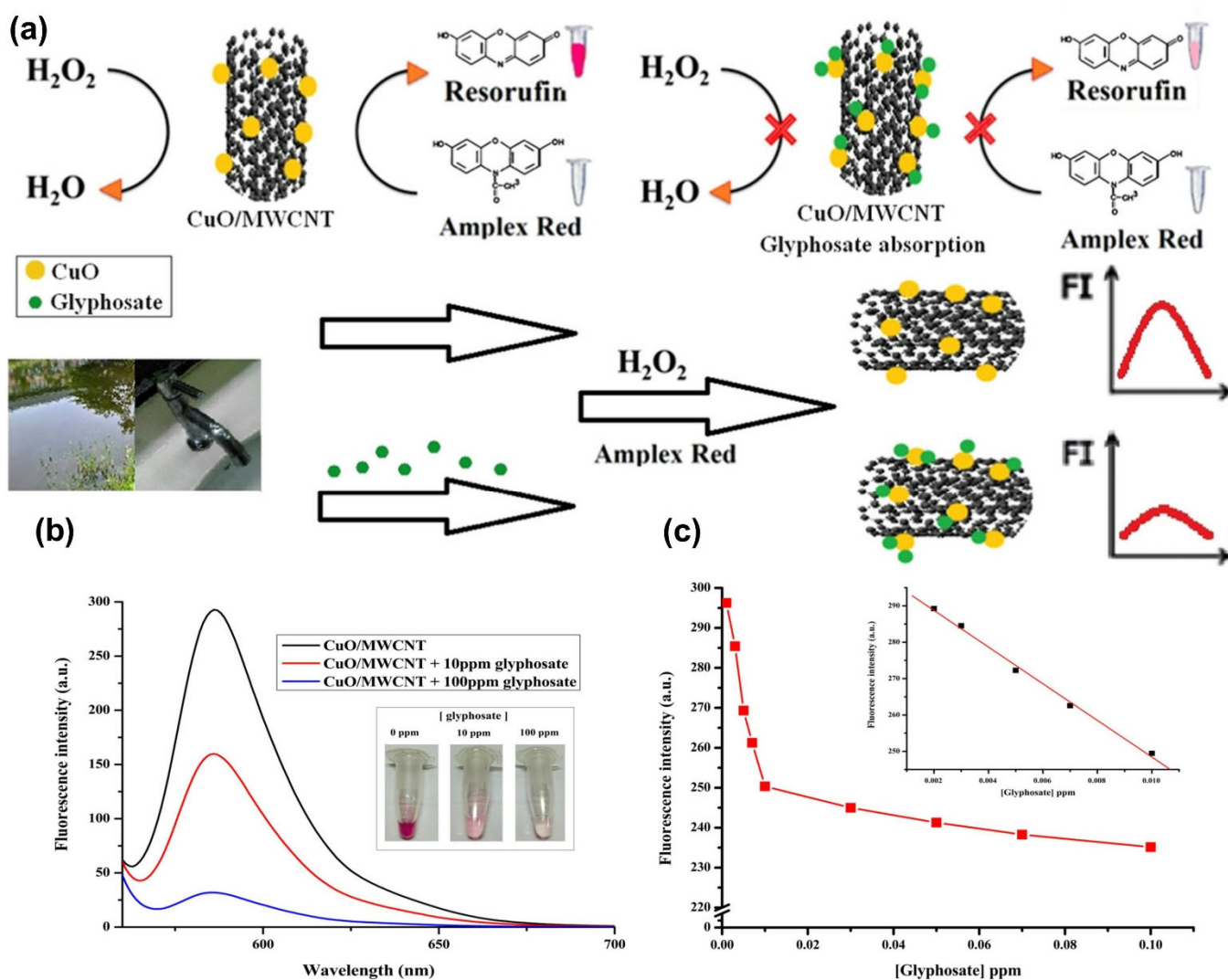
Figure 18. (**a**) Schematic illustration of fluorescence detection based on the inhibition of CuOox/MWCNTs catalytic activity by GLYP. (**b**) Fluorescence spectra of resorufin as a reaction product in the absence and presence at different concentrations of GLYP. (**c**) Fluorescence intensity of resorufin as reaction product at increasing concentration of GLYP. The inset figure presents the linear range. Reprinted with permission from [112]. Copyright 2016 Elsevier.

Gholivand et al. [160] modified a pencil graphite electrode with hollow fiber (HF), which was covered with a multi-walled carbon nanotube (MWCNT)-ionic liquid (IL) composite, and copper oxide nanoparticles (CuO). According to the authors, the combination of the ionic liquids and copper nanoparticles provides a suitable preconcentration and sensitive determination system. Additionally, the further modification of HF with suitable metal oxide nanoparticles such as copper oxide promotes the conductivity of the electrode-coating film. The linear range reported between the current peak and the herbicide concentration was linear over 5 nM to 1.1 μM, with an LOD of 1.3 nM. However, this study showed that the sensor was not highly selective in detecting GLYP in compounds with similar structures or other herbicides, fungicides, pesticides, and insecticides (Figure 19) [160].

Figure 19. (**a**) Schematic illustration of the extraction and in-situ electrochemical detection of GLYP (**b**) Differential pulse voltammetry for GLYP, 0.1 M PBS (pH 7), (**c**) Linear dependence of peak currents on GLYP concentrations as a calibration curve. Reprinted with permission from [160]. Copyright 2018 Elsevier.

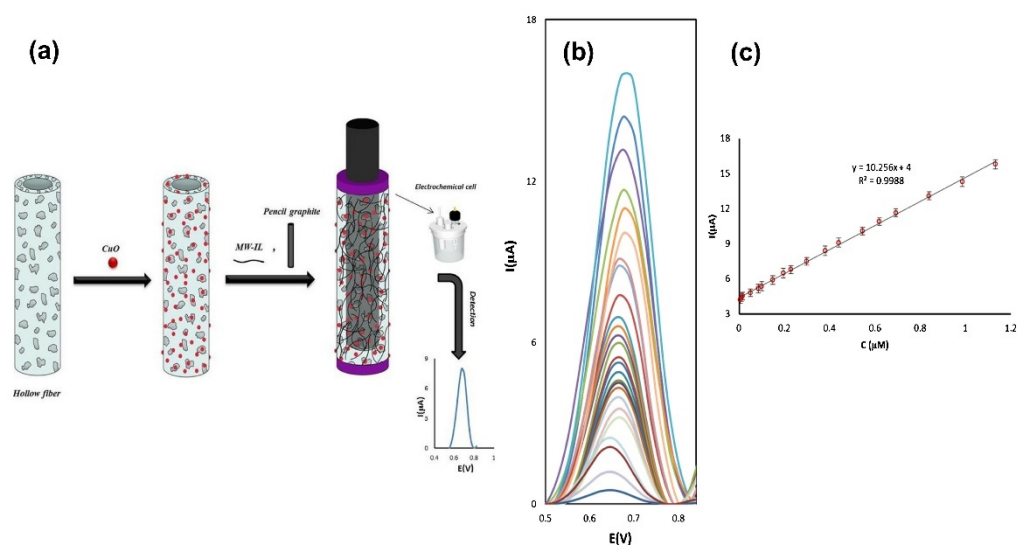Screen-printed electrodes (SPEs) have also emerged as an alternative to the rapid in situ analyses that cannot be done with traditional electrodes [161]. For example, a spectroelectrochemical method for identifying GLYP and AMPA was reported by Habekost et al. [162] based on the compound tris(2,2′-bipyridyl)ruthenium(II) [Ru(bpy)$_3$]$^{2+}$. The main feature of such a spectroelectrochemical approach is its use of screen-printed electrodes (SPE) made from either gold or multi-walled carbon nanotubes (MWCNTs), decorated with nano ZnO, which significantly enhances the ECL signal. As a result, the authors reported an LOD lower than 1 μM [162].

3.2.2. Nanofibers (NFs)

One-dimensional nanofibers have small diameters and are highly porous with good pore interconnectivity, making them materials with a specific surface area. Together with their polymer functionalities, these unique characteristics give nanofibers desirable properties for advanced applications in pesticide sensing. The manufacturing methods of nanofibers include template self-assembly, phase separation, melt-blowing, and electrospinning [163,164]. A susceptible and selective nanofiber-based sensor requires functionalization strategies such as assembling sensing elements and specific binding sites to GLYP. De Almeida et al. [165] proposed a method involving the derivatization of GLYP to a dithiocarbamic acid intermediate, followed by sample application onto Cu-PVA nanofiber sensor strips. A color change in the presence of the GLYP derivative was observed in the nanofiber, with a limit of 0.59 μM. The system exhibited an excellent on-site application potential for the high-throughput screening of GLYP in water [165] (Figure 20).
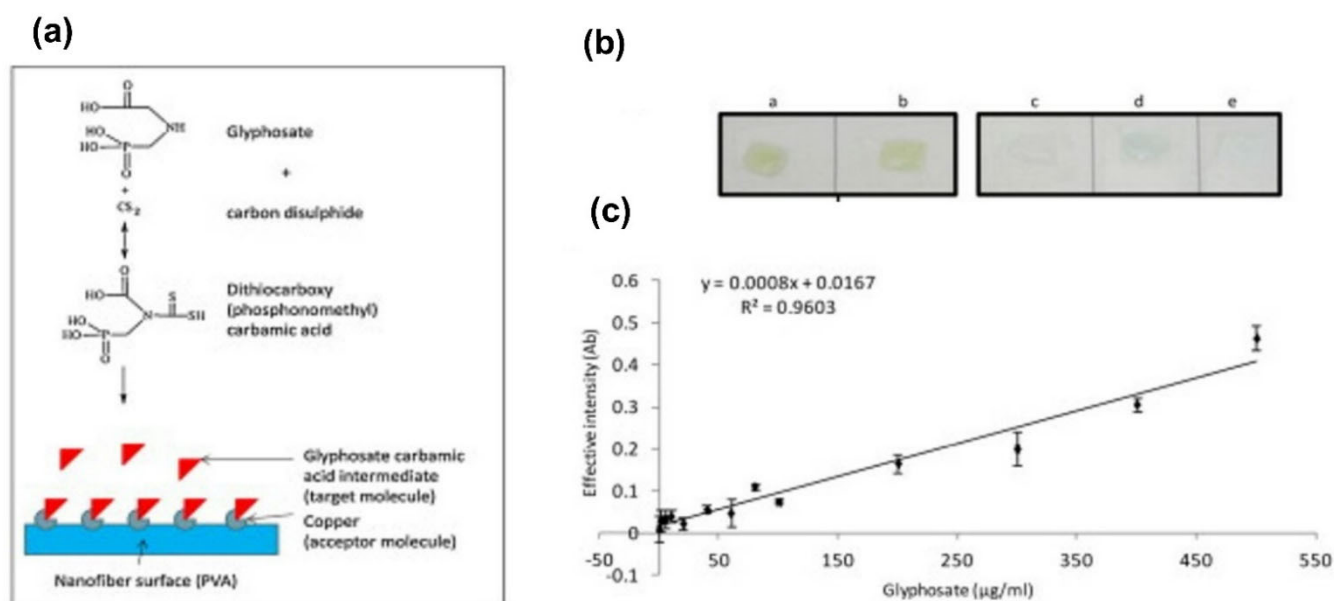
Figure 20. (**a**) The schematic representation of the cd-PVA sensor system. (**b**) The visual colorimetric response of the cd-PVA sensor strips immediately after the addition of 1000 μg/mL of the pure glyphosate derivative (99.5%) a and b: cd-PVA sensor strips after the addition of the glyphosate sample (volume: 30 μL). Values are graphically presented as mean values ± SD (n = 2). Control reactions included: c: no glyphosate, d: no carbon disulfide, e: a no test sensor strip/blank. (**c**) The calibration curve for glyphosate (0.1–500μg/mL). The sample volume was 30 μL and the appropriate controls were used in this study. Values are presented as mean values ±SD (n= 3). Adapted with permission from [165]. Copyright 2015 Elsevier.

3.2.3. Nanorods (NRs)

Gold nanorods (AuNRs) are one-dimensional gold nanocrystals with tunable optical properties, high scattering cross-sections, and the capacity to form core–shell nanostructures with mesoporous silica (MS) [166]. Likewise, AuNRs have attracted significant interest as SERS substrates. Torul et al. [167] reported the attomole detection of GLYP using surface-enhanced Raman spectroscopy (SERS) and gold nanorods derivatized with 4-mercapto phenylboronic acid [167]. The SERS signal exhibited a linear dependence within the glyphosate concentration at $1-10^{-16}$ mM.

3.3. 2D Nanomaterials

The 2D nanomaterials contain only one dimension on the nanoscale. The 2D nanomaterials include single-layered and multi-layered types, crystalline or amorphous types, thin films, nanoplates, and nanocoating. 2D nanostructures such as graphene, MoS_2, MXene, h-BN [168], $g-C_3N_4$, and black phosphorus have demonstrated an unprecedented surface-to-volume ratio, which promises an ultralow material use, ultrafast processing times, and ultrahigh treatment efficiency for water cleaning/monitoring [169]. Inside 2D materials, the nanocarbon-based 2D materials, including graphene (G), graphene oxide (GO), and reduced graphene oxide (rGO), are of interest in the construction of novel interfaces for sensing applications (Table 3) [170].

3.3.1. Graphene and Graphene Analogs Such as Transition Metal Dichalcogenides and Transition Metal Oxide

Setznagl and Cesarino developed an electrochemical sensor composed of a copper nanoparticle system and reduced graphene oxide on a glassy carbon electrode (GC/rGO-CuNPs). The analytic response was based on the differential pulse voltammetry produced

by the anodic peak due to the Cu^0 to Cu^{2+} oxidation process. The DPV signal was inversely dependent on the GLYP concentration, achieving a linear response of 0.1 to 1.1 μM with a LOD of 0.19 μM [108].

MoS_2 nanosheets exhibit peroxidase mimetic activity, which also can be inhibited by GLYP, which when combined with 2D layered structures analogous to graphene, results in a suitable sensor. This principle was used to detect and quantify GLYP. A linear relationship between the absorbance change and GLYP concentration was observed over 2.37– 11.83 μM with an LOD of 0.51 μM [171]. In another example, the inhibition of the peroxidase-mimicking activity of Co_3O_4 nanodiscs by GLYP was also applied. The color variation allows the determination of GLYP in less than 20 min. The LOD was calculated as low as 0.014 μM and displays excellent selectivity against other competitive pesticides and metal ions [172].

Table 3. The 1D, 2D, and 3D nanomaterials used in sensor development for detection of GLYP.

	Detection Method (Transducer)	Linear Range	Detection Limit	Reference
1D Nanomaterials Nanocomposites				
Cu^{2+}-Cu/GC	Electrochemical	0.4–10 μM	0.186 μM	[110]
Inhibiting the catalytic activity of the CuO/MWCNTs	Turn-off fluorescence	0.012–0.06 μM	3.96×10^{-6} μM	[112]
Carbon dot labeled antibodies (lgG-CDs) magnetic nanoparticles Fe_3O_4 and GLYP utilized to couple with the excess lgG-CDs	Immune Reaction	0.06–473 μM	0.05 μM	[127]
Carbon nano-onions (CNOs)	Tyrosinase based Amperometric	0.015–10 μM	6.5 nM	[150]
CdTe-CQD	Photoluminescence (PL) Fluorometric	0–1000 nM	2 pM	[157]
Pencil graphite electrode modified by hollow fiber pregnant by MWCNTS-ionic liquid composite and CuONPs	Electrochemical	5 nM–1.1 μM	1.3 nM	[160]
MWCNTs decorated with nano-ZnO. Nano-ZnO	Spectro electrochemical and electrochemical detection	GLYP: 0–100μM AMPA: 30–100 μM	GLYP:1 μM AMPA:10μM	[162]
GE/MWCNTs-HRP	Electrochemical	0–4.5 mM	1.32 pM	[173]
Carbon paste electrode (spectroscopic-grade graphite powder)	Electrochemical	0.044–2.8 μM	2×10^{-3} μM	[174]
Fluorescent CDs	Turn-on Fluorescence	0.18–59 μM	0.09 μM	[175]
Fluorescent CDs	FRET	0.02–2.0 μM.	0.6 μM	[176]
CDs	Fluorescent quenching	1.5×10^{-3}–30 μM	Diazinon: 1.5×10^{-3} μM GLYP: 0.012 μM	[177]
GQDs-AgNPs system	Fluorometric Luminescence probe	0.18–11.83 μM	0.05 μM	[178]
CdTe-quantum dots	Fluorometric	10–118 μM	3 μM	[179]
2D Nanomaterials Nanocomposites				
Peroxidase Mimetic Activity of MoS_2 Nanosheets	Colorimetric	2.4–12μM	0.51 μM	[171]
Ultrathin two-dimensional	Fluorescence	2.5–45 μM	2.25 μM	[180]

metal-organic framework nanosheets, decorated with tetra-pyridyl calix [4]arene (MOF-Calix)				
GLYP/Ru(bpy)32+system on gold electrodes modified with SAM.	ECL	0–100 μM	0.01 μM	[181]
Calixarene-functionalized luminescent silica nanoparticles [Ru(bpy)3] $^{2+}$ complex.	FRET	0–2 μM	0.8 μM	[182]
3D Nanomaterials Nanocomposites				
Nanoporous Copper film (microelectrode)	Electrochemical	0.030–0.065 μM	4×10^{-3} μM	[111]
Nanobody (CP4-EPSPS protein) and Mesoporous Carbon	Electrochemical immunosensor	6×10^{-6}–0.6 μM	4.3×10^{-6} μM	[123]
ZnS-QDs on ordered mesoporous carbons substrate	HRP and ECL	0.1 nM–10 mM	NR	[183]

Note: NR: Not Reported.

3.3.2. Meso-/Nanoporous

Mesoporous materials show unique features, including high surface areas, large pore sizes (2–50 nm), tunable pore structures, controllable framework compositions, various nanostructures, high stabilities, and easy functionalization. These features have led to their widespread usage [184]. For example, an electrochemiluminescence (ECL) enzymatic biosensor was successfully developed using an ordered mesoporous carbon (OMC) and HRP. The principle of detection was the inhibition of HRP by GLYP. The analytical response was based on the catalytic reaction using HRP, $Na_2S_2O_3$, and H_2O_2 to yield H_2S, which reacts with Zn^{+2} ions to produce ZnS quantum dots. The OMC provided excellent conductivity for detection and ample accommodation for the Zn^{2+} ions; chitosan was added to enhance the Zn^{2+} ions' adsorption. In this way, the enzymatic activity was followed by electrochemiluminescence generated by ZnS QDs. As GLYP can chelate iron from the catalytic center of HRP, its presence decreases the HRP activity and the ECL signal. A wide linear range was reported from 0. 1 nM to 10 mM with an excellent sensitivity, reproducibility, and selectivity. In this report, the IC value of 1.61 μM revealed a pronounced inhibition of HRP by GLYP [183].

In another example, stable covalent organic frameworks (COFs) of melamine and *p*-benzaldehyde (MaBd) were prepared by polycondensation. MaBd catalyzes the glycol and chloroauric acid reaction to generate gold nanoparticles with a strong RRS and surface-enhanced Raman scattering (SERS) effect. On the other hand, an aptamer for GLYP c, able to interact with MaBd was synthesized, but the Aptamer–MaBd complex was catalytically inactive. However, when GLYP was added to the solution, the aptamer interacted preferably with the herbicide, liberating and restoring the MaBd's catalytic activity. Thus, a highly sensitive SERS method was developed with a linear range of 0.003–0.07 nM and a GLYP detection limit of 0.002 nM (Figure 21) [185].
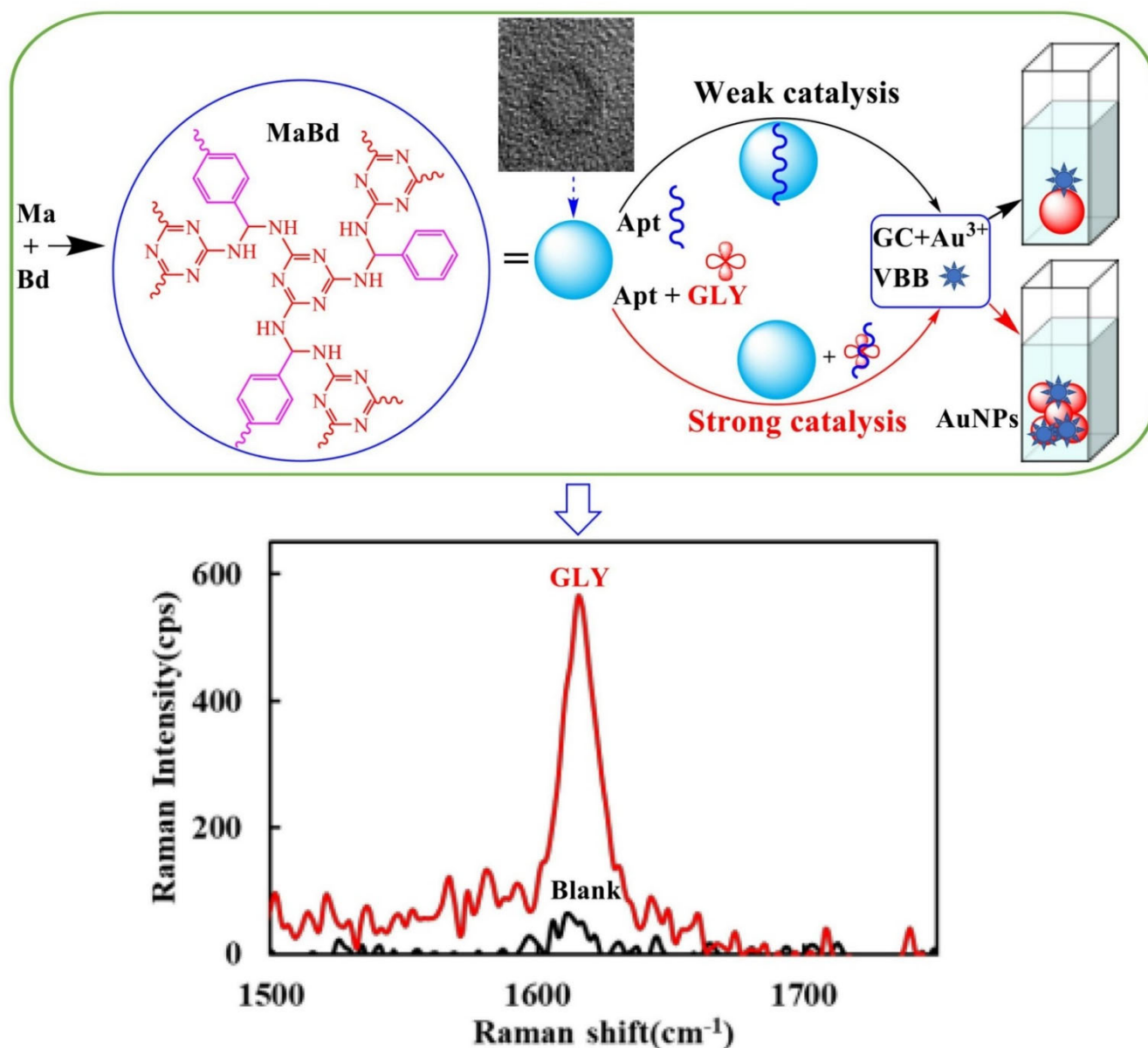
Figure 21. Aptamer regulated-MaBd catalysis of GC-HAuCl₄ nanogold reaction to detect GLYP with two scattering techniques. Reprinted with permission from [185]. Copyright 2021 Elsevier.

In recent years, nanoporous materials-based sensors for pollutants detection have drawn interest as simple novel sensors to overcome the drawbacks of some conventional analytical methods [186]. For instance, a copper microelectrode was modified with nanoporous copper film (NPC) to study the effect of GLYP on the Cu^0 to Cu^{2+} oxidation process (Figure 22). As already known, GLYP is electrochemically inactive, but this compound influences the electrochemical behavior of NPC materials through a chemical reaction with Cu(II) ions. At specific concentrations, the amount of copper oxides decreases due to the formation of soluble Cu(II) complex with GLYP; therefore, less current was obtained in a concentration-dependent manner. An LOD of 3 nM was reported [111]. With the electrodeposition of copper nanoparticles (CuNP) on a screen-printed carbon electrode (SPCE), which was modified with an ordered mesoporous carbon (CMK-8), GLYP was determined electrochemically with an LOD of 5.3×10^{-4} μM [111].

Figure 22. An electrochemically synthesized nanoporous copper microsensor for highly sensitive and selective determination of GLYP. Reprinted with permission from [111]. Copyright 2020 Wiley Online Library.
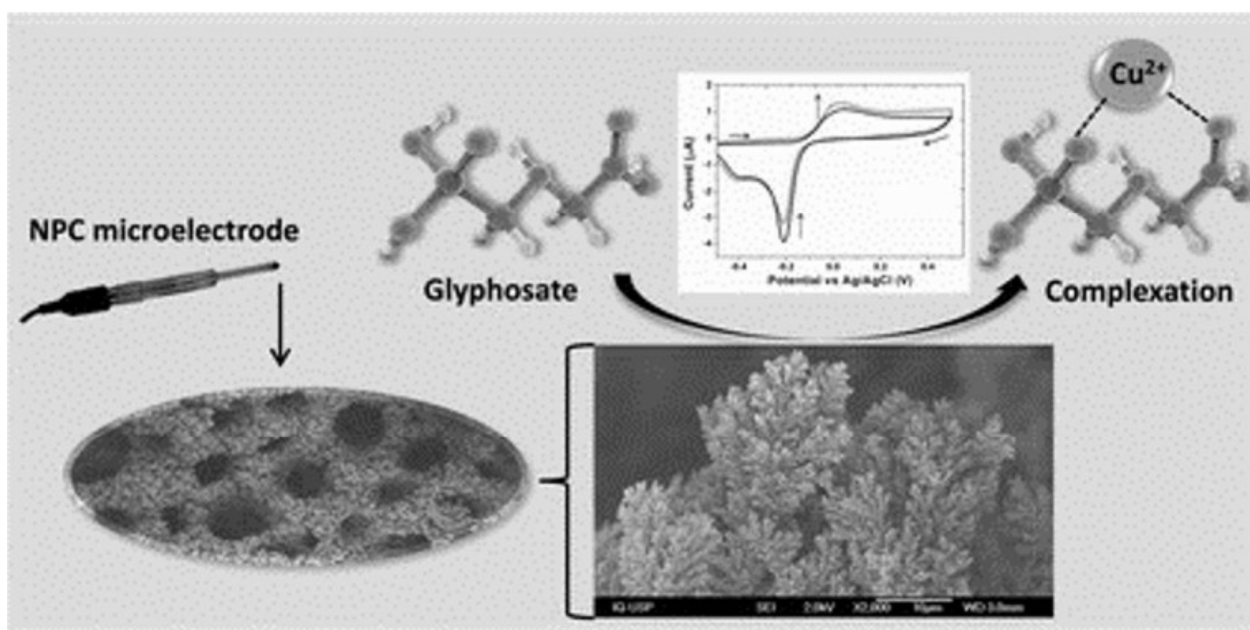
Metal-Organic Frameworks (MOFs)

MOFs are a relevant class of inorganic and organic hybrid crystals of nanostructured porous materials. They have attracted increasing interest from research communities due to their vast surface area, diversity in nanostructures [187], and unique properties [188,189] for optical sensing [190]. MOFs have been extensively investigated to address the challenges associated with the sensitivity of on-site detection in environmental monitoring, which is imperative for developing sensors for pesticides (Table 4) [191,192]. Most of the studies in the literature focus on the application of MOFs as sorbents for GLYP extraction and preconcentration [193–196].

Further progress in the detection of GLYP was achieved with the synthesis of ultrathin 2D metal-organic framework (MOF) nanosheets decorated with tetra-pyridyl calix[4]arene. Calix[n]arenes have been widely used as fluorescent probes because of the fluorescence variation resulting from the interaction between small guest molecules incorporated into their structure. The implementation of 2D MOF-Calix nanosheets with functional groups have enabled the development of the third generation of hosts for the selective and sensitive detection of GLYP by enhancing the fluorescence effect with an LOD of 2.25 μM [180].

The unique characteristics of MOFs are advantageous for constructing novel artificial enzymes, particularly nanozymes. The development of MOF-based nanozymes includes their construction and an analysis of their chemical sensing and biosensing properties [197]. A pesticide sensor based on a glass carbon electrode (GCE) modified by copper oxide @ mesoporous carbon (CuOx@mC) composite was reported (Figure 23). Since copper ions can coordinate with GLYP, the DPV method could record the effect on the electrochemical response signal. This effect was used to determine the GLYP content (Figure 23c). The CuOx@mC/GCE displayed superior sensing performance, the achievement of an LOD of 7.69×10^{-10} μM was achieved, and the acquirement of a linear range of 1.0×10^{-9} to 100 μM [198] (Figure 23).
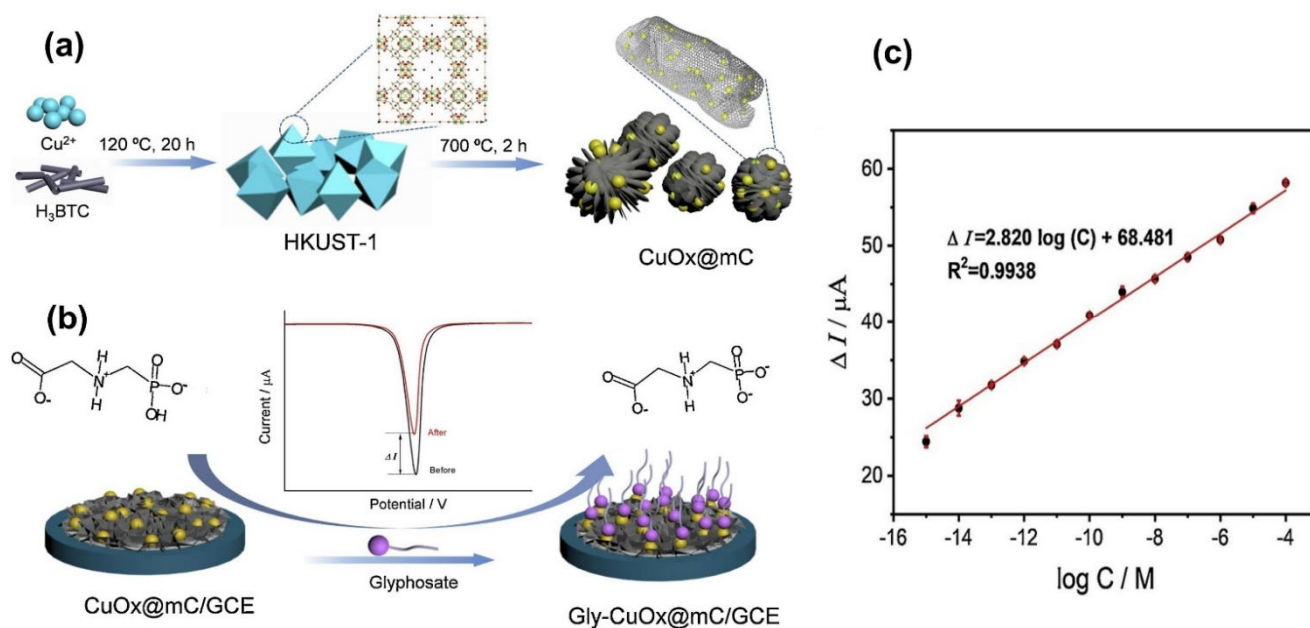
Figure 23. Nanocomposite development for an electrochemical sensor. (**a**) CuOx@mC composite formation, (**b**) Analytical principle of the electrochemical sensor based on the CuOx@mC composite, (**c**) A calibration curves between ΔI and the GLYP concentrations for CuOx@ mC GCE. Reprinted with permission from [198]. Copyright 2020 Elsevier.

An electrochemical sensor was constructed by dropping a hierarchically porous Cu-BTC material on the surface of an ITO electrode [199]. Cu-BTC increases the active surface area of the working electrode, improving its cyclic voltammetry (CV) and differential pulse-stripping voltammetry (DPV) responses. In addition, the large specific surface area of the Cu-BTC enhanced the electrode's accumulation ability, resulting in an improved electrode detection limit. The LOD was as low as 1.4×10^{-7} μM with two detection ranges, 1.0×10^{-6} to 1.0×10^{-3} μM and 1.0×10^{-3} to 0.1 μM [73] (Figure 24).
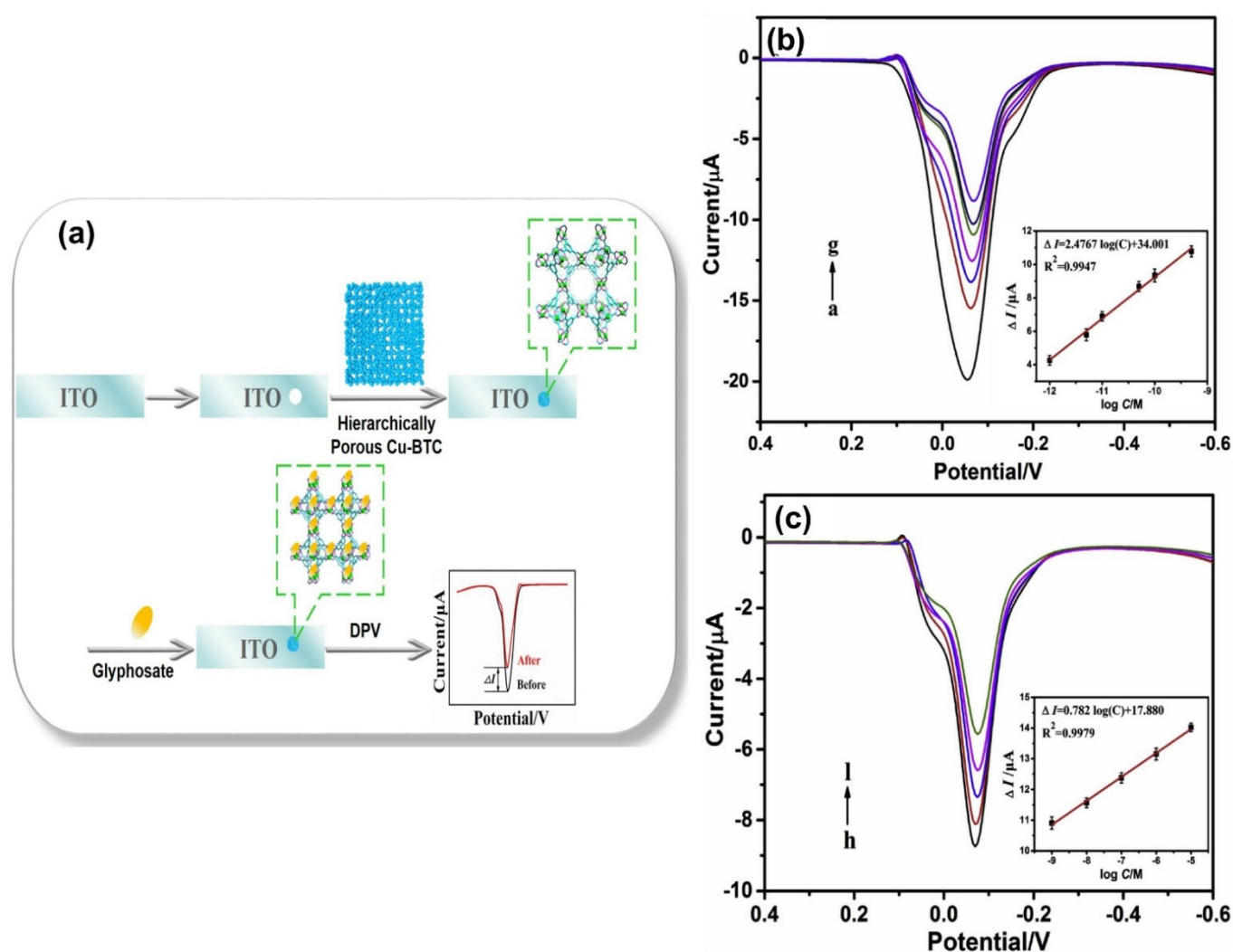
Figure 24. (**a**) Analytical principle of the electrochemical sensor based on the hierarchically porous Cu-BTC MOF material. (**b**) Differential pulse stripping voltammograms of Cu-BTC/ITO at different GLYP concentrations from a to g (0, 1.0×10^{-6}, 5.0×10^{-6}, 1.0×10^{-5}, 5.0×10^{-5}, 1.0×10^{-4}, 5.0×10^{-4}. (**c**) from h to l (1.0×10^{-3}, 1.0×10^{-2}, 1.0×10^{-1}, 1.0, 0.1 μM). Reprinted with permission from [73]. Copyright 2019 Elsevier.

3.4. 3D Nanomaterials Such as Nanocomposites in Sensors for GLYP Detection

3D nanomaterials have dimensions beyond 100nm, allowing multidimensional structures to be constructed. Combining 1D, 2D, and 3D nanomaterials have created a wide range of hybrid NMs, called nanocomposites, with enhanced sensitivity for sensor applications [200–202].

A water-stable 3D metal-organic framework (MOF) with a lanthanide, namely Tb-MOF, resulted in an ideal fluorescence recognition material to detect GLYP. The fluorescence intensity of Tb-MOF varies with the amount of glyphosate. The first emission peak (360 nm) of Tb-MOF was enhanced, but the other emission peaks (490 nm and 545 nm) were reduced, allowing detection of GLYP in the range of 0–630 μM with a limit of detection of 0.0144 μM [203] (Figure 25).

Figure 25. (**a**) The fluorescence spectra of Tb-MOF after different concentrations of GLYP; (**b**) Linear correlation of Tb-MOF and different concentration of GLYP; (**c**) The change of color for the Tb-MOF before and after adding GLYP. Reprinted with permission from [203]. Copyright 2021 Elsevier.

Nanocomposites

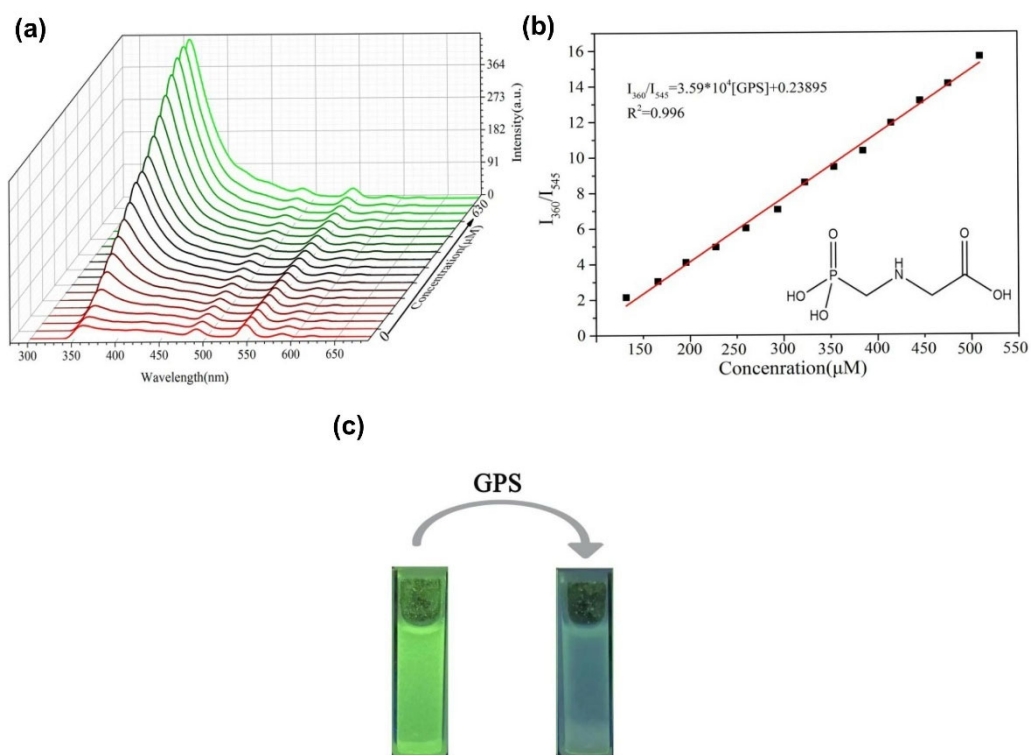Molecularly imprinted polymers (MIPs) have now earned a reputation as ''artificial receptors'' or ''plastic antibodies''. As the mimics of natural receptors, MIPs are reminiscent of some essential functions of natural receptors in living systems, e.g., the ability to interact with or recognize one element target in preference to another that is closely related, which is potentially valuable for the detection of molecules in a sensitive, rapid, and selective way (Table 4) [204,205].

For example, a pencil graphite electrode was modified with a doubly imprinted polymer for the simultaneous detection of GLYP and glufosinate (Glu). Since GLYP is prone to nitrosation, N-nitroso GLYP and Glu were used as templates for anodic stripping voltametric peaks assays. The sensor's fabrication plans initially involved growing a nanostructured polymer film directly on the electrode by immobilizing the AuNPs on its surface. Then, monomeric (N-methacryloyl-L-cysteine) molecules were linked through S-Au bonds and were subjected to free-radical polymerization using a pre-polymer mixture composed of a cross-linker, an initiator, and multiwalled carbon nanotubes (MWCNTs). Finally, a doubly imprinted polymer was obtained by removing the molecule templates (Figure 26). The final sensor could simultaneously detect GLYP and glufosinate in aqueous samples in two wide linear ranges (0.02–1.04 μM and 3.19×10^{-3}–0.02 μM) with LOD of 2.07×10^{-3} and 1.12×10^{-3} μM [206].
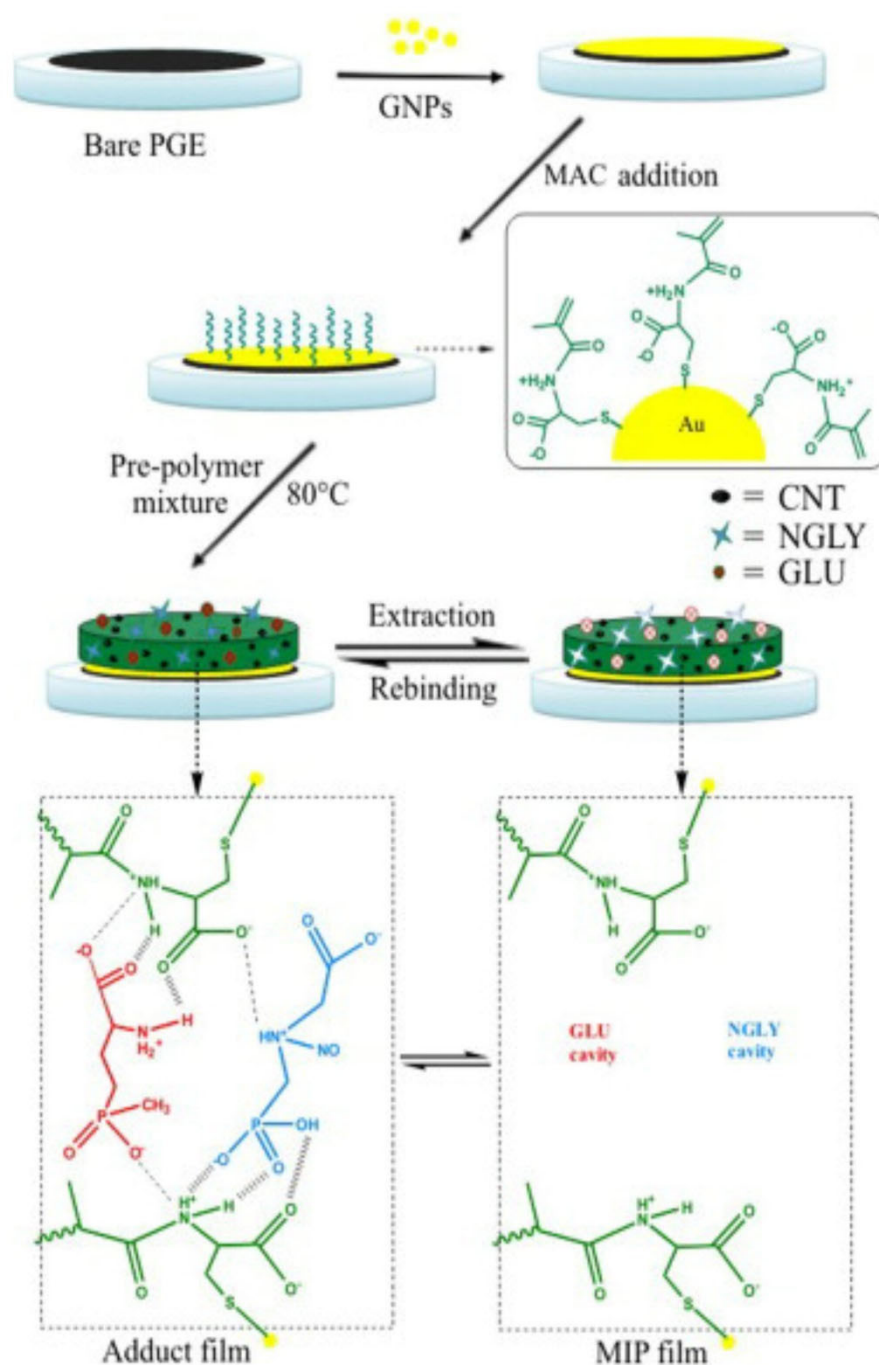
Figure 26. Schematic representation of double-template imprinted polymer-modified GNPs-PGE fabrication and the suggested binding mechanism for simultaneous analysis of GLYP and GLU in their respective MIP cavities. Reprinted with permission from [206]. Copyright 2014 Elsevier.

Heterocycles such as pyrrole, thiophene, or aromatic thiols are commonly partially cross-linked electro-monomers used to construct molecularly imprinted electrochemical sensors [207]. For example, Mazouz et al. [208] made an electrochemical sensor with MIPs, a polypyrrole matrix (Ppy), and GLYP molecules as a template. Two electrodes were obtained: one with a gold surface and the second with ZnO nanorods (grown on an ITO diazonium-modified electrode), and ehe LODs of these sensors were around 10^{-7} μM and 10^{-4} μM, respectively [208]. In another example, a molecularly imprinted mesoporous organosilica (MIMO) for GLYP was synthesized using a zwitterionic functional group (MIMO-z). After removing GLYP, the zwitterionic group remained in the MIMO-z

structure. Then, graphene quantum dots were encapsulated into the MIMO-z's pores (MIMO-zQ). The effect of GLYP on the fluorescence intensity of the graphene dots was monitored. In addition, the authors used another kind of quantum dot, InP/ZnS QD. In both cases, when the MIMO-zQ suspension was incubated into the GLYP solutions, significant fluorescence quenching occurred, which was used as a signal transducer to sensitively detect GLYP to sub-nanomolar concentration levels: $9.2 \pm 0.18\%$ quenching at 0.1 nM (Figure 27) [209].
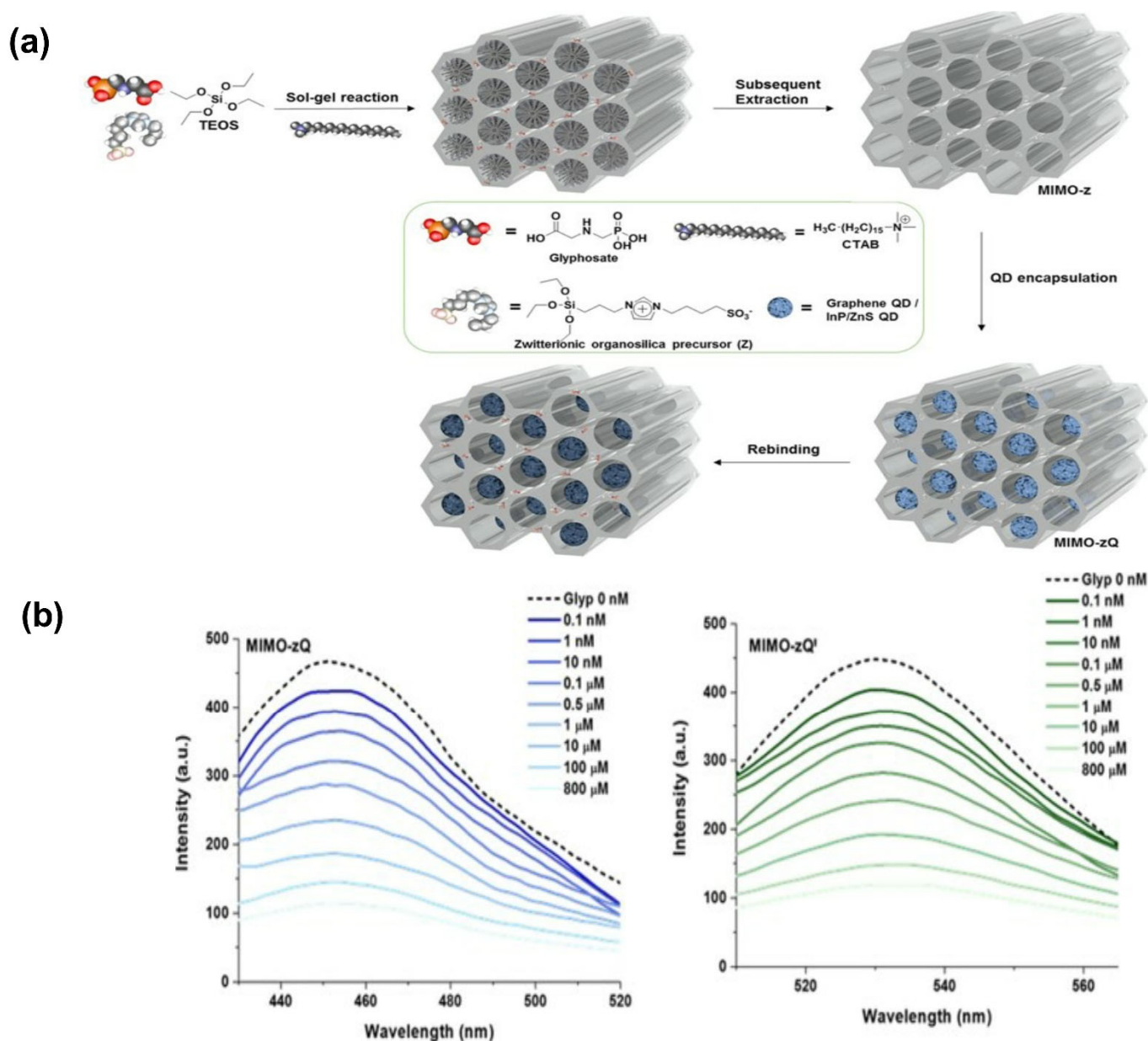
Figure 27. (**a**) Schematic illustration of the synthesis of QD-encapsulated GLYP imprinted mesoporous organosilica (MIMO-zQ), (**b**) Photoluminescence decrease as a function of the GLYP concentration for both MIMO-zQ preparations, graphene QDs (left) and InP/ZnS QD (right). Reprinted with permission from [209]. Copyright 2019 Nature.

A three-dimensional microfluidic paper-based analytical device (3D-μPAD) using Mn–ZnS quantum dots embedded in a molecularly imprinted polymer (Mn-ZnS QD-MIP) was reported. Its detection was based on inhibiting the catalytic activity of Mn-ZnS QD

MIP in the H_2O_2 oxidation of ABTS. A glyphosate-imprinted polymer was successfully synthesized on the Mn-ZnS QD's surface using a poly (N-isopropyl acrylamide) and N, N'-Methylenebisacrylamide as the functional monomers. The catalytic activity depended on the binding or non-binding of the glyphosate molecules on the Mn–ZnS QD-MIP synthetic recognition sites. Glyphosate selectively bonded to the cavities embedded on the Mn–ZnS QD's surface and subsequently turned off or inhibited the ABTS oxidation. An assay on the 3D-µPAD determined the presence of glyphosate via image detection, over an operating range of 2.96×10^{-5} mM–0.296 mM and with a detection limit of 1.18×10^{-5} mM (Figure 28) [210].
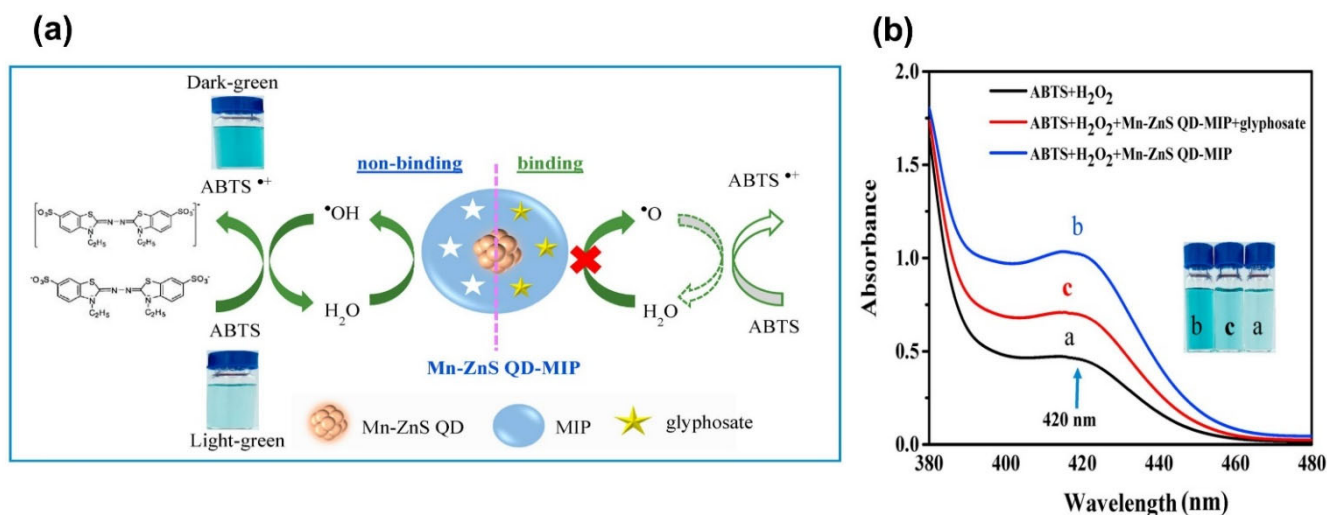
Figure 28. (**a**) Scheme of mechanism of GLYP colorimetric detection based on Mn–ZnS QD-MIP as a competitive inhibitor on the reaction between ABTS and H_2O_2. (**b**) Absorbance spectra of ABTS, a: after the addition of Mn–ZnS QD-MIP, b: ABTS-H_2O_2–Mn–ZnS QD-MIP, c: after addition of GLYP. Reprinted with permission from [210]. Copyright 2021 Elsevier.

In another example, molecularly imprinted Ppy nanotubes (MIPNs) were prepared by imprinting GLYP sites on their surfaces. The GLYP sensor was fabricated by coating a thin layer of the MIPNs on the surface of a screen-printed electrode (SPE). The MIPN-modified SPE produces an oxidation-reduction reaction and thus results in the response current. When GLYP is selectively adsorbed, the transfer of electrons is hindered, and the active surface area is reduced alongside the response current. The decrease in the response current is proportional to the amount of GLYP that has been adsorbed. The results demonstrate that the MIPN-based electrochemical sensor for GLYP exhibits a wide detection range of 1.48×10^{-5}–2.07×10^{-3} mM with an LOD of 1.15×10^{-5} mM [211].

Thimoonnee et al. [212] developed a graphite screen-printed electrode modified with a molecularly imprinted polymer coated on a mesoporous silica-platinum core (MSN-PtNPs@d-MIP/GSPE) for the sensitive, selective, and simultaneous detection of GLYP. The 3D-surface-imprinting strategy enhances the conductivity and monodispersity of the MSN-PtNPs@d-MIP. A quantitative analysis was performed by differential pulse voltammetry. As a result, the MIP sensor showed good linear calibration curves from 0.025–500 mM for both analytes with detection limits of 4.0 nM [212].

Table 4. MOF and MIPs as nanomaterial-based for GLYP detection.

Metal-Organic Framework (MOFs) System Nanomaterial			
Detection Method (Transducer)	Linear Range	Detection Limit	Reference

Hierarchically porous Cu-BTC MOF platform	Electrochemical	1.0×10^{-6}–0.01 μM and 0.01~1000 μM	1.4×10^{-7} μM	[73]
(CuOx@mC/GCE) mesoporous with MOF	Electrochemical	1.0×10^{-9}–100 μM	7.69×10^{-10} μM	[198]
Molecularly Imprinted Polymer (MIP) Nanomaterial System				
PAP-MIP-MOF films- Gly as template molecule/ (AuNPS) / Gold electrode	Electrochemical	6×10^{-9}–6×10^{-3} μM	5 fM	[100]
Coumarin-based ligand (CL) quenched by Cu^{2+} due to the process of photoinduced electron transfer.	Fluorescence	0.12–8.87 μM	0.11 μM	[113]
antibody-modified magnetic particles, using TMB as an enzymatic substrate.	Electrochemical immunoassay (competitive)	0–0.06 μM	3×10^{-5} μM	[129]
Fe_3O_4/molecular-imprinted nanocomposite	Electrochemical	NR	10 μM	[201]
Ppy matrix/molecules GLYP templates	Electrochemical	NR	1×10^{-7} μM	[208]
Molecularly imprinted mesoporous organosilica (MIMO)/QD-encapsulated GLYP imprinted mesoporous organosilica	Fluorescence	0 nM–800 μM	0.1 nM	[209]
Ppy-MIP	Gravimetric [a] and electrochemical [b]	1 pM–1 nM	1 pM	[51]
Ppy-MIP	Electrochemical	0.03–4.73 μM	1.6 μM	[213]
Composite AuNPs-Ppy -MIP on the surface of the ITO electrode	Voltammetric	2.4–7.1 μM	0.5 μM	[214]
Disubstituted polyacetylenes (TZP and PBP) with Cu ions	Fluorescence	NR	0.08 μM	[215]
Poly(2,5dimethoxyaniline) (PDMA) doped with poly (4-styrenesulfonic acid) (PSS)/ HRP	Amperometric	NR	0.09 μM	[216]
Molecularly imprinted polymer (MIPs) made of chitosan (CS)	EIS	2×10^{-6}–0.3 μM	6×10^{-9} μM	[217]

Note: NR Not Reported; [a] Surface acoustic wave (SH-SAW); [b] Chronamperometry (CA); and square wave voltammetry (SWV).

4. Nanosensors Performance Using Real Samples

In some countries, the water contamination from GLYP is a permanent problem due to GLYP's intensive and unregulated use. Therefore, monitoring the presence of GLYP in environmental water samples should be a permanent activity for correctly diagnosing the ecological impact of using this herbicide. Only some analyzed works report the application of nanosensors in environmental water (regarding drinking and urban, subway, or surface environments) (Table 5). From the data in Table 5, it seems that the ecological matrix effects appear to have no significant effect on the selectivity of the determination, accuracy, or precision. In addition, individual interferents also do not affect the performance of the (nano)sensors; the variety of interferents, salts, and pesticides used supports the notion that the development of nanosensors is on the right track.

However, these applications have been tested in fortified water samples but have not been validated with the officially proven technique, namely, HPLC-mass spectrometry. In addition, the interferents have usually been studied individually and not in mixtures, which may have an increased impact. Therefore, the development of nanosensors should also focus on analyzing them in environmental water samples, where the effect of the interferents can be adequately validated. Some other aspects of the integral performance of the system, such as the stability of the components, and the repeatability between days,

are generally not reported; therefore, it is necessary to strengthen the studies to elucidate these issues' real potential outside the laboratory.

Table 5. Accuracy and precision of nanosensors for GLYP determination in environmental water samples.

Sample Matrix	Interferences	Accuracy (Range/AVERAGE Recovery)	Precision	Reference
Tap water samples	AMPA	98.7–102.6%	3.33–4.54%	[100]
Water samples, including local river water and lake water.	Deltamethrin, acetamiprid, chlorpyrifos, carbendazim	98.9–105 %.	3.59–6.52%	[102]
Tap water	Pyrethroid cypermethrin and deltamethrin, diazinon and malathion and mevinphos	96–104%	NR	[108]
River water samples	Simazine, propazine, and atrazine, AMPA, Na^+, K^+, Ni^{2+}, Ca^{2+}, Mg^{2+},	98.7–105.2%	1.58–4.76%	[111]
Real water samples from the Taitung Flowing Lake in the Taitung Forest Park and the tap water of school	Chlorothalonil,Cyanofenphos, Propanil, Chlorpyrifos, Carbendazim, Acetamiprid, Fenvalerate, Carbaryl, Dimethoate	96–107%	1.6–4.1%	[112]
Real samples river and lake water	Dimethoate, malathion, fenitrothion, carbendazim, fluazinam, chlorpyrifos, triadimefon, trichlorfon, and methamidophos.	91.31–105.28%	1.10–3.48%	[113]
Tap water and rice	K^+, Na^+, Ca^{2+}, Zn^{2+}, Mg^{2+}, Fe^{3+}, Pb^{2+}, Ni^{2+}, Co^{2+}, Cr^{2+}, Ag^+, Hg^{2+}, and Cd^{2+}, trichlorfon, profenofos, malathion, fenitrothion, chlorpyrifos, glyphosate. ascorbic acid and glutathione	Cu^{2+} = 92.41–108.38% GLYP = 89.87–109.39%	NR	[116]
Tap water	Dichlorvos, dimethoate, 2–4D, paraquat dichloride, hexaconazole	86%	6%	[117]
Pearl River water, tea, and soil	Na^+, K^+, NH_4^+, NO_3^-, PO_4^{3-}, F^-, Mg^{2+}, Zn^{2+}, Ca^{2+}, and Fe^{3+} pmida, glyphosine, omethoate, phosmet	87.4–103.7%.	4.67%	[127]
River water soil	Zn^{2+}, Cd^{2+}, Ca^{2+}, Mg^{2+}, Na^+, NH_4^+, Br^-, NO_3^-, SO_4^{2-},PO_4^{3-}, Glufosinate. Bialaphos, Tridemorph, Chlorpyrifos, Cypermethrin (Aminomethyl) phosphonic acid	92.19–103.25 %	4.3–5.10%	[160]
Environmental water samples	Na^+, K^+, Mg^{2+}, Ca^{2+}, NO^-_3, CO_3^{2-}, SO_4^{2-}, dimethoate, isocarbophos, phosalone carbaryl, bendiocarb	99–108%	NR	[171]

Water samples collected from Qing Lake, Guanlan Lake and Yan Lake (Changchun, China).	$Na^+, K^+, Mg^{2+}, Ca^{2+}, Ba^{2+}, Zn^{2+}, Ag^+, Cd^{2+}, Fe^{3+}, Hg^{2+}, Mn^{2+}$ $Pb^{2+}, Hg^{2+}, Cd^{2+}, Fe^{3+}, Ag^+$, Ametryn, Metsulfuron-methyl, Metaflumizone, Dinotefuran, Chlorfenapyr, Carbendazim, Pymetrozine, Imidacloprid, Chlorothalonil, Chlorpyrifos, Glufosinate	93.3–106.7%	2.1%	[175]
Environmental water samples	NaCl, KCl, CaCl₂, NH₄Cl, MgCl₂, CdCl₂, ZnSO₄, ascorbic acid, pyridoxine, glycine, lysine, aspartic acid, arginine glucose, sucrose, maltose, quercetin, puerarin, trifluralin, dicamba, acetochlor, atrazine, and AMPA	93.7–102.6%	1.7–3.3%,	[176]
Environmental simples water and cereal samples (amaranth, barley, oat, and quinoa).	K^+, Na^+, Cl^-, NO_3^- $Mg^{2+}, PO_4^{3-}, CO_3^{2-}, SO_4^{2-}$ Ni^{2+} Carbaryl, carbendazim, fipronil, imidacloprid, malathion, nitenpyram, o-phenylphenol, pyraclostrobin, thiabendazole, thiacloprid, thiamethoxam	92–108%	3.7%	[179]
Ground water and rice	Mancozeb, Thiamethoxam, Cartap Hydrochloride, Emamectin Benzoate, Alphamethrin, Fenpropathrin, Triazophos, Imidacloprid, and Chlorpyrifos	94–98%	NR	[182]
Water-quality control and on-site applications	Phenol, caffeine, uric acid, ascorbic acid, hydroquinon, profenofos, chlorpyrifos, and carbofuran	100.00–108.00%	0.10–3.79%	[212]
Cucumber and tap water	AMPA, chlorpyrifos, aldicarb	72.70–98.96%	1.07–4.48%	[213]
Potato, Tap water	Malathion, Fenamiphos, Parathion $Zn^{2+}, Ni^{2+}, Hg^{2+}, Fe^{3+}, Al^{3+}, Cd^{2+}, Co^{2+}, Cu^{2+}$ Na^+	81.3–101%	0.49–4.61%	[218]
Groundwater samples, soybean extracts, and lettuce extracts	Glufosinate, carbaryl, bentazon, monocrotophos, thiram, and carbofuran, AMPA) and sarcosine, $Mn^{4+}, Fe^{2+}, Fe^{3+}, K^+, Cl^-, Zn^{2+}, SO_4^{2-}, BO_3^{3-}, Na^+, NO_3^-, PO_4^{3-}$, and Ca^{2+}	97.9–102.1%.	0.2–2.3%	[219]
Drinking water	$Mn^+ = Al^{3+}, Fe^{3+}, Cr^{3+}, Hg^{2+}, Ni^{2+}, Cu^{2+}, Cd^{2+}, Mn^{2+}, Zn^{2+}, Co^{2+}, Ca^{2+}, Ba^{2+}, Mg^{2+}, K^+$, and Na^+ fenthion, parathion-ethyl, parathion-methyl, chlorpyrifos, dichlorvos, profe- nofos, azinphosethyl, azinphosmethyl, fenitrothion, malathion, diazinon	NR	NR	[220]

Note: NR Not Reported.

5. Future Perspectives and Conclusions

Currently, as a result of the use of herbicides for agricultural purposes, the dispersion of harmful chemical pollutants is a crucial environmental problem. Specifically, GLYP water contamination must be addressed due to the health problems this chemical can provoke in humans. Even though traditional analytical methods have shown good LOD values (in the range of pM-μM), they are usually very time-consuming with respect to preparing and analyzing the samples and the cost of the methodology.

As is has been shown, different coupling nanomaterials have boosted the fabrication of composite sensors with distinct features and vast applications in pesticide sensing. However, none of the available GLYP detection methods can satisfy all the safety requirements and simultaneously achieve high sensitivity, selectivity, portability, and a fast response time. Hence, the nano-materials designed to interact with specific organic/biological compounds and polymers face significant challenges. In addition, nano entity–support matrix interactions are critical in the sensing properties of the nanomaterials. One crucial challenge is finding the optimal immobilization procedure for conjugating a biomolecule and a nanomaterial, in addition to the sample processing before detection (e.g., purification and separation) [158]. Finally, other challenges remain, such as the miniaturization, automation, and integration of the nanostructured-based biosensors.

However, the scope and possibilities that these nanomaterials offer are countless, which has driven various 3D printing technologies to construct sensing devices for pesticide detection, such as using microfluidics [221,222] or 3D-printing technologies [223–225]. With microfluidics and micro-and nanostructures, remarkable progress has been achieved, although there are still many challenges regarding their synthesis, alignment, and application. A microfluidic chip presents several advantages: high portability, versatility in design, a fast and cheap analysis, and multiple and parallel sample detection.

Nevertheless, the detection throughput is low and requires significant and precise sample pretreatment [226,227]. Therefore, future research must focus on the online and accurate monitoring of drinking water supply networks to quickly detect accidental or intentional drinking water contamination.

One possibility is to develop an intelligent sensor that presents a sensing element, a filtering system, which amplifies a signal with software for data processing and compensation. Smart sensors' detection and data processing can be performed while considering the environmental factors. They can be used to develop various optical detection tools, which makes smart sensors even more appropriate for use as portable biosensors, either as a smartphone detector in a direct form or as an instrumental interface. Smart sensors differ from integrated sensors as they have built-in programmable microprocessors. After processing and analyzing the data from a sensor, the information can be transmitted wirelessly to a notification node, reporting the water quality to the end-user. A multi-analytical and portable analysis platform could be used to detect GLYP, which would further the possibility of its day-to-day detection in a simple, effective, and real-time way [228].

With this review, it has been shown that nanosensors can be used as potential devices for GLYP detection in a variety of sample matrices, as they are portable, fast, and sensitive, showing LOD values in a range of μM comparable to the traditional methods. Additionally, nanosensors have the potential for in situ applications. Biological or inorganic compounds can construct these nanosensors. Bio-nanosensors, for example, are made with enzymes, DNA, or antibodies, making their application more attractive because of their specificity. On the other hand, Quantum Dots have captured research interest, and even though they are newly studied materials in this field, there are reports concerning devices with LOD values in the pM range. These kinds of devices are of interest due to their high surface area.

Institutional Review Board Statement: Not applicable.

Informed Consent Statement: Not applicable.

Data Availability Statement: Not applicable.

Conflicts of Interest: The authors declare no conflict of interest.

References

1. Storck, V.; Karpouzas, D.G.; Martin-laurent, F. Towards a better pesticide policy for the European Union. *Sci. Total Environ.* **2017**, *575*, 1027–1033. https://doi.org/10.1016/j.scitotenv.2016.09.167.
2. Kim, K.; Kabir, E.; Ara, S. Exposure to pesticides and the associated human health effects. *Sci. Total Environ.* **2017**, *575*, 525–535. https://doi.org/10.1016/j.scitotenv.2016.09.009.
3. Landrigan, P.J.; Fuller, R.; Acosta, N.J.R.; Adeyi, O.; Arnold, R.; Basu, N.N.; Baldé, A.B.; Bertollini, R.; Bose-O'Reilly, S.; Boufford, J.I.; et al. The Lancet Commission on pollution and health. *Lancet* **2018**, *391*, 462–512.
4. Steingrímsdóttir, M.M.; Petersen, A.; Fantke, P. A screening framework for pesticide substitution in agriculture. *J. Clean. Prod.* **2018**, *192*, 306–315. https://doi.org/10.1016/j.jclepro.2018.04.266.
5. Benbrook, C.M. Trends in glyphosate herbicide use in the United States and globally. *Environ. Sci. Eur.* **2016**, *28*, 3. https://doi.org/10.1186/s12302-016-0070-0.
6. Hossain, M. Recent perspective of herbicide: Review of demand and adoption in world agriculture. *J. Bangladesh Agric. Univ.* **2016**, *13*, 19–30. https://doi.org/10.3329/jbau.v13i1.28707.
7. Lewis, K.A.; Tzilivakis, J.; Warner, D.J.; Green, A. An international database for pesticide risk assessments and management. *Hum. Ecol. Risk Assess.* **2016**, *22*, 1050–1064. https://doi.org/10.1080/10807039.2015.1133242.
8. Myers, J.P.; Antoniou, M.N.; Blumberg, B.; Carroll, L.; Colborn, T.; Everett, L.G.; Hansen, M.; Landrigan, P.J.; Lanphear, B.P.; Mesnage, R.; et al. Concerns over use of glyphosate-based herbicides and risks associated with exposures: A consensus statement. *Environ. Health A Glob. Access Sci. Source* **2016**, *15*, 19. https://doi.org/10.1186/s12940-016-0117-0.
9. Gupta, P.K. Toxicity of Herbicides. In *Veterinary Toxicology: Basic and Clinical Principles*, 3rd ed.; Elsevier Inc.: Amsterdam, The Netherlands, 2018; pp. 553–567, ISBN 9780128114100.
10. Leyva-Soto, L.A.; Balderrama-Carmona, A.P.; Moran-Palacio, E.F.; Diaz-Tenorio, L.M.; Gortares-Moroyoqui, P. Glyphosate and aminomethylphosphonic acid in population of agricultural fields: Health risk assessment overview. *Appl. Ecol. Environ. Res.* **2018**, *16*, 5127–5140. https://doi.org/10.15666/aeer/1604_51275140.
11. Richmond, M.E. Glyphosate: A review of its global use, environmental impact, and potential health effects on humans and other species. *J. Environ. Stud. Sci.* **2018**, *8*, 416–434. https://doi.org/10.1007/s13412-018-0517-2.
12. Heap, I.; Duke, S.O. Overview of glyphosate-resistant weeds worldwide. *Pest Manag.* Sci. **2018**, *74*, 1040–1049. https://doi.org/10.1002/ps.4760.
13. Torretta, V.; Katsoyiannis, I.A.; Viotti, P.; Rada, E.C. Critical review of the effects of glyphosate exposure to the environment and humans through the food supply chain. *Sustainability* **2018**, *10*, 950. https://doi.org/10.3390/su10040950.
14. Gillezeau, C.; Van Gerwen, M.; Shaffer, R.M.; Rana, I.; Zhang, L.; Sheppard, L.; Taioli, E. The evidence of human exposure to glyphosate: A review. *Environ. Health A Glob. Access Sci. Source* **2019**, *18*, 2. https://doi.org/10.1186/s12940-018-0435-5.
15. Peruzzo, P.J.; Porta, A.A.; Ronco, A.E. Levels of glyphosate in surface waters, sediments and soils associated with direct sowing soybean cultivation in north pampasic region of Argentina. *Environ. Pollut.* **2008**, *156*, 61–66. https://doi.org/10.1016/j.envpol.2008.01.015.
16. Vereecken, H. Mobility and leaching of glyphosate: A review. *Pest Manag. Sci. Former. Pestic. Sci.* **2005**, *61*, 1139–1151. https://doi.org/10.1002/ps.1122.
17. Annett, R.; Habibi, H.R.; Hontela, A. Impact of glyphosate and glyphosate-based herbicides on the freshwater environment. *J. Appl. Toxicol.* **2014**, *34*, 458–479. https://doi.org/10.1002/jat.2997.
18. Silva, V.; Montanarella, L.; Jones, A.; Fernández-Ugalde, O.; Mol, H.G.J.; Ritsema, C.J.; Geissen, V. Distribution of glyphosate and aminomethylphosphonic acid (AMPA) in agricultural topsoils of the European Union. *Sci. Total Environ.* **2018**, *621*, 1352–1359. https://doi.org/10.1016/j.scitotenv.2017.10.093.
19. Gill, J.P.K.; Sethi, N.; Mohan, A. Analysis of the glyphosate herbicide in water, soil and food using derivatising agents. *Environ. Chem. Lett. Rev.* **2017**, *15*, 85–100. https://doi.org/10.1007/s10311-016-0585-z.
20. Valavanidis, A. Glyphosate, the Most Widely Used Herbicide. Health and safety issues. Why scientist differ in their evaluation of its adverse health effects. *Sci. Rev.* **2018**, *1*, 1–36.
21. Mariane, R.; Souza, D.; Seibert, D.; Beatriz, H.; Jesus, F. De; Fagundes-klen, M.R.; Bergamasco, R. Occurrence, impacts and general aspects of pesticides in surface water: A review. *Process. Saf. Environ. Prot.* **2020**, *135*, 22–37. https://doi.org/10.1016/j.psep.2019.12.035.

22. Reynoso, E.C.; Torres, E.; Bettazzi, F.; Palchetti, I. Trends and perspectives in immunosensors for determination of currently-used pesticides: The case of glyphosate, organophosphates, and neonicotinoids. *Biosensors* **2019**, *9*, 20. https://doi.org/10.3390/bios9010020.

23. EFSA. Conclusion on the peer review of the pesticide risk assessment of the active substance glyphosate. *EFSA J.* **2017**, *13*, 4302. https://doi.org/10.2903/j.efsa.2015.4302.

24. International Agency for Research on Cancer. *Evaluation of Five Organophosphate Insecticides and Herbicides*; World Health Organization: Lyon, France, 2015.

25. Guyton, K.Z.; Loomis, D.; Grosse, Y.; El Ghissassi, F.; Benbrahim-Tallaa, L.; Guha, N.; Scoccianti, C.; Mattock, H.; Straif, K.; Blair, A.; et al. Carcinogenicity of tetrachlorvinphos, parathion, malathion, diazinon, and glyphosate. *Lancet Oncol.* **2015**, *16*, 490–491. https://doi.org/10.1016/S1470-2045(15)70134-8.

26. Mesnage, R.; Defarge, N.; Spiroux de Vendômois, J.; Séralini, G.E. Potential toxic effects of glyphosate and its commercial formulations below regulatory limits. *Food Chem. Toxicol.* **2015**, *84*, 133–153. https://doi.org/10.1016/j.fct.2015.08.012.

27. Banaee, M.; Akhlaghi, M.; Soltanian, S.; Sureda, A.; Gholamhosseini, A.; Rakhshaninejad, M. Combined effects of exposure to sub-lethal concentration of the insecticide chlorpyrifos and the herbicide glyphosate on the biochemical changes in the freshwater crayfish Pontastacus leptodactylus. *Ecotoxicology* **2020**, *29*, 1500–1515. https://doi.org/10.1007/s10646-020-02233-0.

28. Ingaramo, P.; Alarcón, R.; Muñoz-de-Toro, M.; Luque, E.H. Are glyphosate and glyphosate-based herbicides endocrine disruptors that alter female fertility? *Mol. Cell. Endocrinol.* **2020**, *518*, 110934. https://doi.org/10.1016/j.mce.2020.110934.

29. Meftaul, I.M.; Venkateswarlu, K.; Dharmarajan, R.; Annamalai, P.; Asaduzzaman, M.; Parven, A.; Megharaj, M. Controversies over human health and ecological impacts of glyphosate: Is it to be banned in modern agriculture? *Environ. Pollut.* **2020**, *263*, 114372. https://doi.org/10.1016/j.envpol.2020.114372.

30. Peillex, C.; Pelletier, M. The impact and toxicity of glyphosate and glyphosate-based herbicides on health and immunity. *J. Immunotoxicol.* **2020**, *17*, 163–174. https://doi.org/10.1080/1547691X.2020.1804492.

31. Lu, T.; Xu, N.; Zhang, Q.; Zhang, Z.; Debognies, A.; Zhou, Z.; Sun, L.; Qian, H. Understanding the influence of glyphosate on the structure and function of freshwater microbial community in a microcosm. *Environ. Pollut.* **2020**, *260*, 114012. https://doi.org/10.1016/j.envpol.2020.114012.

32. Valle, A.L.; Mello, F.C.C.; Alves-Balvedi, R.P.; Rodrigues, L.P.; Goulart, L.R. Glyphosate detection: Methods, needs and challenges. *Environ. Chem. Lett.* **2019**, *17*, 291–317. https://doi.org/10.1007/s10311-018-0789-5.

33. European Commission. Council Directive 98/83/EC on the Quality of Water Intended for Human Consumption. Friends of Earth Europe 2013, Friends of Earth Europe. The Environmental Effects of Glyphosate (2013). Available online: https://www.foeeurope.org/sites/default/files/press_releases/foee_5_environmental_impacts_glyphosate.pdf (accessed on 1st April 2022).

34. Environmental Protection Agency. National Primary Drinking Water Regulations EPA 816 F 09 0004. *Epa* **2009**. Available online: https://www.epa.gov/sites/default/files/2016-06/documents/npwdr_complete_table.pdf (accessed on 1 April 2022).

35. US EPA Drinking Water Contaminants: National Primary Drinking Water Regulations. US EPA. 2015. Available online: http//water.epa.gov/drink/contaminants/index.cfm (accessed on 1 April 2022)..

36. Health Canada. *Guidelines for Canadian Drinking Water Quality—Summary Table. Water and Air Quality Bureau, Healthy Environments and Consumer Safety Branch*, Health Canada: Ottawa, ON, Canada, 2020. Available online: https://www.canada.ca/content/dam/hc-sc/migration/hc-sc/ewh-semt/alt_formats/pdf/pubs/water-eau/sum_guide-res_recom/summary-table-EN-2020-02-11.pdf (accessed on 1 April 2022).

37. Secretaría de Salud, S. NOM-201-SSA1-2015, Productos y Servicios. Agua y hielo para Consumo Humano, Envasados y a Granel. Especificaciones Sanitarias. *D. Of. Fed.* Available online: https://dof.gob.mx/nota_detalle.php?codigo=5420977&fecha=22/12/2015#gsc.t (accessed on 1 April 2022).

38. Hamilton, D.J.; Ambrus, Á.; Dieterle, R.M.; Felsot, A.S.; Harris, C.A.; Holland, P.T.; Katayama, A.; Kuriharas, N.; Linders, J.; Unsworth, J.; et al. Regulatory limits for pesticide residues in water (IUPAC technical report). *Pure Appl. Chem.* **2003**, *75*, 1123–1155. https://doi.org/10.1351/pac200375081123.

39. Li, Z.; Jennings, A. Worldwide regulations of standard values of pesticides for human health risk control: A review. *Int. J. Environ. Res. Public Health* **2017**, *14*, 826. https://doi.org/10.3390/ijerph14070826.

40. Tarazona, J.V.; Court-Marques, D.; Tiramani, M.; Reich, H.; Pfeil, R.; Istace, F.; Crivellente, F. Glyphosate toxicity and carcinogenicity: A review of the scientific basis of the European Union assessment and its differences with IARC. *Arch. Toxicol.* **2017**, *91*, 2723–2743. https://doi.org/10.1007/s00204-017-1962-5.

41. Winfield, T.W.; Bashe, W.J.; Baker, T.V. Method 547 Determination of Glyphosate in Drinking Water By Direct-Aqueous-Injection Hplc, Post-Column Derivatization, and Fluorescence Detection. *Technol. Appl.* **1990**, *1*, 1–16.

42. Mitra, S.; Patnaik, P.; Kebbekus, B.B. *Environmental Chemical Analysis*; CRC Press: New York, NY, USA, 2019; ISBN 9780849338380.

43. Okada, E.; Coggan, T.; Anumol, T.; Clarke, B.; Allinson, G. A simple and rapid direct injection method for the determination of glyphosate and AMPA in environmental water samples. *Anal. Bioanal. Chem.* **2019**, *411*, 715–724. https://doi.org/10.1007/s00216-018-1490-z.

44. Begum, S.S.; Sushmaa, B.S.; Vijayaraja, S. Bioanalytical Techniques–An Overview. *PharmaTutor* **2015**, *3*, 14–24.

45. Peng, J.; Tang, F.; Zhou, R.; Xie, X.; Li, S.; Xie, F.; Yu, P.; Mu, L. New techniques of on-line biological sample processing and their application in the field of biopharmaceutical analysis. *Acta Pharm. Sin. B* **2016**, *6*, 540–551. https://doi.org/10.1016/j.apsb.2016.05.016.

46. Koskinen, W.C.; Marek, L.J.; Hall, K.E. Analysis of glyphosate and aminomethylphosphonic acid in water, plant materials and soil. *Pest Manag. Sci.* **2016**, *72*, 423–432. https://doi.org/10.1002/ps.4172.

47. Zouaoui, K.; Dulaurent, S.; Gaulier, J.M.; Moesch, C.; Lacha, G. Determination of glyphosate and AMPA in blood and urine from humans: About 13 cases of acute intoxication. *Forensic Sci. Int. J.* **2013**, *226*, 20–25. https://doi.org/10.1016/j.forsciint.2012.12.010.

48. Oulkar, D.P.; Hingmire, S.; Goon, A.; Jadhav, M.; Ugare, B.; Thekkumpurath, A.S.; Banerjee, K. Optimization and validation of a residue analysis method for glyphosate, glufosinate, and their metabolites in plant matrixes by liquid chromatography with tandem mass spectrometry. *J. AOAC Int.* **2017**, *100*, 631–639. https://doi.org/10.5740/jaoacint.17-0046.

49. Fontàs, C.; Sanchez, J.M. Evaluation and optimization of the derivatization reaction conditions of glyphosate and aminomethylphosphonic acid with 6-aminoquinolyl-N-hydroxysuccinimidyl carbamate using reversed-phase liquid chromatography. *J. Sep. Sci.* **2020**, *43*, 3931–3939. https://doi.org/10.1002/jssc.202000645.

50. Pires, N.L.; Passos, C.J.S.; Morgado, M.G.A.; Mello, D.C.; Infante, C.M.C.; Caldas, E.D. Determination of glyphosate, AMPA and glufosinate by high performance liquid chromatography with fluorescence detection in waters of the Santarém Plateau, Brazilian Amazon. *J. Environ. Sci. Health Part B Pestic. Food Contam. Agric. Wastes* **2020**, *55*, 794–802. https://doi.org/10.1080/03601234.2020.1784668.

51. Mazouz, Z.; Rahali, S.; Fourati, N.; Zerrouki, C.; Aloui, N.; Seydou, M.; Yaakoubi, N.; Chehimi, M.M.; Othmane, A.; Kalfat, R. Highly selective polypyrrole MIP-based gravimetric and electrochemical sensors for picomolar detection of glyphosate. *Sensors* **2017**, *17*, 258. https://doi.org/10.3390/s17112586.

52. Thevenot, D.R.; Toth, K.; Durst, R.A.; Wilson, G.S. International union of pure and applied chemistry physical chemistry division, steering committee on biophysical chemistry analytical chemistry division, commission V.5 (electroanalytical chemistry) Electrochemical biosensors: Proposed definitions and cla. *Sens. Actuators B Chem.* **1996**, 30, 81. https://doi.org/10.1016/0925-4005(95)01816-6.

53. Saxena, U.; Das, A.B. Nanomaterials towards fabrication of cholesterol biosensors: Key roles and design approaches. *Biosens. Bioelectron.* **2016**, *75*, 196–205. https://doi.org/10.1016/j.bios.2015.08.042.

54. Rawtani, D.; Khatri, N.; Tyagi, S.; Pandey, G. Nanotechnology-based recent approaches for sensing and remediation of pesticides. *J. Environ. Manag.* **2018**, *206*, 749–762. https://doi.org/10.1016/j.jenvman.2017.11.037.

55. Bănică, F.G. *Chemical Sensors and Biosensors: Fundamentals and Applications;* John Wiley & Sons: Hoboken, NJ, USA, 2012; ISBN 9780470710661.

56. Korotkaya, E.V. Biosensors: Design, classification, and applications in the food industry. *Foods Raw Mater.* **2014**, *2*, 161–171. https://doi.org/10.12737/5476.

57. Arduini, F.; Cinti, S.; Scognamiglio, V.; Moscone, D.; Palleschi, G. How cutting-edge technologies impact the design of electrochemical (bio)sensors for environmental analysis. A review. *Anal. Chim. Acta* **2017**, *959*, 15–42. https://doi.org/10.1016/j.aca.2016.12.035.

58. Sanchís, J.; Kantiani, L.; Llorca, M.; Rubio, F.; Ginebreda, A.; Fraile, J.; Garrido, T.; Farré, M. Determination of glyphosate in groundwater samples using an ultrasensitive immunoassay and confirmation by on-line solid-phase extraction followed by liquid chromatography coupled to tandem mass spectrometry. *Anal. Bioanal. Chem.* **2012**, *402*, 2335–2345. https://doi.org/10.1007/s00216-011-5541-y.

59. Chuang, H.Y.; Hong, T.P.; Whang, C.W. A simple and rapid screening method for glyphosate in water using flow-injection with electrochemiluminescence detection. *Anal. Methods* **2013**, *5*, 6186–6191. https://doi.org/10.1039/c3ay41059e.

60. Fang, F.; Wei, R.; Liu, X. Novel pre-column derivatisation reagent for glyphosate by high-performance liquid chromatography and ultraviolet detection. *Int. J. Environ. Anal. Chem.* **2014**, *94*, 661–667. https://doi.org/10.1080/03067319.2013.864648.

61. Pérez, A.L.; Tibaldo, G.; Sánchez, G.H.; Siano, G.G.; Marsili, N.R.; Schenone, A.V. A novel fluorimetric method for glyphosate and AMPA determination with NBD-Cl and MCR-ALS. *Spectrochim. Acta Part A Mol. Biomol. Spectrosc.* **2019**, *214*, 119–128. https://doi.org/10.1016/j.saa.2019.01.078.

62. Romero-Natale, A.; Palchetti, I.; Avelar, M.; González-Vergara, E.; Garate-Morales, J.L.; Torres, E. Spectrophotometric detection of glyphosate in water by complex formation between bis 5-phenyldipyrrinate of nickel (II) and glyphosate. *Water* **2019**, *11*, 719. https://doi.org/10.3390/w11040719.

63. Ramirez, C.E.; Bellmund, S.; Gardinali, P.R. A simple method for routine monitoring of glyphosate and its main metabolite in surface waters using lyophilization and LC-FLD + MS/MS. Case study: Canals with influence on Biscayne National Park. *Sci. Total Environ.* **2014**, *496*, 389–401. https://doi.org/10.1016/j.scitotenv.2014.06.118.

64. Guo, H.; Gao, Y.; Guo, D.; Liu, W.; Wang, J.; Zheng, J.; Zhong, J.; Zhao, Q. Sensitive, rapid and non-derivatized determination of glyphosate, glufosinate, bialaphos and metabolites in surface water by LC–MS/MS. *SN Appl. Sci.* **2019**, *1*, 305. https://doi.org/10.1007/s42452-019-0306-x.

65. Wang, S.; Liu, B.; Yuan, D.; Ma, J. A simple method for the determination of glyphosate and aminomethylphosphonic acid in seawater matrix with high performance liquid chromatography and fluorescence detection. *Talanta* **2016**, *161*, 700–706. https://doi.org/10.1016/j.talanta.2016.09.023.

66. Dai, H.; Sang, M.; Wang, Y.; Du, R.; Yuan, W.; Jia, Z.; Cao, Z.; Chen, X. Determination of trace glyphosate in water with a prism coupling optical waveguide configuration. *Sens. Actuators A Phys.* **2014**, *218*, 88–93. https://doi.org/10.1016/j.sna.2014.07.022.

67. Wei, X.; Gao, X.; Zhao, L.; Peng, X.; Zhou, L.; Wang, J.; Pu, Q. Fast and interference-free determination of glyphosate and glufosinate residues through electrophoresis in disposable microfluidic chips. *J. Chromatogr. A* **2013**, *1281*, 148–154. https://doi.org/10.1016/j.chroma.2013.01.039.

68. Mörtl, M.; Németh, G.; Juracsek, J.; Darvas, B.; Kamp, L.; Rubio, F.; Székács, A. Determination of glyphosate residues in Hungarian water samples by immunoassay. *Microchem. J.* **2013**, *107*, 143–151. https://doi.org/10.1016/j.microc.2012.05.021.

69. Zhang, W.; Feng, Y.; Ma, L.; An, J.; Zhang, H.; Cao, M. A method for determining glyphosate and its metabolite aminomethyl phosphonic acid by gas chromatography-flame photometric detection. *J. Chromatogr. A* **2019**, *1589*, 116–121. https://doi.org/10.1016/j.chroma.2018.12.039.

70. Oliveira Pereira, E.A.; Freitas Melo, V.; Abate, G.; Masini, J.C. Determination of glyphosate and aminomethylphosphonic acid by sequential-injection reversed-phase chromatography: Method improvements and application in adsorption studies. *Anal. Bioanal. Chem.* **2019**, *411*, 2317–2326. https://doi.org/10.1007/s00216-019-01672-x.

71. Sharma, P.; Pandey, V.; Sharma, M.M.M.; Patra, A.; Singh, B.; Mehta, S.; Husen, A. A Review on Biosensors and Nanosensors Application in Agroecosystems. *Nanoscale Res. Lett.* **2021**, *16*, 136. https://doi.org/10.1186/s11671-021-03593-0.

72. Vikesland, P.J. Nanosensors for water quality monitoring. *Nat. Nanotechnol.* **2018**, *13*, 651–660. https://doi.org/10.1038/s41565-018-0209-9.

73. Cao, Y.; Wang, L.; Shen, C.; Wang, C.; Hu, X.; Wang, G. An electrochemical sensor on the hierarchically porous Cu-BTC MOF platform for glyphosate determination. *Sens. Actuators B Chem.* **2019**, *283*, 487–494. https://doi.org/10.1016/j.snb.2018.12.064.

74. Gupta, A.; Eral, H.B.; Hatton, T.A.; Doyle, P.S. Nanoemulsions: Formation, properties and applications. *Soft Matter* **2016**, *12*, 2826–2841. https://doi.org/10.1039/c5sm02958a.

75. Kurbanoglu, S.; Ozkan, S.A.; Merkoçi, A. Nanomaterials-based enzyme electrochemical biosensors operating through inhibition for biosensing applications. *Biosens. Bioelectron.* **2017**, *89*, 886–898. https://doi.org/10.1016/j.bios.2016.09.102.

76. Jampílek, J.; Kráľová, K.; Campos, E.V.R.; Fraceto, L.F. Bio-Based Nanoemulsion Formulations Applicable in Agriculture, Medicine, and Food Industry. In *Nanobiotechnology in Bioformulations*; Springer: Cham, Switzerland, 2019; pp. 33–84.

77. Dasgupta, N.; Ranjan, S.; Chakraborty, A.R.; Ramalingam, C.; Shanker, R.; Kumar, A. Nanoagriculture and Water Quality Management. In *Nanoscience in Food and Agriculture 1*; Springer: Cham, Switzerland, 2016; pp. 1–43, ISBN 9783319393056.

78. Chen, J.; Andler, S.M.; Goddard, J.M.; Nugen, S.R.; Rotello, V.M. Integrating recognition elements with nanomaterials for bacteria sensing. *Chem. Soc. Rev.* **2017**, *46*, 1272–1283. https://doi.org/10.1039/c6cs00313c.

79. Reynoso, E.C.; Romero-Guido, C.; Rebollar-Pérez, G.; Torres, E. Chapter 16—Enzymatic biosensors for the detection of water pollutants. In *Enzymatic Biosensors for the Detection of Water Pollutants*; Elsevier: Amsterdam, The Netherlands, 2022; pp. 463–511.

80. Pokropivny, V.V.; Skorokhod, V.V. Classification of nanostructures by dimensionality and concept of surface forms engineering in nanomaterial science. *Mater. Sci. Eng. C* **2007**, 27, 990–993. https://doi.org/10.1016/j.msec.2006.09.023.

81. Saleh, T.A. Nanomaterials: Classification, properties, and environmental toxicities. *Environ. Technol. Innov.* **2020**, *20*, 101067. https://doi.org/10.1016/j.eti.2020.101067.

82. Wang, Z.; Hu, T.; Liang, R.; Wei, M. Application of Zero-Dimensional Nanomaterials in Biosensing. *Front. Chem.* **2020**, *8*, 320. https://doi.org/10.3389/fchem.2020.00320.

83. Zhou, Y.; Tang, L.; Zeng, G.; Zhang, C.; Zhang, Y.; Xie, X. Sensors and Actuators B : Chemical Current progress in biosensors for heavy metal ions based on DNAzymes / DNA molecules functionalized nanostructures : A review. *Sens. Actuators B. Chem.* **2016**, *223*, 280–294. https://doi.org/10.1016/j.snb.2015.09.090.

84. Srivastava, A.K.; Dev, A.; Karmakar, S. Nanosensors and nanobiosensors in food and agriculture. *Environ. Chem. Lett.* **2018**, *16*, 161–182. https://doi.org/10.1007/s10311-017-0674-7.

85. Campbell, F.W.; Compton, R.G. The use of nanoparticles in electroanalysis: An updated review. *Anal. Bioanal. Chem.* **2010**, *396*, 241–259. https://doi.org/10.1007/s00216-009-3063-7.

86. Maduraiveeran, G.; Sasidharan, M.; Ganesan, V. Electrochemical sensor and biosensor platforms based on advanced nanomaterials for biological and biomedical applications. *Biosens. Bioelectron.* **2018**, *103*, 113–129. https://doi.org/10.1016/j.bios.2017.12.031.

87. Li, Z.; Li, X.; Jian, M.; Geleta, G.S.; Wang, Z. Two-Dimensional Layered Nanomaterial-Based Electrochemical Biosensors for Detecting Microbial Toxins. *Toxins* **2019**, *12*, 20.

88. Su, S.; Sun, Q.; Gu, X.; Xu, Y.; Shen, J.; Zhu, D.; Chao, J.; Fan, C.; Wang, L. Two-dimensional nanomaterials for biosensing applications. *TrAC Trends Anal. Chem.* **2019**, *119*, 115610. https://doi.org/10.1016/j.trac.2019.07.021.

89. Zeng, Y.; Zhu, Z.; Du, D.; Lin, Y. Nanomaterial-based electrochemical biosensors for food safety. *J. Electroanal. Chem.* **2016**, *781*, 147–154. https://doi.org/10.1016/j.jelechem.2016.10.030.

90. Lv, M.; Liu, Y.; Geng, J.; Kou, X.; Xin, Z.; Yang, D. Engineering nanomaterials-based biosensors for food safety detection. *Biosens. Bioelectron.* **2018**, *106*, 122–128. https://doi.org/10.1016/j.bios.2018.01.049.

91. Banwaskar, M.R.; Dachawar, S.N. Dachawar Nanotechnology: A New Perspective for Management of Environment. *Int. Journal Res. Anal. Rev.* **2019**, *6*, 78–82.

92. Messina, G.A.; Regiart, M.; Pereira, S.V.; Bertolino, F.A.; Aranda, P.R.; Raba, J.; Fernández-Baldo, M.A. Nanomaterials in the Development of Biosensor and Application in the Determination of Pollutants in Water. In *Advanced Research in Nanosciences for Water Technology*; Springer: Cham, Switzerland, 2019; pp. 195–215.

93. Chen, H.; Zhang, L.; Hu, Y.; Zhou, C.; Lan, W.; Fu, H.; She, Y. Nanomaterials as optical sensors for application in rapid detection of food contaminants, quality and authenticity. *Sens. Actuators B. Chem.* **2021**, *329*, 129135. https://doi.org/10.1016/j.snb.2020.129135.

94. Wu, Z.; Yang, S.; Wu, W. Shape control of inorganic nanoparticles from solution. *Nanoscale* **2016**, *8*, 1237–1259. https://doi.org/10.1039/c5nr07681a.

95. Liu, G.; Lu, M.; Huang, X.; Li, T.; Xu, D. Application of gold-nanoparticle colorimetric sensing to rapid food safety screening. *Sensors* **2018**, *18*, 416. https://doi.org/10.3390/s18124166.

96. Priyadarshini, E.; Pradhan, N. Gold nanoparticles as efficient sensors in colorimetric detection of toxic metal ions: A review. *Sens. Actuators B Chem.* **2017**, *238*, 888–902. https://doi.org/10.1016/j.snb.2016.06.081.

97. Gaviña, P.; Parra, M.; Gil, S.; Costero, A.M. *Red or Blue? Gold Nanoparticles in Colorimetric Sensing*; IntechOpen: London, UK, 2018; pp. 3–15. https://doi.org/10.1016/j.colsurfa.2011.12.014.

98. Csáki, A.; Stranik, O.; Fritzsche, W. Localized surface plasmon resonance based biosensing. *Expert Rev. Mol. Diagn.* **2018**, *18*, 279–296. https://doi.org/10.1080/14737159.2018.1440208.

99. Zheng, J.; Zhang, H.; Qu, J.; Zhu, Q.; Chen, X. Visual detection of glyphosate in environmental water samples using cysteamine-stabilized gold nanoparticles as colorimetric probe. *Anal. Methods* **2013**, *5*, 917–924. https://doi.org/10.1039/c2ay26391b.

100. Do, M.H.; Florea, A.; Farre, C.; Bonhomme, A.; Bessueille, F.; Vocanson, F.; Tran-Thi, N.T.; Jaffrezic-Renault, N. Molecularly imprinted polymer-based electrochemical sensor for the sensitive detection of glyphosate herbicide. *Int. J. Environ. Anal. Chem.* **2015**, *95*, 1489–1501. https://doi.org/10.1080/03067319.2015.1114109.

101. Nafisah, S.; Morsin, M.; Jumadi, N.A.; Nayan, N.; Mohd Shah, N.S.; Razali, N.L.; An'nisa, N.Z. Improved Sensitivity and Selectivity of Direct Localized Surface Plasmon Resonance Sensor Using Gold Nanobipyramids for Glyphosate Detection. *IEEE Sens. J.* **2020**, *20*, 2378–2389. https://doi.org/10.1109/JSEN.2019.2953928.

102. Liu, H.; Chen, P.; Liu, Z.; Liu, J.; Yi, J.; Xia, F.; Zhou, C. Electrochemical luminescence sensor based on double suppression for highly sensitive detection of glyphosate. *Sens. Actuators B Chem.* **2020**, *304*, 127364. https://doi.org/10.1016/j.snb.2019.127364.

103. Song, D.; Wang, Y.; Lu, X.; Gao, Y.; Li, Y.; Gao, F. Ag nanoparticles-decorated nitrogen-fluorine co-doped monolayer MoS2 nanosheet for highly sensitive electrochemical sensing of organophosphorus pesticides. *Sens. Actuators B Chem.* **2018**, *267*, 5–13. https://doi.org/10.1016/j.snb.2018.04.016.

104. Xie, Y.; Yu, Y.; Lu, L.; Ma, X.; Gong, L.; Huang, X.; Liu, G.; Yu, Y. CuO nanoparticles decorated 3D graphene nanocomposite as non-enzymatic electrochemical sensing platform for malathion detection. *J. Electroanal. Chem.* **2018**, *812*, 82–89. https://doi.org/10.1016/j.jelechem.2018.01.043.

105. Tan, M.J.; Hong, Z.Y.; Chang, M.H.; Liu, C.C.; Cheng, H.F.; Loh, X.J.; Chen, C.H.; Liao, C.D.; Kong, K.V. Metal carbonyl-gold nanoparticle conjugates for highly sensitive SERS detection of organophosphorus pesticides. *Biosens. Bioelectron.* **2017**, *96*, 167–172. https://doi.org/10.1016/j.bios.2017.05.005.

106. Wang, L.; Bi, Y.; Hou, J.; Li, H.; Xu, Y.; Wang, B.; Ding, H.; Ding, L. Facile, green and clean one-step synthesis of carbon dots from wool: Application as a sensor for glyphosate detection based on the inner filter effect. *Talanta* **2016**, *160*, 268–275. https://doi.org/10.1016/j.talanta.2016.07.020.

107. De Goes, R.E.; Possetti, G.R.C.; Muller, M.; Fabris, J.L. Tuning of Citrate-Stabilized Laser Ablated Silver Nanoparticles for Glyphosate Detection. *IEEE Sens. J.* **2020**, *20*, 1843–1850. https://doi.org/10.1109/JSEN.2019.2950161.

108. Setznagl, S.; Cesarino, I. Copper nanoparticles and reduced graphene oxide modified a glassy carbon electrode for the determination of glyphosate in water samples. *Int. J. Environ. Anal. Chem.* **2022**, *102*, 293–305. https://doi.org/10.1080/03067319.2020.1720667.

109. Bataller, R.; Campos, I.; Laguarda-Miro, N.; Alcañiz, M.; Soto, J.; Martínez-Máñez, R.; Gil, L.; García-Breijo, E.; Ibáñez-Civera, J. Glyphosate detection by means of a voltammetric electronic tongue and discrimination of potential interferents. *Sensors* **2012**, *12*, 17553–17568. https://doi.org/10.3390/s121217553.

110. Del Carmen Aguirre, M.; Urreta, S.E.; Gomez, C.G. A Cu2+-Cu/glassy carbon system for glyphosate determination. *Sens. Actuators B Chem.* **2019**, *284*, 675–683. https://doi.org/10.1016/j.snb.2018.12.124.

111. Regiart, M.; Kumar, A.; Gonçalves, J.M.; Junior, G.J.S.; Masini, J.C.; Angnes, L.; Bertottii, M. An Electrochemically Synthesized Nanoporous Copper Microsensor for Highly Sensitive and Selective Determination of Glyphosate. *ChemElectroChem* **2020**, *7*, 1558–1566. https://doi.org/10.1002/celc.202000064.

112. Chang, Y.C.; Lin, Y.S.; Xiao, G.T.; Chiu, T.C.; Hu, C.C. A highly selective and sensitive nanosensor for the detection of glyphosate. *Talanta* **2016**, *161*, 94–98. https://doi.org/10.1016/j.talanta.2016.08.029.

113. Wang, X.; Sakinati, M.; Yang, Y.; Ma, Y.; Yang, M.; Luo, H.; Hou, C.; Huo, D. The construction of a CND/Cu2+ fluorescence sensing system for the ultrasensitive detection of glyphosate. *Anal. Methods* **2020**, *12*, 520–527. https://doi.org/10.1039/c9ay02303h.

114. Liu, Z.; Yang, L.; Sharma, A.S.; Chen, M.; Chen, Q. A system composed of polyethylenimine-capped upconversion nanoparticles, copper(II), hydrogen peroxide and 3,3',5,5'-tetramethylbenzidine for colorimetric and fluorometric determination of glyphosate. *Microchim. Acta* **2019**, *186*, 835. https://doi.org/10.1007/s00604-019-3936-1.

115. Jiang, R.; Pang, Y.H.; Yang, Q.Y.; Wan, C.Q.; Shen, X.F. Copper porphyrin metal-organic framework modified carbon paper for electrochemical sensing of glyphosate. *Sens. Actuators B Chem.* **2022**, *358*, 131492. https://doi.org/10.1016/j.snb.2022.131492.

116. Yang, Y.; Li, L.; Lin, L.; Wang, X.; Li, J.; Liu, H.; Liu, X.; Huo, D.; Hou, C. A dual-signal sensing strategy based on ratiometric fluorescence and colorimetry for determination of Cu2+ and glyphosate. *Anal. Bioanal. Chem.* **2022**, *414*, 2619–2628. https://doi.org/10.1007/s00216-022-03898-8.

117. Vaghela, C.; Kulkarni, M.; Haram, S.; Aiyer, R.; Karve, M. A novel inhibition based biosensor using urease nanoconjugate entrapped biocomposite membrane for potentiometric glyphosate detection. *Int. J. Biol. Macromol.* **2018**, *108*, 32–40. https://doi.org/10.1016/j.ijbiomac.2017.11.136.

118. Zhang, Z.; Zeng, K.; Liu, J. Immunochemical detection of emerging organic contaminants in environmental waters. *TrAC Trends Anal. Chem.* **2017**, *87*, 49–57. https://doi.org/10.1016/j.trac.2016.12.002.

119. Stavra, E.; Petrou, P.S.; Koukouvinos, G.; Economou, A.; Goustouridis, D.; Misiakos, K.; Raptis, I.; Kakabakos, S.E. Fast, sensitive and selective determination of herbicide glyphosate in water samples with a White Light Reflectance Spectroscopy immunosensor. *Talanta* **2020**, *214*, 120854. https://doi.org/10.1016/j.talanta.2020.120854.

120. Sharma, R.; Ragavan, K.V.; Thakur, M.S.; Raghavarao, K.S.M.S. Recent advances in nanoparticle based aptasensors for food contaminants. *Biosens. Bioelectron.* **2015**, *74*, 612–627. https://doi.org/10.1016/j.bios.2015.07.017.

121. Viirlaid, E.; Ilisson, M.; Kopanchuk, S.; Mäeorg, U.; Rinken, A.; Rinken, T. Immunoassay for rapid on-site detection of glyphosate herbicide. *Environ. Monit. Assess.* **2019**, *191*, 507. https://doi.org/10.1007/s10661-019-7657-z.

122. Chen, F.; Li, G.; Liu, H.; Leung, C.; Ma, D. G-quadruplex-based detection of glyphosate in complex biological systems by a time-resolved luminescent assay. *Sens. Actuators B Chem.* **2020**, *320*, 128393. https://doi.org/10.1016/j.snb.2020.128393.

123. Zhang, M.; Li, G.; Zhou, Q.; Pan, D.; Zhu, M.; Xiao, R.; Zhang, Y.; Wu, G.; Wan, Y.; Shen, Y. Boosted Electrochemical Immunosensing of Genetically Modified Crop Markers Using Nanobody and Mesoporous Carbon. *ACS Sens.* **2018**, *3*, 684–691. https://doi.org/10.1021/acssensors.8b00011.

124. Wang, X.; Qin, L.; Zhou, M.; Lou, Z.; Wei, H. Nanozyme Sensor Arrays for Detecting Versatile Analytes from Small Molecules to Proteins and Cells. *Anal. Chem.* **2018**, *90*, 11696–11702. https://doi.org/10.1021/acs.analchem.8b03374.

125. Qiu, L.; Lv, P.; Zhao, C.; Feng, X.; Fang, G.; Liu, J.; Wang, S. Electrochemical detection of organophosphorus pesticides based on amino acids conjugated nanoenzyme modified electrodes. *Sens. Actuators B Chem.* **2019**, *286*, 386–393. https://doi.org/10.1016/j.snb.2019.02.007.

126. Ma, J.; Feng, G.; Ying, Y.; Shao, Y.; She, Y.; Zheng, L.; Ei-aty, A.M.A.; Wang, J. Sensitive SERS assay for glyphosate based on the prevention of L -cysteine inhibition of a Au–Pt nanozyme. *Analyst* **2021**, *146*, 956–963. https://doi.org/10.1039/d0an01919d.

127. Wang, D.; Lin, B.; Cao, Y.; Guo, M.; Yu, Y. A Highly Selective and Sensitive Fluorescence Detection Method of Glyphosate Based on an Immune Reaction Strategy of Carbon Dot Labeled Antibody and Antigen Magnetic Beads. *J. Agric. Food Chem.* **2016**, *64*, 6042–6050. https://doi.org/10.1021/acs.jafc.6b01088.

128. Li, X.; Tang, X.; Chen, X.; Qu, B.; Lu, L. Label-free and enzyme-free fluorescent isocarbophos aptasensor based on MWCNTs and G-quadruplex. *Talanta* **2018**, *188*, 232–237. https://doi.org/10.1016/j.talanta.2018.05.092.

129. Bettazzi, F.; Natale, A.R.; Torres, E.; Palchetti, I. Glyphosate determination by coupling an immuno-magnetic assay with electrochemical sensors. *Sensors* **2018**, *18*, 2965. https://doi.org/10.3390/s18092965.

130. Guan, N.; Li, Y.; Yang, H.; Hu, P.; Lu, S.; Ren, H.; Liu, Z.; Soo Park, K.; Zhou, Y. Dual-functionalized gold nanoparticles probe based bio-barcode immuno-PCR for the detection of glyphosate. *Food Chem.* **2021**, *338*, 128133. https://doi.org/10.1016/j.foodchem.2020.128133.

131. Bala, R.; Kumar, M.; Bansal, K.; Sharma, R.K.; Wangoo, N. Ultrasensitive aptamer biosensor for malathion detection based on cationic polymer and gold nanoparticles. *Biosens. Bioelectron.* **2016**, *85*, 445–449. https://doi.org/10.1016/j.bios.2016.05.042.

132. Bala, R.; Sharma, R.K.; Wangoo, N. Development of gold nanoparticles-based aptasensor for the colorimetric detection of organophosphorus pesticide phorate. *Anal. Bioanal. Chem.* **2016**, *408*, 333–338. https://doi.org/10.1007/s00216-015-9085-4.

133. Bala, R.; Dhingra, S.; Kumar, M.; Bansal, K.; Mittal, S.; Sharma, R.K.; Wangoo, N. Detection of organophosphorus pesticide–Malathion in environmental samples using peptide and aptamer based nanoprobes. *Chem. Eng. J.* **2017**, *311*, 111–116. https://doi.org/10.1016/j.cej.2016.11.070.

134. Bala, R.; Mittal, S.; Sharma, R.K.; Wangoo, N. A supersensitive silver nanoprobe based aptasensor for low cost detection of malathion residues in water and food samples. *Spectrochim. Acta Part A Mol. Biomol. Spectrosc.* **2018**, *196*, 268–273. https://doi.org/10.1016/j.saa.2018.02.007.

135. Bala, R.; Swami, A.; Tabujew, I.; Peneva, K.; Wangoo, N.; Sharma, R.K. Ultra-sensitive detection of malathion using quantum dots-polymer based fluorescence aptasensor. *Biosens. Bioelectron.* **2018**, *104*, 45–49. https://doi.org/10.1016/j.bios.2017.12.034.

136. Madianos, L.; Skotadis, E.; Tsekenis, G.; Patsiouras, L.; Tsigkourakos, M.; Tsoukalas, D. Impedimetric Nanoparticle Aptasensor for Selective and Label Free Pesticide Detection. *Microelectron. Eng.* **2018**, *189*, 39–45. https://doi.org/10.1016/j.mee.2017.12.016.

137. Madianos, L.; Tsekenis, G.; Skotadis, E.; Patsiouras, L.; Tsoukalas, D. A highly sensitive impedimetric aptasensor for the selective detection of acetamiprid and atrazine based on microwires formed by platinum nanoparticles. *Biosens. Bioelectron.* **2018**, *101*, 268–274. https://doi.org/10.1016/j.bios.2017.10.034.

138. Fu, J.; An, X.; Yao, Y.; Guo, Y.; Sun, X. Electrochemical aptasensor based on one step co-electrodeposition of aptamer and GO-CuNPs nanocomposite for organophosphorus pesticide detection. *Sens. Actuators B Chem.* **2019**, *287*, 503–509. https://doi.org/10.1016/j.snb.2019.02.057.

139. Liu, H.; Cheng, S.; Shi, X.; Zhang, H.; Zhao, Q.; Dong, H.; Guo, Y.; Sun, X. Electrochemiluminescence Aptasensor for Profenofos Detection Based on Silver Nanoparticles Enhanced Luminol Luminescence System. *J. Electrochem. Soc.* **2019**, *166*, B1562–B1566. https://doi.org/10.1149/2.0801915jes.

140. Jiang, M.; Chen, C.; He, J.; Zhang, H.; Xu, Z. Fluorescence assay for three organophosphorus pesticides in agricultural products based on Magnetic-Assisted fluorescence labeling aptamer probe. *Food Chem.* **2020**, *307*, 125534. https://doi.org/10.1016/j.foodchem.2019.125534.

141. Bucur, B.; Munteanu, F.D.; Marty, J.L.; Vasilescu, A. Advances in enzyme-based biosensors for pesticide detection. *Biosensors* **2018**, *8*, 27. https://doi.org/10.3390/bios8020027.

142. Sun, Y.; Wei, J.; Zou, J.; Cheng, Z.; Huang, Z.; Gu, L.; Zhong, Z.; Li, S.; Wang, Y.; Li, P. Electrochemical detection of methyl-paraoxon based on bifunctional cerium oxide nanozyme with catalytic activity and signal amplification effect. *J. Pharm. Anal.* **2021**, *11*, 653–660. https://doi.org/10.1016/j.jpha.2020.09.002.

143. Boruah, P.K.; Darabdhara, G.; Das, M.R. Polydopamine functionalized graphene sheets decorated with magnetic metal oxide nanoparticles as efficient nanozyme for the detection and degradation of harmful triazine pesticides. *Chemosphere* **2021**, *268*, 129328. https://doi.org/10.1016/j.chemosphere.2020.129328.

144. Huang, Y.; Ren, J.; Qu, X. Nanozymes: Classification, Catalytic Mechanisms, Activity Regulation, and Applications. *Chem. Rev.* **2019**, *119*, 4357–4412. https://doi.org/10.1021/acs.chemrev.8b00672.

145. Wu, J.; Wang, X.; Wang, Q.; Lou, Z.; Li, S.; Zhu, Y.; Qin, L.; Wei, H. Nanomaterials with enzyme-like characteristics (nanozymes): Next-generation artificial enzymes (II). *Chem. Soc. Rev.* **2019**, *48*, 1004–1076. https://doi.org/10.1039/c8cs00457a.

146. Wei, J.; Yang, L.; Luo, M.; Wang, Y.; Li, P. Nanozyme-assisted technique for dual mode detection of organophosphorus pesticide. *Ecotoxicol. Environ. Saf.* **2019**, *179*, 17–23. https://doi.org/10.1016/j.ecoenv.2019.04.041.

147. Luo, D.; Huang, X.; Liu, B.; Zou, W.; Wu, Y. Facile Colorimetric Nanozyme Sheet for the Rapid Detection of Glyphosate in Agricultural Products Based on Inhibiting Peroxidase-Like Catalytic Activity of Porous Co_3O_4 Nanoplates. *J. Agric. Food Chem.* **2021**, *69*, 3537–3547.

148. Yang, Y.; Ghalandari, B.; Lin, L.; Sang, X.; Su, W.; Divsalar, A.; Ding, X. A turn-on fluorescence sensor based on Cu^{2+} modulated DNA-templated silver nanoclusters for glyphosate detection and mechanism investigation. *Food Chem.* **2022**, *367*, 130617. https://doi.org/10.1016/j.foodchem.2021.130617.

149. Li, H.; Chen, H.; Li, M.; Lu, Q.; Zhang, Y.; Yao, S. Template protection of gold nanoclusters for the detection of organophosphorus pesticides. *New J. Chem.* **2019**, *43*, 5423–5428. https://doi.org/10.1039/C9NJ01007F.

150. Sok, V.; Fragoso, A. Amperometric biosensor for glyphosate based on the inhibition of tyrosinase conjugated to carbon nano-onions in a chitosan matrix on a screen-printed electrode. *Microchim. Acta* **2019**, *186*, 569. https://doi.org/10.1007/s00604-019-3672-6.

151. Prasad, R. *Advanced Research in Nanosciences for Water Technology*; Springer: Cham, Switzerland, 2019; ISBN 978-3-030-02380-5.

152. Faridbod, F.; Sanati, A.L. Graphene Quantum Dots in Electrochemical Sensors/Biosensors. *Curr. Anal. Chem.* **2018**, *15*, 103–123. https://doi.org/10.2174/1573411014666180319145506.

153. Masteri-Farahani, M.; Mahdavi, S.; Khanmohammadi, H. Chemically functionalized ZnS quantum dots as new optical nanosensor of herbicides. *Mater. Res. Express* **2018**, *5*, 035055. https://doi.org/10.1088/2053-1591/aab7b0.

154. Lesiak, A.; Drzozga, K.; Cabaj, J.; Ba'nski, M.; Malecha, K.; Podhorodecki, A. Optical Sensors Based on II-VI Quantum Dots. *Nanomaterials* **2019**, *9*, 192. https://doi.org/10.3390/nano9020192.

155. Sahoo, D.; Mandal, A.; Mitra, T.; Chakraborty, K.; Bardhan, M.; Dasgupta, A.K. Nanosensing of Pesticides by Zinc Oxide Quantum Dot: An Optical and Electrochemical Approach for the Detection of Pesticides in Water. *J. Agric. Food Chem.* **2018**, *66*, 414–423. https://doi.org/10.1021/acs.jafc.7b04188.

156. Bonilla, J.C.; Bozkurt, F.; Ansari, S.; Sozer, N.; Kokini, J.L. Applications of quantum dots in Food Science and biology. *Trends Food Sci. Technol.* **2016**, *53*, 75–89. https://doi.org/10.1016/j.tifs.2016.04.006.

157. Bera, M.K.; Mohapatra, S. Ultrasensitive detection of glyphosate through effective photoelectron transfer between CdTe and chitosan derived carbon dot. *Colloids Surf. A Physicochem. Eng. Asp.* **2020**, *596*, 124710. https://doi.org/10.1016/j.colsurfa.2020.124710.

158. Xing, Y.; Dittrich, P.S. One-dimensional nanostructures: Microfluidic-based synthesis, alignment and integration towards functional sensing devices. *Sensors* **2018**, *18*, 134. https://doi.org/10.3390/s18010134.

159. Jiang, B.; Lu, M.; Xu, M. Amperometric sensing of organophosphorus pesticides based on covalently attached multilayer assemblies of diazo-resin, Prussian blue single-walled carbon nanotubes, and acetylcholinesterase. *Rev. Roum. Chim.* **2019**, *64*, 763–774. https://doi.org/10.33224/rrch.2019.64.9.03.

160. Gholivand, M.B.; Akbari, A.; Norouzi, L. Development of a novel hollow fiber- pencil graphite modified electrochemical sensor for the ultra-trace analysis of glyphosate. *Sens. Actuators B Chem.* **2018**, *272*, 415–424. https://doi.org/10.1016/j.snb.2018.05.170.

161. O. Domínguez Renedo, M.A. Alonso-Lomillo, M.J.A.M. Recent developments in the field of screen-printed electrodes and their related applications. *Talanta* **2007**, *73*, 202–219. https://doi.org/10.1016/j.talanta.2007.03.050.

162. Habekost, A. Rapid and sensitive spectroelectrochemical and electrochemical detection of glyphosate and AMPA with screen-printed electrodes. *Talanta* **2017**, *162*, 583–588. https://doi.org/10.1016/j.talanta.2016.10.074.

163. Jian Fang, Xungai Wang, T.L. Functional Applications of Electrospun Nano. *Nanofibers Prod. Prop. Funct. Appls.* **2011**, *14*, 287–302.

164. Srivastava, A.K.; Bajpai, P.; Awasthi, P.; Kumar, A.; Prasad, N.E. Nanofiber Based Sensors for Water Pollution Monitoring. In *Sensors in Water Pollutants Monitoring: Role of Material*; Springer: Singapore, 2020.

165. De Almeida, L.K.S.; Chigome, S.; Torto, N.; Frost, C.L.; Pletschke, B.I. A novel colorimetric sensor strip for the detection of glyphosate in water. *Sens. Actuators B Chem.* **2015**, *206*, 357–363. https://doi.org/10.1016/j.snb.2014.09.039.

166. Cui, H.F.; Zhang, T.T.; Lv, Q.Y.; Song, X.; Zhai, X.J.; Wang, G.G. An acetylcholinesterase biosensor based on doping Au nanorod@SiO2 nanoparticles into TiO2-chitosan hydrogel for detection of organophosphate pesticides. *Biosens. Bioelectron.* **2019**, *141*, 111452. https://doi.org/10.1016/j.bios.2019.111452.

167. Torul, H.; Boyaci, I.H.; Tamer, U. Attomole detection of glyphosate by surface-enhanced raman spectroscopy using gold nanorods. *Fabad J. Pharm. Sci.* **2010**, *35*, 179–184.

168. Yola, M.L. Electrochemical activity enhancement of monodisperse boron nitride quantum dots on graphene oxide: Its application for simultaneous detection of organophosphate pesticides in real samples. *J. Mol. Liq.* **2019**, *277*, 50–57.

169. Zeng, M.; Chen, M.; Huang, D.; Lei, S.; Zhang, X.; Wang, L.; Cheng, Z. Engineered two-dimensional nanomaterials: An emerging paradigm for water purification and monitoring. *Mater. Horizons* **2021**, *8*, 758–802. https://doi.org/10.1039/d0mh01358g.

170. Mao, H.; Yan, Y.; Hao, N.; Liu, Q.; Qian, J.; Chen, S.; Wang, K. Dual signal amplification coupling dual inhibition effect for fabricating photoelectrochemical chlorpyrifos biosensor. *Sens. Actuators B Chem.* **2017**, *238*, 239–248. https://doi.org/10.1016/j.snb.2016.07.072.

171. Chen, Q.; Chen, H.; Li, Z.; Pang, J.; Lin, T.; Guo, L.; Fu, F.F. Colorimetric sensing of glyphosate in environmental water based on peroxidase mimetic activity of MoS2 nanosheets. *J. Nanosci. Nanotechnol.* **2017**, *17*, 5730–5734. https://doi.org/10.1166/jnn.2017.13821.

172. Wu, Z.; Hu, Y.; Pan, X.; Tang, Y.; Dai, Y.; Wu, Y. A liquid colorimetric chemosensor for ultrasensitive detection of glyphosate residues in vegetables using a metal oxide with intrinsic peroxidase catalytic activity. *Food Addit. Contam. Part A* **2022**, *39*, 710–723.

173. Cahuantzi-Muñoz, S.L.; González-Fuentes, M.A.; Ortiz-Frade, L.A.; Torres, E.; Țălu, Ș.; Trejo, G.; Méndez-Albores, A. Electrochemical Biosensor for Sensitive Quantification of Glyphosate in Maize Kernels. *Electroanalysis* **2019**, *31*, 927–935. https://doi.org/10.1002/elan.201800759.

174. Oliveira, P.C.; Maximiano, E.M.; Oliveira, P.A.; Camargo, J.S.; Fiorucci, A.R.; Arruda, G.J. Direct electrochemical detection of glyphosate at carbon paste electrode and its determination in samples of milk, orange juice, and agricultural formulation. *J. Environ. Sci. Health Part B Pestic. Food Contam. Agric. Wastes* **2018**, *53*, 817–823. https://doi.org/10.1080/03601234.2018.1505081.

175. Wang, L.; Bi, Y.; Gao, J.; Li, Y.; Ding, H.; Ding, L. Carbon dots based turn-on fluorescent probes for the sensitive determination of glyphosate in environmental water samples. *RSC Adv.* **2016**, *6*, 85820–85828. https://doi.org/10.1039/c6ra10115a.

176. Yuan, Y.; Jiang, J.; Liu, S.; Yang, J.; zhang, H.; Yan, J.; Hu, X. Fluorescent carbon dots for glyphosate determination based on fluorescence resonance energy transfer and logic gate operation. *Sens. Actuators B Chem.* **2017**, *242*, 545–553. https://doi.org/10.1016/j.snb.2016.11.050.

177. Ashrafi Tafreshi, F.; Fatahi, Z.; Ghasemi, S.F.; Taherian, A.; Esfandiari, N. Ultrasensitive fluorescent detection of pesticides in real sample by using green carbon dots. *PLoS ONE* **2020**, *15*, e0230646. https://doi.org/10.1371/journal.pone.0230646.

178. Jiménez-López, J.; Llorent-Martínez, E.J.; Ortega-Barrales, P.; Ruiz-Medina, A. Graphene quantum dots-silver nanoparticles as a novel sensitive and selective luminescence probe for the detection of glyphosate in food samples. *Talanta* **2020**, *207*, 120344. https://doi.org/10.1016/j.talanta.2019.120344.

179. Jiménez-López, J.; Llorent-Martínez, E.J.; Ortega-Barrales, P.; Ruiz-Medina, A. Multicommutated Flow System for the Determination of Glyphosate Based on Its Quenching Effect on CdTe-Quantum Dots Fluorescence. *Food Anal. Methods* **2018**, *11*, 1840–1848. https://doi.org/10.1007/s12161-018-1192-3.

180. Yu, C.X.; Hu, F.L.; Song, J.G.; Zhang, J. Lou; Liu, S.S.; Wang, B.X.; Meng, H.; Liu, L.L.; Ma, L.F. Ultrathin two-dimensional metal-organic framework nanosheets decorated with tetra-pyridyl calix[4]arene: Design, synthesis and application in pesticide detection. *Sens. Actuators B Chem.* **2020**, *310*, 127819. https://doi.org/10.1016/j.snb.2020.127819.

181. Marzari, G.; Cappellari, M.V.; Morales, G.M.; Fungo, F. Electrochemiluminescent detection of glyphosate using electrodes modified with self-assembled monolayers. *Anal. Methods* **2017**, *9*, 2452–2457. https://doi.org/10.1039/c7ay00506g.

182. Ashwin, B.C.M.A.; Saravanan, C.; Stalin, T.; Muthu Mareeswaran, P.; Rajagopal, S. FRET-based Solid-state Luminescent Glyphosate Sensor Using Calixarene-grafted Ruthenium(II)bipyridine Doped Silica Nanoparticles. *ChemPhysChem* **2018**, *19*, 2768–2775. https://doi.org/10.1002/cphc.201800447.

183. Zhang, Q.; Xu, G.; Gong, L.; Dai, H.; Zhang, S.; Li, Y.; Lin, Y. An enzyme-assisted electrochemiluminescent biosensor developed on order mesoporous carbons substrate for ultrasensitive glyphosate sensing. *Electrochim. Acta* **2015**, *186*, 624–630. https://doi.org/10.1016/j.electacta.2015.10.081.

184. Duan, L.; Wang, C.; Zhang, W.; Ma, B.; Deng, Y.; Li, W.; Zhao, D. Interfacial Assembly and Applications of Functional Mesoporous Materials. *Chem. Rev.* **2021**, *121*, 14349–14429. https://doi.org/10.1021/acs.chemrev.1c00236.

185. Liu, Q.; Zhang, R.; Yu, B.; Liang, A.; Jiang, Z. A highly sensitive gold nanosol SERS aptamer assay for glyphosate with a new COF nanocatalytic reaction of glycol-Au(III). *Sens. Actuators B Chem.* **2021**, *344*, 130288. https://doi.org/10.1016/j.snb.2021.130288.

186. Zhou, Y.; Zhang, Y.; Tang, L.; Long, B.; Zeng, G. Nanoporous Materials Based Sensors for Pollutant Detection. In *Nanohybrid and Nanoporous Materials for Aquatic Pollution Control*; Elsevier Inc.: Amsterdam, The Netherlands, 2018; pp. 265–291, ISBN 9780128141557.

187. Song, D.; Jiang, X.; Li, Y.; Lu, X.; Luan, S.; Wang, Y.; Li, Y.; Gao, F. Metal−organic frameworks-derived MnO2/Mn3O4 microcuboids with hierarchically ordered nanosheets and Ti3C2 MXene / Au NPs composites for electrochemical pesticide detection. *J. Hazard. Mater.* **2019**, *373*, 367–376. https://doi.org/10.1016/j.jhazmat.2019.03.083.

188. He, K.; Li, Z.; Wang, L.; Fu, Y.; Quan, H.; Li, Y.; Wang, X.; Gunasekaran, S.; Xu, X. A Water-Stable Luminescent Metal − Organic Framework for Rapid and Visible Sensing of Organophosphorus Pesticides. *Appl. Mater. Interfaces* **2019**, *11*, 26250–26260. https://doi.org/10.1021/acsami.9b06151.

189. Pan, S.; Chen, X.; Li, X.; Jin, M. Nonderivatization method for determination of glyphosate, glufosinate, bialaphos, and their main metabolites in environmental waters based on magnetic metal-organic framework pretreatment. *J. Sep. Sci.* **2019**, *42*, 1045–1050. https://doi.org/10.1002/jssc.201800957.

190. Mahmoudi, E.; Fakhri, H.; Hajian, A.; Afkhami, A.; Bagheri, H. High-performance electrochemical enzyme sensor for organophosphate pesticide detection using modified metal-organic framework sensing platforms. *Bioelectrochemistry* **2019**, *130*, 107348. https://doi.org/10.1016/j.bioelechem.2019.107348.

191. Xie, Z.; Xu, W.; Cui, X.; Wang, Y. Recent Progress in Metal–Organic Frameworks and Their Derived Nanostructures for Energy and Environmental Applications. *ChemSusChem* **2017**, *10*, 1645–1663. https://doi.org/10.1002/cssc.201601855.

192. Vikrant, K.; Tsang, D.C.W.; Raza, N.; Giri, B.S.; Kukkar, D.; Kim, K.H. Potential Utility of Metal-Organic Framework-Based Platform for Sensing Pesticides. *ACS Appl. Mater. Interfaces* **2018**, *10*, 8797–8817. https://doi.org/10.1021/acsami.8b00664.

193. Yang, Q.; Wang, J.; Chen, X.; Yang, W.; Pei, H.; Hu, N.; Li, Z.; Suo, Y.; Li, T.; Wang, J. The simultaneous detection and removal of organophosphorus pesticides by a novel Zr-MOF based smart adsorbent. *J. Mater. Chem. A* **2018**, *6*, 2184–2192. https://doi.org/10.1039/c7ta08399h.

194. Marin, P.; Bergamasco, R.; Módenes, A.N.; Paraiso, P.R.; Hamoudi, S. Synthesis and characterization of graphene oxide functionalized with MnFe2O4 and supported on activated carbon for glyphosate adsorption in fixed bed column. *Process Saf. Environ. Prot.* **2019**, *123*, 59–71. https://doi.org/10.1016/j.psep.2018.12.027.

195. Santos, T.R.T.; Andrade, M.B.; Silva, M.F.; Bergamasco, R.; Hamoudi, S. Development of α- and γ-Fe2O3 decorated graphene oxides for glyphosate removal from water. *Environ. Technol.* **2019**, *40*, 1118–1137. https://doi.org/10.1080/09593330.2017.1411397.

196. Park, H.; May, A.; Portilla, L.; Dietrich, H.; Münch, F.; Rejek, T.; Sarcletti, M.; Banspach, L.; Zahn, D.; Halik, M. Magnetite nanoparticles as efficient materials for removal of glyphosate from water. *Nat. Sustain.* **2020**, *3*, 129–135. https://doi.org/10.1038/s41893-019-0452-6.

197. Li, S.; Liu, X.; Chai, H.; Huang, Y. Recent advances in the construction and analytical applications of metal-organic frameworks-based nanozymes. *TrAC Trends Anal. Chem.* **2018**, *105*, 391–403. https://doi.org/10.1016/j.trac.2018.06.001.

198. Gu, C.; Wang, Q.; Zhang, L.; Yang, P.; Xie, Y.; Fei, J. Ultrasensitive non-enzymatic pesticide electrochemical sensor based on HKUST-1-derived copper oxide @ mesoporous carbon composite. *Sens. Actuators B Chem.* **2020**, *305*, 127478. https://doi.org/10.1016/j.snb.2019.127478.

199. Cao, Y.; Wang, T.; Wang, X.; Huo, Q.; Liu, Y. Facile Fabricating Hierarchically Porous Metal−Organic Frameworks via a Template-Free Strategy. *Cryst. Growth Des.* **2016**, *16*, 504–510. https://doi.org/10.1021/acs.cgd.5b01559.

200. Bao, J.; Huang, T.; Wang, Z.; Yang, H.; Geng, X.; Xu, G.; Samalo, M.; Sakinati, M.; Huo, D.; Hou, C. 3D graphene/copper oxide nano-flowers based acetylcholinesterase biosensor for sensitive detection of organophosphate pesticides. *Sens. Actuators B Chem.* **2019**, *279*, 95–101. https://doi.org/10.1016/j.snb.2018.09.118.

201. Duan, G.W.; Zhang, J.; Li, Y.; Xu, Y.M.; Yin, F.; Fu, Y.Z. The preparation of Fe3O4/molecular-imprinted nanocomposite and the application on the recognition and separation of glyphosate. *Inorg. Nano-Metal Chem.* **2017**, *47*, 481–487. https://doi.org/10.1080/15533174.2016.1186052.

202. Wu, S.; Huang, F.; Lan, X.; Wang, X.; Wang, J.; Meng, C. Electrochemically reduced graphene oxide and Nafion nanocomposite for ultralow potential detection of organophosphate pesticide. *Sens. Actuators B Chem.* **2013**, *177*, 724–729. https://doi.org/10.1016/j.snb.2012.11.069.

203. Li, Y.; Wu, S.; Zhang, Y.; Ma, Z.; Zhu, M.; Gao, E. A lanthanide metal–organic framework as ratio fluorescence probe to detect pesticides in water. *Inorganica Chim. Acta* **2021**, *528*, 120632. https://doi.org/10.1016/j.ica.2021.120632.

204. Pan, J.; Chen, W.; Ma, Y.; Pan, G. Molecularly imprinted polymers as receptor mimics for selective cell recognition. *Chem. Soc. Rev.* **2018**, *47*, 5574–5587. https://doi.org/10.1039/c7cs00854f.

205. Saylan, Y.; Yilmaz, F.; Özgür, E.; Derazshamshir, A.; Yavuz, H.; Denizli, A. Molecular imprinting of macromolecules for sensor applications. *Sensors* **2017**, *17*, 898. https://doi.org/10.3390/s17040898.

206. Prasad, B.B.; Jauhari, D.; Tiwari, M.P. Doubly imprinted polymer nanofilm-modified electrochemical sensor for ultra-trace simultaneous analysis of glyphosate and glufosinate. *Biosens. Bioelectron.* **2014**, *59*, 81–88. https://doi.org/10.1016/j.bios.2014.03.019.

207. Chen, L.; Wang, X.; Lu, W.; Wu, X.; Li, J. Molecular imprinting: Perspectives and applications. *Chem. Soc. Rev.* **2016**, *45*, 2137–2211. https://doi.org/10.1039/c6cs00061d.

208. Mazouz, Z.; Touchente, Z.A.; Laradi, H.; Fourati, N.; Yaakoubi, N.; Touzani, R.; Chehimi, M.M.; Kalfat, R.; Othmane, A.; Zerrouki, C. Design of Novel Electrochemical Sensors for the Selective Detection of Glyphosate. *Proceedings* **2017**, *1*, 483. https://doi.org/10.3390/proceedings1040483.

209. Kim, Y.; Lee, J.; Shin, I.S. Advanced method for fabrication of molecularly imprinted mesoporous organosilica with highly sensitive and selective recognition of glyphosate. *Sci. Rep.* **2019**, *9*, 10293. https://doi.org/10.1038/s41598-019-46881-7.

210. Sawetwong, P.; Chairam, S.; Jarujamrus, P.; Amatatongchai, M. Enhanced selectivity and sensitivity for colorimetric determination of glyphosate using Mn–ZnS quantum dot embedded molecularly imprinted polymers combined with a 3D-microfluidic paper-based analytical device. *Talanta* **2021**, *225*, 122077. https://doi.org/10.1016/j.talanta.2020.122077.

211. Ding, S.; Lyu, Z.; Li, S.; Ruan, X.; Fei, M.; Zhou, Y.; Niu, X.; Zhu, W.; Du, D.; Lin, Y. Molecularly imprinted polypyrrole nanotubes based electrochemical sensor for glyphosate detection. *Biosens. Bioelectron.* **2021**, *191*, 113434.

212. Thimoonnee, S.; Somnet, K.; Ngaosri, P.; Chairam, S.; Karuwan, C.; Kamsong, W.; Tuantranont, A.; Amatatongchai, M. Fast, sensitive and selective simultaneous determination of paraquat and glyphosate herbicides in water samples using a compact electrochemical sensor. *Anal. Methods* **2022**, *14*, 820–833. https://doi.org/10.1039/d1ay02201f.

213. Zhang, C.; She, Y.; Li, T.; Zhao, F.; Jin, M.; Guo, Y.; Zheng, L.; Wang, S.; Jin, F.; Shao, H.; et al. A highly selective electrochemical sensor based on molecularly imprinted polypyrrole-modified gold electrode for the determination of glyphosate in cucumber and tap water. *Anal. Bioanal. Chem.* **2017**, *409*, 7133–7144. https://doi.org/10.1007/s00216-017-0671-5.

214. Xu, J.; Zhang, Y.; Wu, K.; Zhang, L.; Ge, S.; Yu, J. A molecularly imprinted polypyrrole for ultrasensitive voltammetric determination of glyphosate. *Microchim. Acta* **2017**, *184*, 1959–1967. https://doi.org/10.1007/s00604-017-2200-9.

215. Gui, M.; Jiang, J.; Wang, X.; Yan, Y.; Li, S.; Xiao, X.; Liu, T.; Liu, T.; Feng, Y. Copper ion-mediated glyphosate detection with N-heterocycle based polyacetylene as a sensing platform. *Sens. Actuators B Chem.* **2017**, *243*, 696–703. https://doi.org/10.1016/j.snb.2016.12.037.

216. Songa, E.A.; Waryo, T.; Jahed, N.; Baker, P.G.L.; Kgarebe, B.V.; Iwuoha, E.I. Electrochemical nanobiosensor for glyphosate herbicide and Its metabolite. *Electroanalysis* **2009**, *21*, 671–674. https://doi.org/10.1002/elan.200804452.

217. Zouaoui, F.; Bourouina-Bacha, S.; Bourouina, M.; Abroa-Nemeir, I.; Halima, H. Ben; Gallardo-Gonzalez, J.; El Alami El Hassani, N.; Alcacer, A.; Bausells, J.; Jaffrezic-Renault, N.; et al. Electrochemical impedance spectroscopy determination of glyphosate using a molecularly imprinted chitosan. *Sens. Actuators B Chem.* **2020**, *309*, 127753. https://doi.org/10.1016/j.snb.2020.127753.

218. Aydin, Z.; Keleş, M. A reaction-based system for the colorimetric detection of glyphosate in real samples. *Spectrochim. Acta Part A Mol. Biomol. Spectrosc.* **2022**, *267*, 120501. https://doi.org/10.1016/j.saa.2021.120501.

219. Santos, J.S.; Pontes, M.S.; Santiago, E.F.; Fiorucci, A.R.; Arruda, G.J. An efficient and simple method using a graphite oxide electrochemical sensor for the determination of glyphosate in environmental samples. *Sci. Total Environ.* **2020**, *749*, 142385. https://doi.org/10.1016/j.scitotenv.2020.142385.

220. Wiwasuku, T.; Boonmak, J.; Burakham, R.; Hadsadee, S.; Jungsuttiwong, S.; Bureekaew, S.; Promarak, V.; Youngme, S. Turn-on fluorescent probe towards glyphosate and Cr3+ based on Cd(ii)-metal organic framework with Lewis basic sites. *Inorg. Chem. Front.* **2021**, *8*, 977–988. https://doi.org/10.1039/d0qi00947d.

221. Hu, T.; Xu, J.; Ye, Y.; Han, Y.; Li, X.; Wang, Z.; Sun, D.; Zhou, Y.; Ni, Z. Visual detection of mixed organophosphorous pesticide using QD-AChE aerogel based microfluidic arrays sensor. *Biosens. Bioelectron.* **2019**, *136*, 112–117. https://doi.org/10.1016/j.bios.2019.04.036.

222. Li, Y.; Zhu, Y.; Wang, C.; He, M.; Lin, Q. Selective detection of water pollutants using a differential aptamer-based graphene biosensor. *Biosens. Bioelectron.* **2019**, *126*, 59–67. https://doi.org/10.1016/j.bios.2018.10.047.

223. Liu, Y.; Bonizzoni, M. A supramolecular sensing array for qualitative and quantitative analysis of organophosphates in water. *J. Am. Chem. Soc.* **2014**, *136*, 14223–14229. https://doi.org/10.1021/ja507905r.

224. Banna, M.; Bera, K.; Sochol, R.; Lin, L.; Najjaran, H.; Sadiq, R.; Hoorfar, M. 3D printing-based integrated water quality sensing system. *Sensors* **2017**, *17*, 1336. https://doi.org/10.3390/s17061336.

225. Saftics, A.; Türk, B.; Sulyok, A.; Nagy, N.; Gerecsei, T.; Szekacs, I.; Kurunczi, S.; Horvath, R. Biomimetic Dextran-Based Hydrogel Layers for Cell Micropatterning over Large Areas Using the FluidFM BOT Technology. *Langmuir* **2019**, *35*, 2412–2421. https://doi.org/10.1021/acs.langmuir.8b03249.

226. Fan, Y.; Dong, D.; Li, Q.; Si, H.; Pei, H.; Li, L.; Tang, B. Fluorescent analysis of bioactive molecules in single cells based on microfluidic chips. *Lab Chip* **2018**, *18*, 1151–1173. https://doi.org/10.1039/c7lc01333g.

227. Liao, Z.; Wang, J.; Zhang, P.; Zhang, Y.; Miao, Y.; Gao, S.; Deng, Y.; Geng, L. Recent advances in microfluidic chip integrated electronic biosensors for multiplexed detection. *Biosens. Bioelectron.* **2018**, *121*, 272–280. https://doi.org/10.1016/j.bios.2018.08.061.

228. Silva Freire, C. Da; Da Silva Moreira, C.; De Souza Filho, C.A.; Moreno Santa Cruz, R.; Falqueto, A.; Valle, A.L.; Goulart Filho, L.R.; Souto De Medeiros, E.; Nascimento Ferreira, K. Do Application of a Smartphone-based SPR platform for Glyphosate detection. In Proceedings of the 2019 IEEE Sensors Applications Symposium (SAS), Sophia Antipolis, France, 11–13 March 2019; pp. 1–6. https://doi.org/10.1109/SAS.2019.8706024.